# SANDIA REPORT

SAND98–0566 • UC–706
Unlimited Release
Printed March 1998

# GaAs Photonic Integrated Circuit (PIC) Development for High Performance Communications

C. T. Sullivan

Prepared by
Sandia National Laboratories
Albuquerque, New Mexico 87185 and Livermore, California 94550

Sandia is a multiprogram laboratory operated by Sandia Corporation, a Lockheed Martin Company, for the United States Department of Energy under Contract DE-AC04-94AL85000.



Sandia National Laboratories

Issued by Sandia National Laboratories, operated for the United States Department of Energy by Sandia Corporation.


Available to DOE and DOE contractors from
Office of Scientific and Technical Information
P.O. Box 62
Oak Ridge, TN 37831

Prices available from (615) 576-8401, FTS 626-8401

Available to the public from
National Technical Information Service
U.S. Department of Commerce
5285 Port Royal Rd
Springfield, VA 22161

NTIS price codes
Printed copy: A04
Microfiche copy: A01

SAND98-0566
Unlimited Release
Printed March 1998

Distribution

Category UC-706

# GaAs Photonic Integrated Circuit (PIC) Development for High Performance Communications

**C. T. Sullivan**
**Advanced Compound Semiconductor Technologies Department**
**P. O. Box 5800**
**Sandia National Laboratories**
**Albuquerque, New Mexico 87185-0603**

## Abstract

Sandia has established a foundational technology in photonic integrated circuits (PICs) based on the (Al,Ga,In)As material system for optical communication, radar control and testing, and network switching applications at the important 1.3μm/1.55μm wavelengths. We investigated the optical, electrooptical, and microwave performance characteristics of the fundamental building-block PIC elements designed to be as simple and process-tolerant as possible, with particular emphasis placed on reducing optical insertion loss. Relatively conventional device array and circuit designs were built using these PIC elements to establish a baseline performance standard; to assess the impact of epitaxial growth accuracy and uniformity, and of fabrication uniformity and yield; to validate our theoretical and numerical models; and to resolve the optical and microwave packaging issues associated with building fully packaged prototypes. Novel and more complex PIC designs and fabrication processes, viewed as higher payoff but higher risk, were explored in a parallel effort with the intention of meshing those advances into our baseline higher-yield capability as they mature. The application focus targeted the design and fabrication of packaged solitary modulators meeting the requirements of future wideband and high-speed analog and digital data links. Successfully prototyped devices are expected to feed into more complex PICs solving specific problems in high-performance communications, such as optical beamforming networks for phased array antennas.

## Acknowledgment

Many individuals are responsible for the success of this program. The principal investigators are M. G. Armendariz, G. R. Hadley, M. J. Hafich, B. E. Hammons, V. M. Hietala, H. Q. Hou, J. F. Klem, S. H. Kravitz, J. Reno, R. J. Shul, R. E. Smith, C. T. Sullivan, G. A. Vawter, and J. R. Wendt.

This program benefited from numerous invaluable technical contributions from C. I. Ashby, T. Bauer, T. Brennan, F. G. Cajas, R. F. Carson, D. Chu, H. Chui, R. F. Corless, T. Drummond, B. A. Fuchs, C. T. Fuller, L. Griego, H. P. Hjalmarson, M. Housel, G. M. McClellan, T. A. Plut, D. J. Reiger, C. E. Sandoval, P. K. Seigal, M. Slayton, M. B. Snipes, D. Tibbets, C. P. Tigges, M. E. Warren, J. C. Word, and W. Zuberzycki.

Sandia is a multiprogram laboratory operated by Sandia Corporation , a Lockheed Martin Company, for the United States Department of Energy under contract DE-AC04-94AL85000.

## Contents

## Objective

The objective of this program has been to establish a foundational technology in photonic integrated circuits (PICs) based on the (Al,Ga,In)As material system for optical communication, radar and antenna control and testing, and network switching applications at the important 1.3μm/1.55μm wavelengths. As these operating wavelengths are substantially below the bandedge, and the primary modulation mechanism is the linear electrooptic effect, we anticipate that these materials are quite hard to damaging radiation effects and can be engineered in device geometries capable of operating from DC to deep into the millimeter-wave range. These attributes may therefor become very attractive to the nuclear weapons community (primarily for its spaceborne surveillance and treaty verification missions), the military and commercial space applications community, and the terrestrial fiber data and telecommunications communities. While beyond the scope of the present program, the potential exists to integrate PICs monolithically with electronic circuits made from epitaxially compatible materials. Indeed, many of the requisite fabrication steps developed for PICs under this program were borrowed from the knowledge base at Sandia and elsewhere in GaAs digital integrated circuits and GaAs millimeter-wave and microwave integrated circuits (MMICs) to maintain the capability for eventual integration.

We investigated the optical, electrooptical, and microwave performance characteristics of the fundamental building-block PIC elements designed to be as simple and process-tolerant as possible, with particular emphasis placed on reducing optical insertion loss. This has been a key issue for the semiconductor PIC community since the fiber-PIC-fiber insertion loss had been prohibitively large, with typical values in excess of 20 dBo (40 dBe). This loss problem has been substantially solved as a result of progress under this program. Relatively conventional device array and circuit designs were built using these low-loss PIC elements to establish a baseline performance standard (versus state-of-the-art lithium niobate and chromophore-doped polymer devices); to assess the impact of epitaxial growth accuracy and uniformity, and of fabrication uniformity and yield; to validate our newly-developed theoretical and numerical models for photonic devices and circuits; and to resolve the optical and microwave packaging issues associated with building fully packaged prototypes suitable for some system applications. Novel and much more complex PIC designs and fabrication processes, viewed as higher payoff but higher risk, were explored in a parallel effort with the intention of meshing those advances into our baseline higher-yield capability as they mature.

The application focus targeted the design and fabrication of packaged solitary modulators meeting the requirements of future wideband and high-speed analog and digital data links. Successfully prototyped devices are expected to feed into more complex PICs solving specific problems in high-performance communications, such as optical beamforming networks for phased array antennas.

## Technical Accomplishments

On our baseline effort, we demonstrated record low-loss optical waveguide routing and distribution components for (Al,Ga)As PICs, including: (1) singlemode attenuations < 0.5 dB/cm (our best 0.4 ± 0.1 dB/cm), (2) right-angle turning mirror insertion loss of 0.4 ± 0.1 dB, a world-best record, and (3) excess loss of 0.4 ± 0.2 dB for lateral mode interference (LMI) 1X2, 1X4, 1X8, and 1X32 splitters, all with typically ~95% on-chip yields. These accomplishments represent a tremendous advance in the state-of-the-art of semiconductor-based PICs. The optical loss performance now surpasses nonlinearoptic polymeric devices and nearly matches that of lithium niobate devices, but of course without the many disadvantages of those material systems.

We developed an approach to velocity match (<10% mismatch) low-loss transmission line electrodes to undoped (Al,Ga)As optical waveguide modulators with ~95% on-chip yields, fabricated wideband electrooptic waveguide modulators, and developed fiber packaging for loss-limited small-signal bandwidth >50 GHz and fiber-waveguide-fiber insertion loss of <6 dB. We have theorized and then demonstrated experimentally that the use of highly form-birefringent waveguide designs are a practical solution to obtaining high-extinction ratio Mach-Zehnder interferometers, thus resolving the long-standing problem of device depolarization in semiconductor PICs. Our novel approach is based on high-index-contrast digital alloys. The origin of the otherwise unpredictable lightwave depolarization is associated with uncontrolled strain introduced by residual electrode stresses and submicron misalignment on our deeply-etched waveguide features, feature micro-roughness (esp. sidewall roughness), and crystallographic misorientation of the starting substrates. Typical interferometer extinction ratios are now routinely measured to be in the 30 dB to 40 dB range, with a best value of about 43 dB, for devices that exhibit on-chip optical losses of 2~5 dB, and half-wave voltages of 4~10 V, depending on the design specifics. This accomplishment represents a vast improvement over the previous state-of-the-art. (For example, previous Sandia art had uncontrolled extinction ratios in the 3 dB to 15 dB range with fiber-PIC-fiber losses much greater than 20 dB.)

A novel fiber-waveguide coupler has been invented and demonstrated to have ~1.5dB insertion loss with substantial misalignment tolerance, a dramatic improvement over the 8~10dB range typically expected for very high electrooptic figure-of-merit (FOM) modulators. In fact, this invention has now made high-FOM modulators relevant to a variety of defense and commercial applications. High-FOM modulators with 15.5dB ($V^1$ = 2.6V) and 14dB extinction ratios have been demonstrated using novel XY combiner and cutoff mesa waveguide designs, respectively, and have on-chip losses of about 7 dB.

Novel traveling-wave optical photodetectors using high-InAs-mode-fraction absorbing layers on standard low-loss AlGaAs waveguides have been invented and are being developed for wideband, high-optical-saturation-power RF applications. A novel 1X32 switch based on LMI splitters, phased-modulated arrayed waveguides and electrooptic in-plane focusing effects has been invented to address optical control problems in phased array radars.

**Publications**

The following thirty publications resulted from the subject program. Some of the more important publications are reprinted in the Appendices.

Vawter, G. A., C. T. Sullivan, J. R. Wendt, R. E. Smith, H. Q. Hou, and J. F. Klem, "Tapered rib adiabatic following fiber couplers in etched GaAs materials for monolithic spot-size transformation," (Invited) *to be published in IEEE J. of Selected Topics in Quantum Electron.*, (1997).

Childs, T. E., V. Sokolov, and C. T. Sullivan, "Lattice-engineered MBE growth of high-indium mole fraction InGaAs for low cost MMICs and 1.3-1.55μm OEICs," *Design and Manufacturing of WDM Devices, Proceedings of the Society of Photo-Optical Instrumentation Engineers*, Vol. 3234 (Paper 20), Dallas, TX (1997).

Sullivan, C. T., G. McClellan, T. Plut, C. Fuller, T. Bauer, M. Armendariz, V. Hietala, J. Reno, A. Vawter, D. Reiger, J. Wendt, D. Chu, R. Smith, B. Snipes, and P. Seigal, "Packaging of (Al,Ga)As photonic integrated circuits," (Invited) *1997 IEEE MTT-S Inter. Microwave Symp., Microwave and Millimeter-Wave Optoelectronic Integrated Circuit Modules: Manufacturing and Applic. Workshop*, Denver, CO (1997).

Seigal, P. K., M. G. Armendariz, D. J. Rieger, K. L. Lear, and C. T. Sullivan, "Metallization and packaging of compound semiconductor devices at Sandia National Laboratories," (Invited) *Proceedings of the 190th Electrochemical Society Meeting: State-of-the-Art Program on Compound Semiconductors XXV,* Vol. 96-15, San Antonio, TX, 158 (1996).

Smith, R. E., G. A. Vawter, G. R. Hadley, C. T. Sullivan, J. R. Wendt, M. B. Snipes, S. H. Kravitz, and J. F. Klem, "Reduced coupling loss using a tapered-rib adiabatic-following fiber coupler," *IEEE Photonics Technology Letters,* Vol. 8, No. 8, 1052 (1996).

Vawter, G. A., V. M. Hietala, J. R. Wendt, B. A. Fuchs, M. Hafich, M. Housel, M. Armendariz, and C. T. Sullivan, "High speed traveling wave electrooptic intensity modulator with a doped PIN semiconductor junction," *OSA/IEEE Technical Digest on Integrated Photonics Research (IPR 1996)*, Vol. 6, Boston, MA, 384 (1996).

Smith, R. E., G. A. Vawter, G. R. Hadley, C. T. Sullivan, J. R. Wendt, M. B. Snipes, and J. F. Klem, "Tapered-rib adiabatic-following fiber coupler," *OSA/IEEE Technical Digest on Integrated Photonics Research*, Vol. 6, Boston, MA, 171 (1996).

McClellan, G. B., R. J. Shul, and C. T. Sullivan, "Dry etching of GaAs using an inductively coupled plasma," *32nd Annual Symposium of the New Mexico Chapter of The American Vacuum Society*, Albuquerque, NM (1996).

Sullivan, C. T., "Guided-wave optics developments at Sandia National Laboratories," *Workshop on Electro-Optics for the Next Century*, University of California at San Diego, La Jolla, CA (1996).

Vawter, G. A., R. E. Smith, B. Fuchs, J. R. Wendt, M. Hafich, and G. R. Hadley, "A rib optical waveguide with cutoff mesa isolation," *IEEE J. Lightwave Technol.,* Vol. 14, No. 2, 169 (1996).

Smith, R. E., C. T. Sullivan, G. R. Hadley, G. A. Vawter, J. R. Wendt, M. B. Snipes, and J. F. Klem, "Reduced coupling loss using a tapered-rib adiabatic-following fiber coupler," *IEEE Lasers and Electro-Optics Society Meeting (LEOS'95)*, San Francisco, CA, 15 (1995).

Shul, R. J., C. T. Sullivan, B. Snipes, G. McClellan, M. Hafich, and C. T. Fuller, "Attenuation losses in electron cyclotron resonance plasma etched AlGaAs waveguides," *Solid-State Electronics*, Vol. 38, No. 12, 2047 (1995).

Constantine, C., R. J. Shul, C. T. Sullivan, M. B. Snipes, G. B. McClellan, M. J. Hafich, C. T. Fuller, J. R. Mileham, and S. J. Pearton, "Etching of GaAs/AlGaAs rib waveguide structures using $BCl_3/Cl_2/N_2$/Ar electron cyclotron resonance," *J. of Vacuum Science and Technology B*, Vol. 13, No. 5, 2025 (1995).

McClellan, G. B., C. T. Sullivan, R. J. Shul, M. B. Snipes, C. T. Fuller, and M. J. Hafich, "Minimization of process induced fundamental mode attenuation in GaAs/AlGaAs rib waveguides using electron cyclotron resonance plasmas," *31st Annual Symposium of the New Mexico Chapter of The American Vacuum Society*, Albuquerque, NM (1995).

Snipes, M. B., C. T. Sullivan, R. J. Shul, G. B. McClellan, and C. T. Fuller, "Deep etching of GaAs for self-aligned fiber troughs in photonic integrated circuits," *31st Annual Symposium of the New Mexico Chapter of The American Vacuum Society*, Albuquerque, NM (1995).

Borges, B. V., W. Zubrzycki, P. R. Herczfeld, S. H. Kravitz, G. R. Hadley, G. A. Vawter, R. F. Corless, R. E. Smith, J. R. Wendt, J. C. Word, and T. M. Bauer, "GaAs Fabry-Perot modulator for microwave applications," *1995 SBMO/IEEE MTT-S Inter. Microwave and Optoelectronic. Conf.,* paper H2.3, Rio de Janeiro, Brazil (1995).

Kravitz, S. H., W. J. Zubrzycki, J. C. Word, R. E. Smith, G. R. Hadley, P. R. Herczfeld, R. F. Corless, G. A. Vawter, T. M. Bauer, J. R. Wendt, and B. V. Borges, "Integrated Fabry-Perot intensity modulators using in-line distributed Bragg reflectors for microwave integrated circuits," *Proc. of Prog. in Electromag. Res. Symp. (PIERS 1995),* 520 (1995).

Vawter, G. A., G. R. Hadley, B. Fuchs, J. R. Wendt, and J. F. Klem, "An integrated optical XY coupler for phase sensitive optical power combining and suppression of radiated light," *IEEE Photon. Technol. Lett*, Vol 7, No. 4, 394 (1995).

Zubryzycki, W., B. V. Borges, P. R. Herczfeld, S. H. Kravitz, G. R. Hadley, G. A. Vawter, R. F. Corless, R. E. Smith, J. R. Wendt, J. C. Word, and T. M. Bauer, "Integrated optic distributed

Bragg reflector Fabry-Perot modulator for microwave applications," *Inter. Microwave Symposium,* paper 95CH 3577-4, Orlando, FL, 259 (1995).

Vawter, G. A., R. E. Smith, B. Fuchs, J. R. Wendt, M. Hafich, and G. R. Hadley, "Demonstration of a rib optical waveguide with cutoff mesa isolation," *LEOS'95 8th Annual Meeting*, San Francisco, CA (1995).

Hietala, V. M., G. A. Vawter, T. M. Brennan, and B. E. Hammons, "Traveling-wave photodetectors for high-power, large-bandwidth applications," *IEEE Trans. on Microwave Theory and Techniques*, Vol. 43., No. 9/2, 2291 (1995).

Vawter, G. A., J. F. Klem, and R. E. Leibenguth, "Improved epitaxial layer design for real-time monitoring of dry-etching in III-V compound heterostructures with depth accuracy of +/- 8 nm," *J. of Vac. Sci and Technol. A (Vacuum, Surfaces, and Films),* Vol. 12, 1973 (1994).

Carson, R. F., and C. T. Sullivan, "Guided-wave packaging efforts at Sandia," *Advanced Technology Workshop on Optoelectronics, International Society for Hybrid Manufacturing* and *International Electronic Packaging Society (ISHM/IEPS),* Ojai, CA (1994).

Shul, R. J., M. L. Lovejoy, D. L. Hetherington, D. J. Rieger, G. A. Vawter, and J. F. Klem, "Investigation of plasma etch induced damage in compound semiconductor devices," *J. Vac. Sci. and Technol. A*, Vol. 12, No. 4, 1351 (1994).

Constantine, C., R. J. Shul, and C. T. Sullivan, "Dry etch processing of GaAs/AlGaAs laser structures using electron cyclotron resonance plasmas," *186th Meeting of The Electrochemical Society*, Miami Beach, FL (1994).

Kravitz, S. H., V. M. Hietala, G. A. Vawter, M. E. Warren, G. R. Hadley, M. G. Armendariz, J. C. Word, M. B. Snipes, J. R. Wendt, R. F. Carson, R. F. Corless, B. E. Hammons, J. F. Klem, and R. E. Leibenguth, "High performance GaAs/AlGaAs optical modulators: their performance and packaging for microwave photonic integrated circuits," *1994 Asia-Pacific Microwave Conf.*, Tokyo, Japan (1994).

Vawter, G. A., V. M. Hietala, S. H. Kravitz, and M. G. Armendariz, "Unlimited-bandwidth distributed optical phase modulators and detectors: design and fabrication issues," *Proc. of IEEE MTT-S & LEOS Top. Meeting on Optical Microwave Interactions,* Ile-de-France, France (1994).

Hietala, V. M., S. H. Kravitz, M. G. Armendariz, G. A. Vawter, R. F. Carson, and R. E. Leibenguth, "High-performance GaAs/AlGaAs optical phase modulators for microwave/photonic integrated circuits," *Proc. of the Society of Photo-Optical Instrumentation Engineers*, Vol. 2155, 215 (1994).

Vawter, G. A., and G. R. Hadley, "III-V compound semiconductor strip-loaded waveguide devices for PICs: design for minimum crosstalk and high density," *Proc. of the Society of Photo-Optical Instrumentation Engineers*, Vol. 2146, 2 (1994).

Hietala, V. M., S. H. Kravitz, M. G. Armendariz, G. A. Vawter, and R. F. Carson, "High-performance GaAs/AlGaAs optical phase modulators for microwave photonic integrated circuits," *IEEE MTT-S Inter. Microwave Symp.,* Vol. 3, 1497 (1994).

**Patent Disclosures**

The following patent disclosures resulted from the subject program:

Vawter, G. A., and R. E. Smith, "A semiconductor diode laser using a tapered rib waveguide for expanded output optical mode size," SD-5901, S-86, 546 (1996).

Smith, R. E., and G. A. Vawter, "Tapered rib adiabatic fiber coupler," SD-5588, S-82-946 (1995).

Vawter, G. A., R. E. Smith, "Cutoff mesa isolated rib optical waveguide for III-V heterostructure photonic integrated circuits," SD-5491, S-81-584 (1994).

**Patents**

U. S. Patent No. 5,627,929, "Integrated optical XY coupler," G. A. Vawter and G. R. Hadley (May 6, 1997)

## Conclusion

This program has developed the essentials of a foundational guided-wave technology in the (Al,Ga)As material system. All the requisite building-block components have been demonstrated, most with the world's best performance in these materials. While additional developmental work is required to assure high uniformity and yield, and run-to-run repeatability of any particular device or device array, all the basic constituent components are in place. Thus, the objectives of the program have been substantially met.

Sandia is now pursuing several business opportunities focused on application-specific development of this basic foundational technology. These include the development of high-sensitivity packaged solitary 20 GHz-bandwidth microwave modulators for a military satellite applications, 1x32 optical switch matrices supporting novel optical beamforming networks for phased array antennas, and monolithic electrooptic steering systems for laser satellite communication crosslinks.

## Appendices

The following seven publications are included as appendices:

1. Tapered Rib Adiabatic Following Fiber Couplers in Etched GaAs Materials for Monolithic Spot-Size Transformers
2. High Speed Traveling Wave Electrooptic Intensity Modulator with a Doped PIN Semiconductor Junction
3. Traveling-Wave Electrooptic Intensity Modulator Using a Doped PIN Semiconductor Junction for DC to >40GHz Modulation Bandwidth
4. Reduced Coupling Loss Using a Tapered-Rib Adiabatic-Following Fiber Coupler
5. A Rib Optical Waveguide with Cutoff Mesa Isolation
6. An Integrated Optical XY Coupler for Phase-Sensitive Optical Power Combining and Suppression of Radiated Light
7. Attenuation Losses in Electron Cyclotron Resonance Plasma Etched AlGaAs Waveguides
8. Etching of GaAs/AlGaAs Rib Waveguide Structures Using $BCl_3/Cl_2/N_2/Ar$ Electron Cyclotron Resonance
9. Unlimited Bandwidth Distributed Optical Phase Modulators and Detectors: Design and Fabrication Issues

# Tapered Rib Adiabatic Following Fiber Couplers in Etched GaAs Materials for Monolithic Spot-Size Transformation

G. Allen Vawter, *Member, IEEE,* Charles T. Sullivan, *Senior Member, IEEE,* Joel R. Wendt, *Member, IEEE,* Robert E. Smith, Hong Q. Hou, *Member, IEEE,* and John F. Klem

*(Invited Paper)*

*Abstract*—**Design details and demonstration data are presented for an (Al,Ga)As monolithic tapered rib waveguide achieving modal spot-size transformation. The tapered rib adiabatic following fiber coupler structure (TRAFFiC) achieves two-dimensional (2-D) expansion of the output optical mode of single-transverse-mode semiconductor waveguide modulators and lasers using a one-dimensional (1-D) taper between noncritical initial and final taper widths which are compatible with optical lithographic techniques. Measurements are presented of total mode expansion losses between ~1.5–2.0 dB and semiconductor to single-mode-fiber waveguide coupling losses of ~0.5–1.0 dB for doped pin optical-modulator-type waveguides using the TRAFFiC wave guide. A semiconductor laser with a TRAFFiC tapered-rib mode-expansion section and measured coupling loss between the laser output and single-mode fiber of only 0.9 dB is described. Finally, a TRAFFiC spot-size transformer for undoped waveguide modulators with total mode expansion losses of 1.84 dB and excellent modal behavior at 1.32-$\mu$m wavelength is presented. The TRAFFiC structure is particularly well suited for integration with both active and passive etched rib waveguide devices. Fabrication is relatively simple, requiring only patterning and etching of the tapered waveguide and uniform-width outer mesa waveguide without any epitaxial regrowth.**

*Index Terms*— **Adiabatic transformation, alignment tolerant structures, coupling efficiency, mode expanders, optical waveguide couplers, optoelectronic devices, semiconductor quantum-well lasers.**

## I. Introduction

HIGH-PERFORMANCE optoelectronic systems using optical fiber signal routing require low-cost and low-loss coupling between single-mode fibers (SMF's) and active or passive semiconductor waveguide devices and circuits. However, the 1–3-$\mu$m elliptical modal spot of typical semiconductor waveguides is poorly matched to the 8–9-$\mu$m circular modal spot of conventional single-mode optical fibers. This modal mismatch results in a 7–10-dB insertion loss when directly coupling light between these single-mode fibers and semiconductor waveguides. Nonintegrated solutions that improve this coupling efficiency often do so at the cost of tight alignment requirements and are thus not well suited for low-cost package using passive alignment systems [1]. Tapered waveguide transitions [2]–[10] offer a monolithically integrated means by which efficient coupling can be achieved with relaxed alignment requirements. Most of these approaches, however, require complex growth or processing steps such as multiple etch-regrowth sequences or lithographic patterning of extremely small radius waveguide tips in order to achieve the desired coupler performance. Because of these limitations, a new class of tapered mode expander [11]–[13] has been developed requiring only a single epitaxial growth and etch. Two of these [11], [12] have demonstrated less than 1 dB coupling loss to SMF.

We describe here the tapered rib adiabatic following fiber coupler [11], [12] (TRAFFiC) and its application to both passive optical modulators at 1.3-$\mu$m wavelength and active diode lasers at 0.98-$\mu$m wavelength. All of the TRAFFiC structures achieve less than 1-dB coupling loss to SMF at the design wavelength and may be fabricated with a single epitaxial growth step followed by conventional lithography and etch steps. One of the TRAFFiC devices has even been designed using 1-$\mu$m minimum feature sizes and fabricated using contact-print optical lithography. This is the first reported use of standard contact-print photolithography in the successful fabrication of a laterally tapered adiabatic mode expander.

The paper is structured as follows: First the theoretical basis of the TRAFFiC device is explained using a doped pin-diode waveguide as an example. Spot-size transformation efficiency is calculated at different tapered rib waveguide etch depths and for etched ribs with rounded bases. Excess loss and fiber coupling performance data is then presented for TRAFFiC devices fabricated using the example design. Then, using the pin-waveguide as a starting point, a 980 nm wavelength InGaAs–AlGaAs diode laser design is presented and performance data of fabricated TRAFFiC lasers is shown. Finally, a TRAFFiC waveguide design suitable for unintentionally doped Schottky diode waveguide modulators is presented and mode-expansion performance data given.

Manuscript received August 9, 1997; revised October 6, 1997. This work was supported by the United States Department of Energy under Contract DE-AC04-94AL85000.

The authors are with Sandia National Laboratories Albuquerque, NM 87185-0603 USA.

Publisher Item Identifier S 1077-260X(97)09221-6.

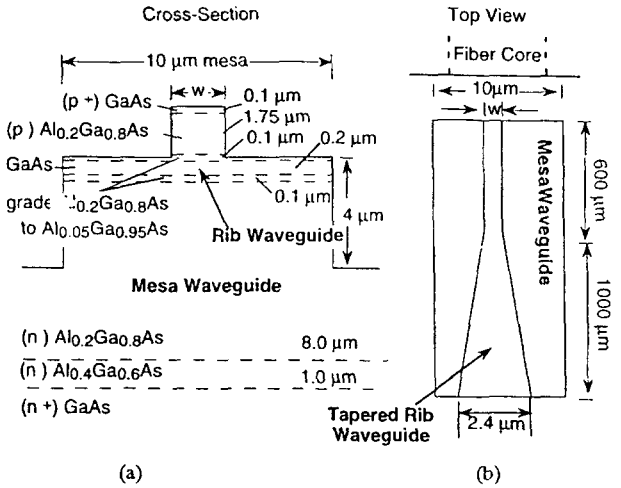


Fig. 1. (a) Cross-section diagram of TRAFFiC device for high-efficiency pin modulator application at 1.32-$\mu$m wavelength and (b) top view of waveguide taper configuration showing orientation of taper to single-mode optical fiber.

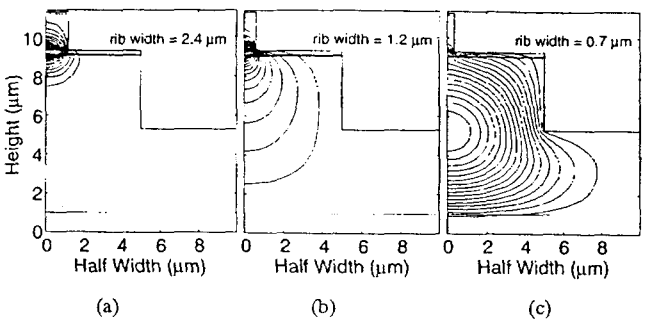


Fig. 2. Contour plots of constant field of eigenmodes at three different TRAFFiC taper widths: (a) wide rib with small spot size; (b) intermediate rib with spot size in transition; and (c) narrow rib with large spot size.

## II. Theory and Design of Coupler for a PIN Waveguide Modulator

One particular design of a TRAFFiC device, intended for use with a pin junction optical phase modulator at 1.3-$\mu$m wavelength, is shown in Fig. 1. In this figure, a small rib waveguide is located on top of a thick lower cladding which is partially etched to form a mesa structure. When the small rib is sufficiently wide the fundamental optical mode is confined to the small rib [Fig. 2(a)] and the device functions as an efficient modulator with high confinement of light within the undoped GaAs layer. At the other extreme, when the small rib is sufficiently narrow, the fundamental mode expands to fill the larger mesa waveguide [Fig. 2(c)]. This behavior is a consequence of the design of the waveguide layers. The thickness and composition of the GaAs and graded AlGaAs layers at the top of the mesa and extending under the small rib are such as to prevent guiding of light [14] within these layers if the upper layers comprising the small rib are etched away. The resulting waveguide allows separate optimization of the optical mode properties of the rib and mesa waveguides at the two extremes of rib width. At large rib widths high-performance modulator function can be achieved while at small rib widths the dimensions of the large mesa and thickness of the lower cladding materials establish the optical mode size of the mesa waveguide for optimum coupling to SMF. The expanded mode [Fig. 2(c)] has been designed for optimum coupling directly to single-mode 1.3-$\mu$m telecommunication fiber. Modal overlap integral calculations predict greater than 90% power coupling between the expanded mode and an 8-$\mu$m-mode diameter optical fiber.

Numerical modeling is required to ensure that the mode expansion occurs with a minimum of excess loss. Selection of the most appropriate modeling tool requires consideration of the actual fabrication method and its influence on the final waveguide topology. The TRAFFiC structure is fabricated using electron-beam direct write or optical contact print lithography followed by highly anisotropic reactive-ion-beam etching (RIBE) [15]. These techniques result in a waveguide taper comprising abruptly joined straight segments whose widths progressively decrease in precise (e.g., 0.025 $\mu$m) steps. An example of a stepped taper is shown in Fig. 3. The modal evolution of such a waveguide made up of longitudinally invariant segments is well described using a two-dimensional (2-D) finite-element model to find the fundamental mode at each segment along the taper provided that the taper slope is sufficiently gradual. The radiation loss of the taper can then be calculated using modal overlap integrals to estimate the coupling efficiency across each step and then multiplying all of the individual step-coupling efficiencies to determine the overall power-conversion efficiency. For low-loss waveguides, this radiation loss is the excess taper loss. Such an approach is computationally faster than three-dimensional (3-D) beam-propagation method and provides accurate eigenmode solutions at each rib width. All 2-D modal calculations employ a variable mesh size between 20–200 nm with finer meshing used at refractive-index discontinuities.

Fig. 4 shows the individual step coupling efficiency through the taper in Fig. 1 as a function of segment width. Steps are 0.025 $\mu$m and alternate between the left and right sides of the taper. For large rib halfwidths, the mode is confined to the small rib as seen in Fig. 2(a) where the halfwidth is 1.2 $\mu$m. As the rib sections narrow, the segment-to-segment coupling is high and varies only slightly with width until the halfwidth reaches roughly 0.7 $\mu$m. The flat coupling efficiency for large halfwidths results from the mode shape changing only slightly in this section of the taper. Below 0.7 $\mu$m halfwidth the mode begins to change shape more rapidly and gradually shift power down into the lower mesa below the rib. Fig. 2(b) shows one of these transitional modes. The changing mode shape and peak intensity location results in a dip of the segment-to-segment coupling between 0.7 and 0.3-$\mu$m halfwidth. Below 0.3 $\mu$m halfwidth the mode is largely confined in the mesa waveguide [Fig. 2(c)] such that further reduction of the small rib width has little influence on the optical mode. Completion of the mode expansion into the large mesa waveguide occurs at significantly large rib widths which can readily be resolved using conventional optical contact lithography. In the present example mode expansion is complete when the rib halfwidth is 0.3 $\mu$m. In fact, the rib may be abruptly terminated at any full width below 0.7 $\mu$m without significant penalty. Overall taper radiation loss is the product of all the individual segment-to-segment coupling efficiencies. In the present example this

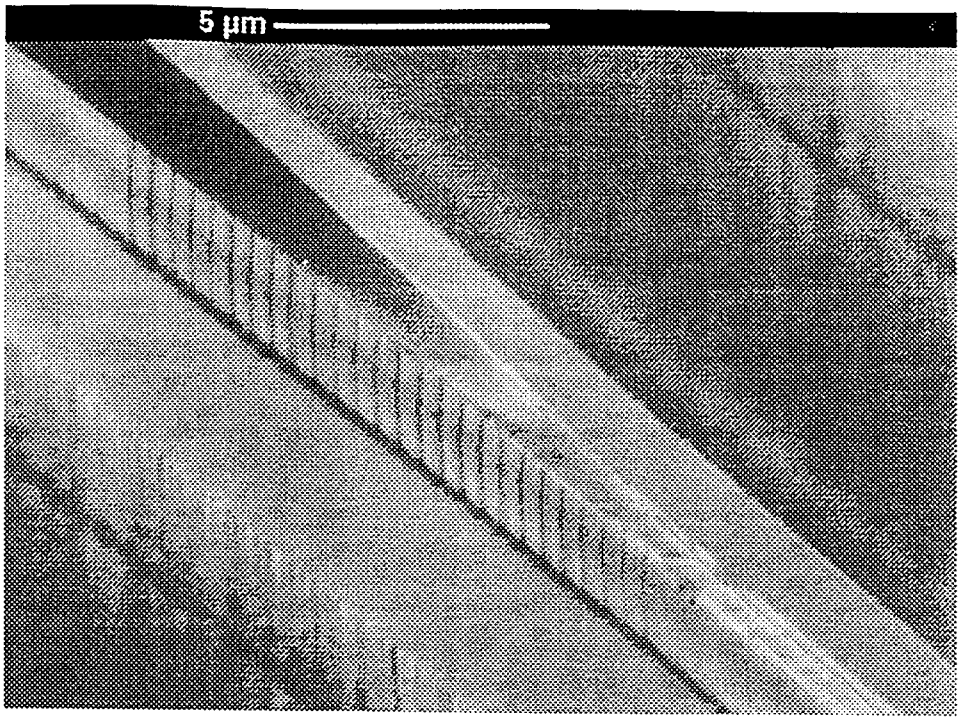


Fig. 3. SEM image of tapered rib waveguide showing discrete 0.025-$\mu$m steps in rib width. This particular rib was made very short in order to obtain this image.

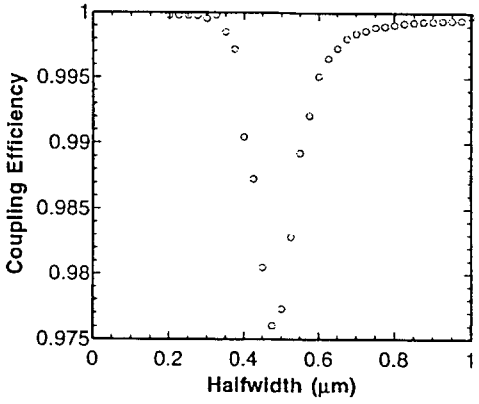


Fig. 4. Individual step coupling efficiency through the taper in Fig. 1 as a function of segment width.

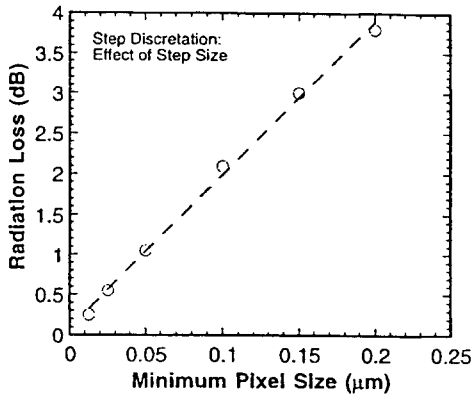


Fig. 5. TRAFFiC radiation loss versus minimum pixel (or step) size used to pattern the tapered rib waveguide.

is 85.7% (equivalent to 0.67 dB radiation loss). A 3-D beam propagation calculation was used to benchmark the successive modal overlap model and to aid in selecting a taper length for good mode conversion. Results of this calculation are in good agreement with the successive modal overlap model and suggest that tapers with >500-$\mu$m length have the desired <1-dB theoretical radiation loss.

The two key physical parameters influencing the power conversion efficiency are the step size used in patterning the taper and the etch depth of the rib. Additional modeling has shown that the excess loss of the taper expressed in decibels is essentially linearly proportional to the step size used in creating the taper (Fig. 5). It is this dependence of radiation loss on sidewall step size that has prompted the use of electron-beam direct write in the initial demonstration of the TRAFFiC wave guide. Although the minimum dimensions of the taper are within the capabilities of conventional contact lithography, the step size of 0.025 $\mu$m required for less than 1-dB excess loss is not available from commercial mask vendors without the use of a reducing reticle. Fabrication of a different TRAFFiC design using conventional contact printing with a specially made photolithographic plate is described later in this article.

Variation of excess loss with etch depth of the small rib is shown in Fig. 6. Power conversion efficiency drops linearly with etch depth from the best value of approximately 86% down to only 60% for etching 0.4 $\mu$m deeper than shown on Fig. 1. Careful examination of the individual step coupling efficiencies of tapers with different etch depths (Fig. 7) provides some insight into the function of the TRAFFiC wave guide. As is clearly evident in Fig. 7, as the etch depth is increased the transition point where the greatest variation in the mode shape occurs moves to larger rib sizes. Movement of the transition point to larger rib sizes for deeper etches is a result of

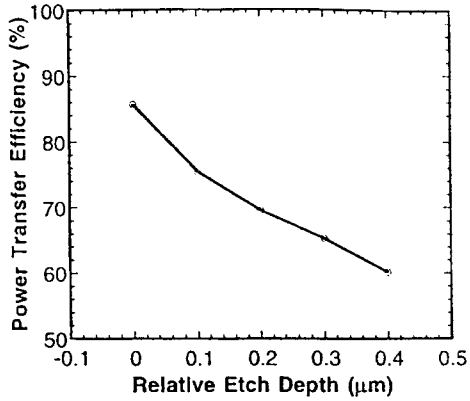


Fig. 6. Power transfer efficiency of spot-size transformation as a function of rib waveguide etch depth. Depths are relative to the rib depth shown in Fig. 1.

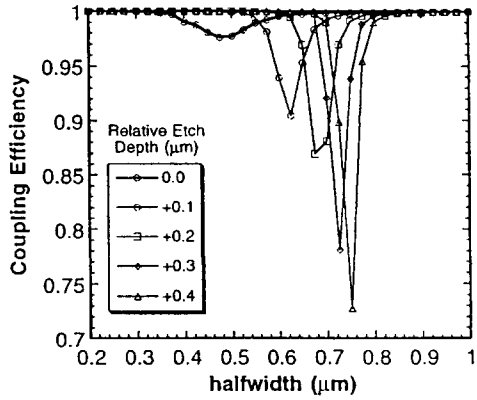


Fig. 7. Individual step coupling efficiencies through the taper in Fig. 1 as a function of segment width for a variety of different rib waveguide etch depths. Depths are relative to the rib depth shown in Fig. 1.

the reduced modal effective index of the more deeply etched ribs approaching the effective modal index of the eventual mesa mode more quickly as the rib narrows along the length of the taper. In addition the mode evolution tends to "snap" more quickly from confinement in the rib to confinement in the mesa. In other words, the bulk of the mode transition occurs in just a few segments of the TRAFFiC waveguide and these few transitions have reduced coupling efficiency. Etching 0.1 $\mu$m less deeply than shown in Fig. 1 (a relative etch depth of $-0.1$ $\mu$m in Figs. 6 and 7) results in confinement of the expanded optical mode by the layers at the top of the mesa and no vertical mode expansion. Calculated power coupling efficiency of the expanded-mode waveguide output into an 8-$\mu$m spot-size ($1/e^2$ intensity diameter) single-mode optical fiber remains between 91.7%–93.7% for all the waveguides plotted in Fig. 6.

Clearly, control of the etch depth to within 0.05 $\mu$m is required for fabrication of high-quality TRAFFiC spot-size transformers. *In situ* reflectometry monitoring of etch depth is used [15] to achieve the needed etch-depth control and reproducible mode-expansion efficiency. As a further aid in fabrication of TRAFFiC waveguides, the use of linear tapers with width variation in excess of the minimum required for spot-size transformation provides substantial tolerance to rib width, etch depth variations, and inaccuracies in epitaxial layer

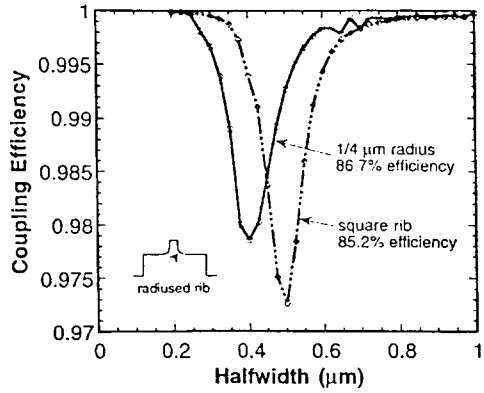


Fig. 8. Individual step coupling efficiencies through the taper in Fig.(1) as a function of segment width for square and rounded rib-to-mesa interface transitions. The rounded transition (inset) has a 0.25-$\mu$m radius curvature. The small oscillation in the calculation near 0.7-$\mu$m halfwidth is due to numerical instability.

composition and thickness. Nonlinear tapers, with a rapid width variation in regions where the mode shape is relatively insensitive to rib width and much slower variation in the critical width region where the bulk of the mode transformation occurs, offer much shorter overall coupler lengths (and lower absorption losses) but also have significantly reduced processing tolerances for fabrication of low-loss couplers.

A common result of semiconductor rib waveguide etching is a rounded transition between the vertical rib sidewall and the horizontal mesa surface. Ribs with such a fillet behave within a TRAFFiC device as though the rib were square but slightly larger than the desired width. Fig. 8 shows plots of the individual step coupling efficiency through the taper both with and without an actual 0.25-$\mu$m radius fillet at the bottom of the etched rib for the same etch depth used in Fig. 4. Addition of the radius to the rib reduces the halfwidth of the rib where spot-size transformation occurs by $\sim$0.1 $\mu$m and slightly improves the power conversion efficiency. The 1.5% improvement in efficiency is a direct result of the more gradual transition between the rib sidewall and mesa top.

## III. Demonstration of Coupler for High-Efficiency PIN Modulators

The TRAFFiC structure discussed above is intended for use with high figure-of-merit pin phase modulators or Mach–Zehnder interferometers at 1.3-$\mu$m wavelength [14], [16]. Demonstration of coupler operation was done using discrete straight rib waveguides [Fig. 2(a)] and mesa waveguides [Fig. 2(c)] along with tapered rib waveguide structures on mesa waveguides [Figs. 2(a)–(c) and 1(b)]. These were fabricated using (Al)GaAs waveguides identical to Fig. 1(a). The linearly tapered waveguides used $w$ = 0.7 $\mu$m final narrow width. Epitaxial layers were grown by molecular-beam epitaxy. The upper and lower cladding layers were doped p- and n-type, respectively, so that the 2.4-$\mu$m-wide rib waveguides are compatible with reverse-biased pin-junction phase modulators. Waveguide rib structures were patterned using electron-beam direct-write lithography with negative-acting electron-beam resist and a 25 nm exposed

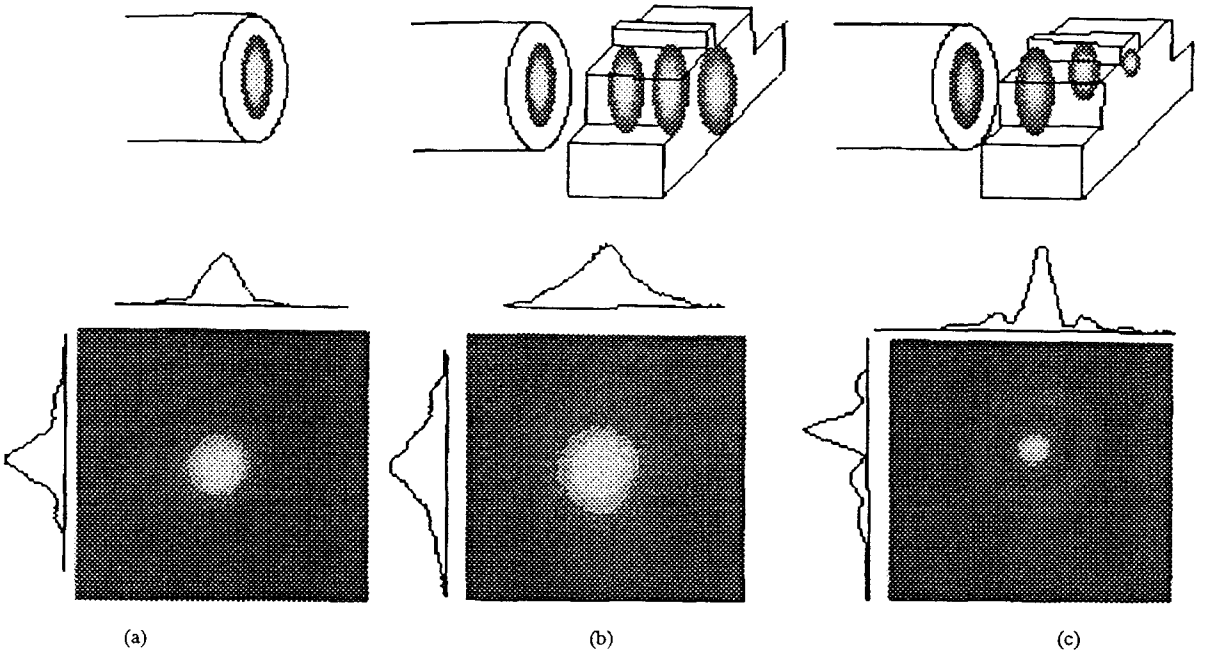


Fig. 9. Experimental results showing near-field images of the: (a) light exiting the optical fiber, (b) light coupled from a fiber and traveling though a mesa waveguide without a taper, and (c) light coupled from a fiber to a mesa waveguide then traveling through a tapered-rib adiabatic-following Fiber Coupler and exiting from a rib wave guide. (c) Demonstrates the desired spot size transformation. Each of the three images is accompanied with a schematic representation of the configuration used to obtain the image.

pixel spacing. Spacing between the 25 nm rib-width steps was approximately 15 $\mu$m for a 1-mm taper length. The mesa waveguide was patterned using conventional optical contact-print lithography. Etching of both the rib waveguide and mesa used chlorine reactive-ion-beam etching [15]. Although these devices were patterned with direct-write techniques, the 0.7-$\mu$m minimum width of the waveguide taper could be defined using optical methods.

To evaluate mode spot-size transformation, a mesa waveguide and a tapered-rib mode converter were alternately excited using a single-mode fiber (3M, FS-HB-6621, design wavelength = 1.3 $\mu$m and modal field diameter = 7.1 $\pm$ 0.2 $\mu$m) emitting light at 1.31-$\mu$m wavelength. Near field images for the fiber, the mesa, and the tapered rib waveguide are shown in Fig. 9(a)–(c), respectively. Notice that the mesa guide and fiber are well matched and that the tapered rib output is very different. Unfortunately, the limitations of the imaging optics result in the much smaller rib mode appearing relatively larger than its size compared to the mesa and fiber modes. Power measurements demonstrate total mesa to rib waveguide coupling losses (excess loss) of ~1.5–2.0 dB and fiber to mesa coupling losses of ~0.5–1.0 dB. The larger than expected total mesa to rib waveguide coupling losses are understood by the unusually large straight waveguide propagation losses of 9.2 $\pm$ 0.8 dB/cm exhibited by both the straight rib and mesa waveguides on this sample.

## IV. Design and Demonstration of 980 nm Laser with Expanded Mode Output

An InAlGaAs diode laser with a TRAFFiC output was demonstrated at 980-nm wavelength. Such expanded-mode semiconductor lasers [12], [13] are of great interest due to the benefits of reduced far-field divergence and improved coupling efficiency to single-mode optical fiber. The TRAFFiC laser description (Fig. 10) follows closely that of the previous discussion and comprises a uniform 2-$\mu$m-wide AlGaAs–InGaAs heterostructure gain section and TRAFFiC waveguide mode converter tapered down to a 0.7-$\mu$m final width. Using a procedure identical to that described above for the 1.3-$\mu$m wavelength pin wave guide, overall power-conversion efficiency of the mode expansion is estimated to be 90%. The expanded mode supported by the mesa guide has a simulated coupling efficiency to single-mode fiber of greater than 95%.

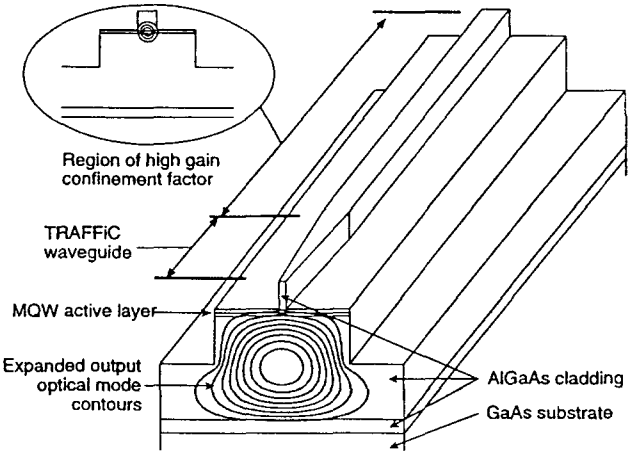


Fig. 10. Representation of the TRAFFiC laser showing the tapered-rib upper cladding shape and the approximate form and size of the optical mode in the active gain section in the wide rib region (inset) and the expanded size and shape of the output optical mode at the cleaved end where the rib is most narrow.

The laser is a strained-quantum-well separate-confinement heterostructure type described in Table I. A 2-$\mu$m-wide rib

TABLE I
EPITAXIAL STRUCTURE OF TRAFFIC LASER FOR 980-nm OPERATION

| Material | Thickness (nm) | Doping ($cm^{-3}$) | Description |
|---|---|---|---|
| GaAs | 100 | p = 8e19 | Cap Layer |
| $Al_{0.1}Ga_{0.9}As$ | 500 | p = 2e18 | Upper Cladding |
| $Al_{0.1}Ga_{0.9}As$ | 1500 | p = 5e17 | Upper Cladding |
| grade from $Al_{0.05}Ga_{0.95}As$ | 90 | uid | Graded Interface |
| GaAs | 60 | uid | Active Waveguide |
| $In_{0.2}Ga_{0.8}As$ | 8 | uid | Quantum Well |
| GaAs | 15 | uid | Barrier |
| $In_{0.2}Ga_{0.8}As$ | 8 | uid | Quantum Well |
| GaAs | 60 | uid | Active Waveguide |
| grade to $Al_{0.05}Ga_{0.95}As$ | 100 | uid | Graded Interface |
| $Al_{0.1}Ga_{0.9}As$ | 2000 | n = 5e17 | Mesa Waveguide |
| $Al_{0.1}Ga_{0.9}As$ | 5000 | n = 1e18 | Mesa Waveguide |
| $Al_{0.1}Ga_{0.9}As$ | 1000 | n = 2e18 | Mesa Waveguide |
| $Al_{0.4}Ga_{0.6}As$ | 1000 | n = 3e18 | Waveguide Barrier |
| GaAs | substrate | n+ | |

Resonant periodic marker layers [15] used for *in situ* monitoring of the etches, but having virtually no impact on device performance have been omitted for clarity.

waveguide is etched in the cladding region above the quantum wells to define the active lasing section in a region of high vertical confinement factor. A TRAFFiC output coupler section is inserted between the active waveguide and one of the cleaved facets by tapering the rib waveguide width from 2 to 0.7 $\mu$m over a length of 1.0 mm. A second 10 $\mu$m-wide outer mesa provides lateral confinement of the expanded optical mode propagating within the thick lower cladding. The low 10% Al content of the cladding material prevents formation of modes guided by the remaining GaAs material at the top of the mesa and subsequent failure of the mode expansion. Overall length of the lasers is 1.5 mm, of which 1 mm is contacted for electrical current injection. The TRAFFiC section is electrically injected only in the first half of the coupler where significant overlap of the optical mode and InGaAs quantum wells exists.

Lasers were fabricated in MOCVD-grown material using two lithography-and-etch steps. The tapered rib waveguide was defined using electron-beam direct-write lithography. The wide mesa was patterned using optical contact printing. Both were etched using nonselective $Cl_2$ dry etching. After etching, the surface was coated with plasma deposited $SiO_2$, a window opened on top of the rib for p-side ohmic metallization and BeAu ohmic contacts formed. The backside of the wafer was coated with AuGeNiAu ohmic contact metallization prior to rapid-thermal annealing at 360 °C. Fig. 11 shows an SEM image of a completed TRAFFiC laser. As experimental control devices, uniform 2-$\mu$m-wide lasers were also fabricated on the same wafer as the TRAFFiC lasers. Final lasers were tested as-cleaved without facet coatings or heat sink. Injection current was pulsed using 2-$\mu$s pulses at a 1-kHz repetition rate. Fig. 12 shows the light output characteristic of a TRAFFiC laser and a 2-$\mu$m-wide × 1.25-mm-long control device. Although slope efficiencies are comparable, threshold current of the TRAFFiC laser is 110 mA compared to 81 mA for the control. In addition, a kink is seen at approximately 150-mA injection current in the TRAFFiC laser output which is not seen in the control device output. This behavior may be due to nonideal current injection in the taper section. Only a portion of the taper is contacted for current injection as shown in Fig. 11. Current injection into the taper stops at a point approximately midway along the length where the width of the rib becomes

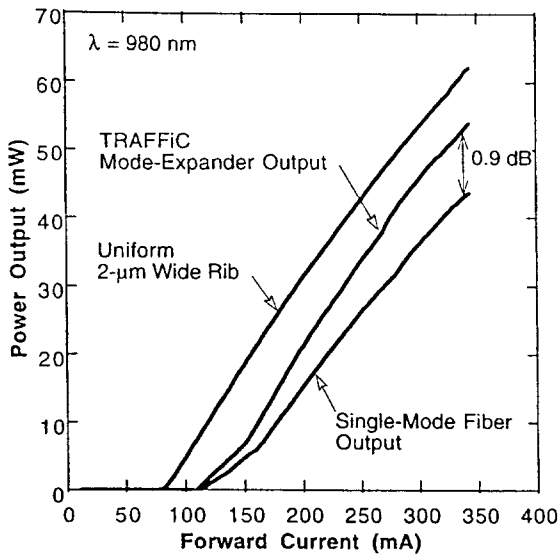


Fig. 12. Threshold characteristics of TRAFFiC and 2-$\mu$m wide control lasers. Data is for 2-$\mu$s pulses at 1-kHz repetition rate.

too small to open a contact window in the dielectric cap using conventional contact lithography. As a result light confined in the quantum wells below the uncontacted taper region will experience higher absorption. This higher absorption increases the lasing threshold current and reduces efficiency. However, as the current injection increases the quantum-well refractive index will decrease in the contacted regions of the rib causing the mode to move into the mesa at relatively larger rib widths. Therefore, at higher injection levels the overall absorption loss of the taper will decrease resulting in an increase in laser efficiency. The kink at ~150 mA injection current is consistent with increased laser efficiency resulting from reduced taper losses. More uniform current injection using optimized layer doping, taper length, processing and electrical contacting are expected to give reduced lasing threshold compared to these demonstration devices.

Coupling efficiency of the TRAFFiC output to optical fiber was measured using a 1-m length of Spectran SMB-E1310B fiber (this fiber is single mode above 1.25-$\mu$m wavelength and has an NA = 0.17 at $\lambda$ = 1.3 $\mu$m) butt-coupled to the laser facet. The fiber ends were as-cleaved without polishing or lensing of any kind and the bulk of the fiber length was wrapped around a 9-cm-diameter spool. TRAFFiC laser output including transmission into and through the length of single-mode fiber is shown as the lower curve in Fig. 12. Measured coupling loss from the laser into the fiber is only 0.9 dB.

The far-field optical emission pattern was measured using a 25-mm-long Si CCD array placed 38 mm from the facet. Fig. 13 shows the far-field intensity pattern of two representative TRAFFiC lasers both perpendicular and parallel to the plane of the epitaxial layers. The far-field patterns are quite stable over a wide range of injection current. The solid line of Fig. 13 is the one-dimensional (1-D) far-field calculation [16], [17] based on two-dimensional (2-D) numerical simulations of the TRAFFiC output. Excellent correlation between the observed and theoretical patterns is observed. The 5.6° and 7.4° full-width at half-maximum (FWHM) far fields in the

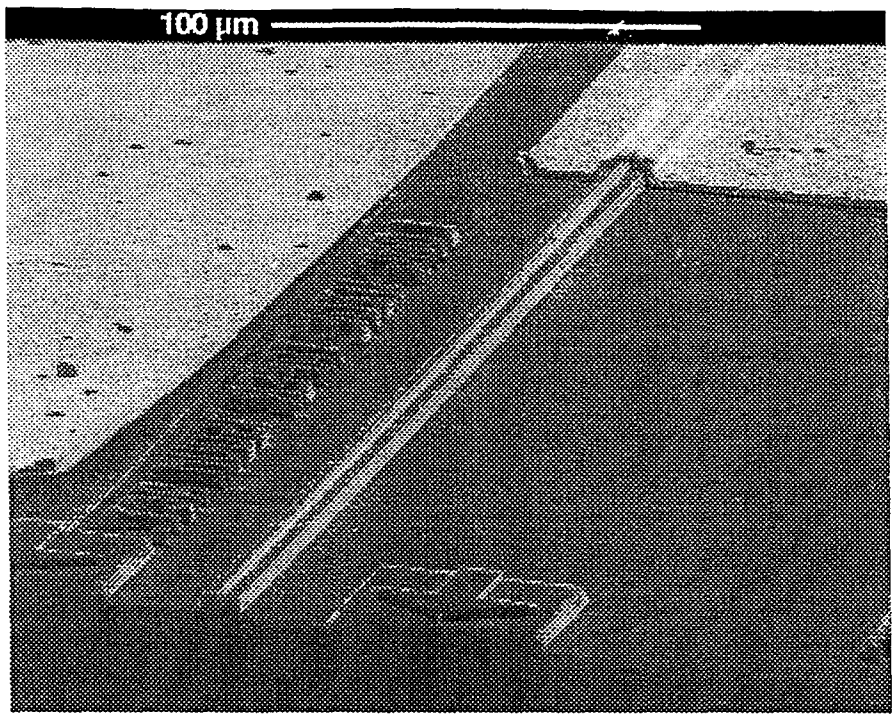


Fig. 11. SEM image of TRAFFiC laser mode-expansion section. Metallization on gain section is seen at the top of the image. Passive rib and mesa comprising the TRAFFiC 2-D mode-expander are seen extending between the metal and the cleaved output facet.

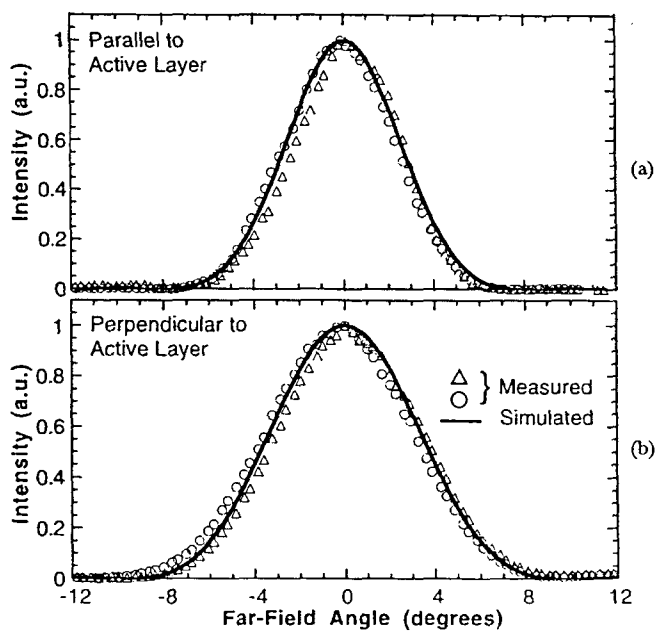


Fig. 13. Far-field emission patterns of TRAFFiC laser output along axes (a) parallel and (b) perpendicular to the epitaxial layers. Symbols are measured data from two different lasers. Solid line is simulation result.

perpendicular and parallel axes respectively are significantly smaller and more symmetric than the ~35° and ~9° FWHM values commonly seen in conventional double-heterostructure AlGaAs lasers.

Near-field image measurements of both a TRAFFiC laser and a 2-$\mu$m-wide control laser are shown in Fig. 14. The TRAFFiC laser is clearly seen to have a much larger fundamental optical mode as compared to the control device. As seen schematically in Fig. 10 and in the measured profile of Fig. 14(b), the output mode is intended to be roughly as tall as it is wide with a characteristic inverted mushroom shape. Back facet emission image of the TRAFFiC laser is indistinguishable from that of the control laser, Fig. 14(a). No evidence of high-order modes is seen at any tested current level.

## V. Design and Demonstration of Coupler for Low-Loss UID Modulators Using Contact Lithography

Unintentionally doped (UID) AlGaAs ridge waveguides for Schottky-barrier Mach–Zehnder interferometers [18], [19] operating at 1.32-$\mu$m wavelength represent a third class of waveguide design for which TRAFFiC sections have recently been used demonstrated to improve fiber coupling performance. In these devices, the waveguide core is often relatively thicker and the core-to-cladding index steps smaller than that used for the pin modulator and diode laser. This results in a slightly larger waveguide with different design and performance details for integrated TRAFFiC waveguides. However, the principle of operation is the same as that of the pin modulator and laser diode. Table II gives the complete epitaxial layer design for a UID waveguide modulator with a TRAFFiC waveguide mode converter. This UID modulator design uses an $n^+$ contact layer between the rib and the mesa for improved electrooptic efficiency. The calculated unexpanded and expanded fundamental modes for the wide and narrow rib are shown in Fig. 15(a) and (b), respectively. Fig. 16 shows the individual step coupling efficiencies through the taper for various etch depths relative to the rib shown in Fig. 15. Transition of the mode between the small rib and large mesa waveguide occurs at larger rib widths compared to the pin modulator and laser diode. In all cases the narrow

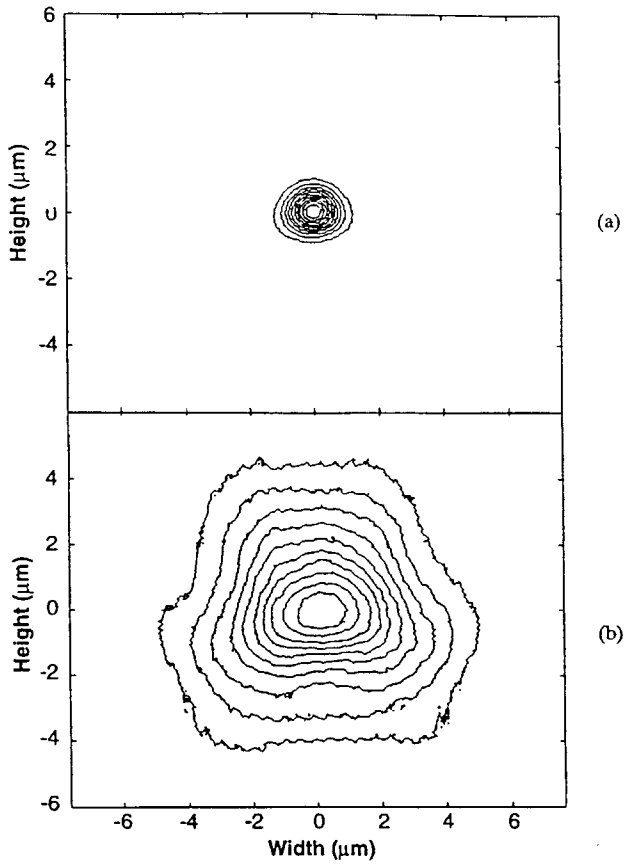


Fig. 14. Linearly spaced contour plots of measured near-field emission intensity pattern of (a) 2-$\mu$m-wide control laser and (b) expanded-mode TRAFFiC laser.

TABLE II
EPITAXIAL STRUCTURE OF UID MODULATOR WAVEGUIDE WITH INTEGRATED TRAFFiC MODE EXPANDER

| Material | Thickness (nm) | Doping ($cm^3$) | Description |
|---|---|---|---|
| $Al_{0.1}Ga_{0.9}As$ | 1250 | uid | Upper Cladding |
| GaAs | 1250 | uid | Waveguide |
| $Al_{0.002}Ga_{0.8}As$ | 50 | uid | Waveguide |
| grade 1.2% to 0.2% AlAs | 250 | uid | Waveguide |
| grade 3.8% to 1.2% AlAs | 600 | n = 1e17 | Waveguide |
| $Al_{0.038}Ga_{0.962}As$ | 50 | n = 1e17 | Waveguide |
| $Al_{0.03}Ga_{0.97}As$ | 500 | n = 1e18 | Contact Layer |
| $Al_{0.04}Ga_{0.96}As$ | 8000 | uid | Mesa Guide |
| $Al_{0.1}Ga_{0.9}As$ | 1000 | uid | Lower Cladding |
| GaAs | substrate | uid | Substrate |

AlGaAs graded layers show only AlAs content. Remainder is GaAs.

dimension of the taper does not need to be any smaller than 1.4–1.6 $\mu$m for complete mode expansion to occur. Calculation of the power conversion efficiency for mode expansion is shown in Fig. 17 for tapers starting at 3 $\mu$m and reducing to 1 $\mu$m in width. Power transfer efficiency varies from 64–89% as the rib etch depth is varied from the bottom to the top of the graded layers in Table II. Selection of an ideal etch depth must take into account the conflicting requirements of shallow etching for best spot-size transformation and deep etching for high lateral optical confinement and reduced loss of turning mirrors fabricated with the same etch. An etch depth 0.125 $\mu$m deeper than shown in Fig. 15 and corresponding to a relative depth = +0.125 $\mu$m in Figs. 16 and 17 was chosen for its combined high 73% transfer efficiency and good lateral confinement. Calculated power coupling efficiency of

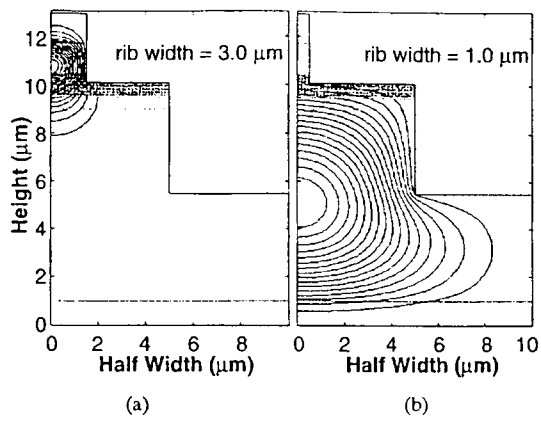


Fig. 15. Contour plots of constant field of eigenmodes at both ends of the UID TRAFFiC device. (a) Wide rib with small spot size. (b) Narrow rib with large spot size.

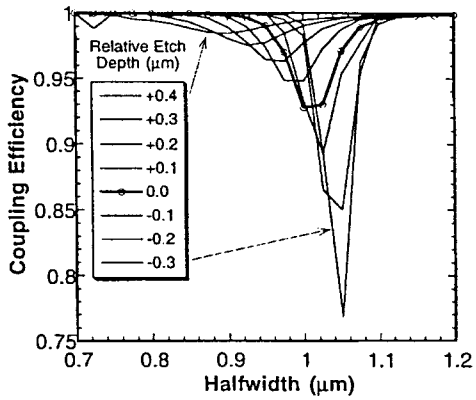


Fig. 16. Individual step coupling efficiencies through the UID taper as a function of segment width for a variety of different rib waveguide etch depths. Depths are relative to the rib depth shown in Fig. 15.

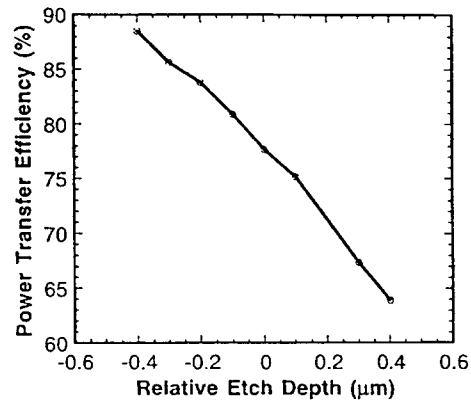


Fig. 17. Power transfer efficiency of spot-size transformation as a function of rib waveguide etch depth for the UID TRAFFiC device. Depths are relative to the rib depth shown in Fig. 15.

the expanded-mode waveguide output into an 8-$\mu$m spot size ($1/e^2$ intensity diameter) single-mode optical fiber remains between 93.7%–94.5% for all the waveguides plotted in Fig. 17.

The 1-$\mu$m final taper width makes this TRAFFiC structure particularly well suited for fabrication by optical contact printing. As discussed above, the step size between straight

segments of the taper is very important in determining the overall power conversion efficiency. Our model predicts that 0.1-$\mu$m steps will yield a significantly lower power transfer efficiency compared to the 0.025-$\mu$m steps used in the calculation for Figs. 16 and 17. For patterning of the UID modulator TRAFFiC waveguide a contact-print mask plate was fabricated in our laboratory using electron-beam direct write lithography with 0.025-$\mu$m pixel spacing (step size). This contact-print lithography mask was used in a conventional contact print exposure system for photolithographic pattern definition of the desired TRAFFiC waveguide taper shape. As before, RIBE was used to etch the rib and mesa waveguides to the desired depth.

The UID TRAFFiC waveguide mode quality and beam expansion were measured at 1.32-$\mu$m wavelength. Fig. 18 shows infrared video camera near field images of both a 3.5-$\mu$m-wide rib waveguide with a small mode spot size [Fig. 18(a)] and a 1.0-$\mu$m-wide rib waveguide on a 10-$\mu$m-wide mesa with a large mode spot size [Fig. 18(b)]. Very good mode expansion and filling of the mesa waveguide is observed when the rib width is reduced to 1.0 $\mu$m. Far-field measurements of the expanded mode (radiation pattern of the mode seen in Fig. 18(b) using a 10-mm-wide 2-D optical beam profiler placed 11.5 mm away from the exit facet confirm the correct behavior of the TRAFFiC waveguide mode expansion. Fig. 19(a) and (b) shows the measured and calculated far-field profiles of on an 8-$\mu$m-wide mesa waveguide with a 1.0-$\mu$m-wide rib along axes parallel and perpendicular to the epitaxial layers. The calculated far-field patterns were obtained using the same method as for the TRAFFiC laser described above. General good agreement between the measured and calculated far-field patterns is seen although the measured pattern parallel to the layers does show some broadening compared to the calculation. The 8.9° and 9.7° FWHM far fields in the perpendicular and parallel axes, respectively, are close to the respective calculated values of 9.1° and 7.7°. Calculations of the far-field radiation pattern of the unexpanded mode [Fig 18(a)] predict 20° and 29° FWHM along the perpendicular and parallel axes, respectively. The combined small far-field radiation pattern and large near-field modal spot size where both are in good agreement with theoretical prediction confirm that the UID TRAFFiC waveguide is operating as expected.

In order to get an accurate measure of excess loss within the TRAFFiC waveguide, several tapers were fabricated end-to-end so that the optical mode was repeatedly compressed and expanded. These multiple taper waveguides were compared to straight rib and mesa waveguides fabricated on the same wafer. Losses were measured at 1.32-$\mu$m wavelength using the Fabry–Perot interference method, tuning the cavity length by adjusting the temperature of the waveguide. Straight rib waveguide loss was 1.02 $\pm$ 0.17 dB/cm while mesa waveguide losses were 0.77 $\pm$ 0.13 dB/cm. Using these straight waveguide losses, the deduced TRAFFiC waveguide excess loss was 1.84 $\pm$ 0.50 dB. This loss corresponds to between 58.3%–73.4% power transfer efficiency through the mode expander. The upper limit of 73.4% measured power transfer efficiency is consistent with the calculated 73% efficiency including only the effect of radiation at the steps in the rib width.

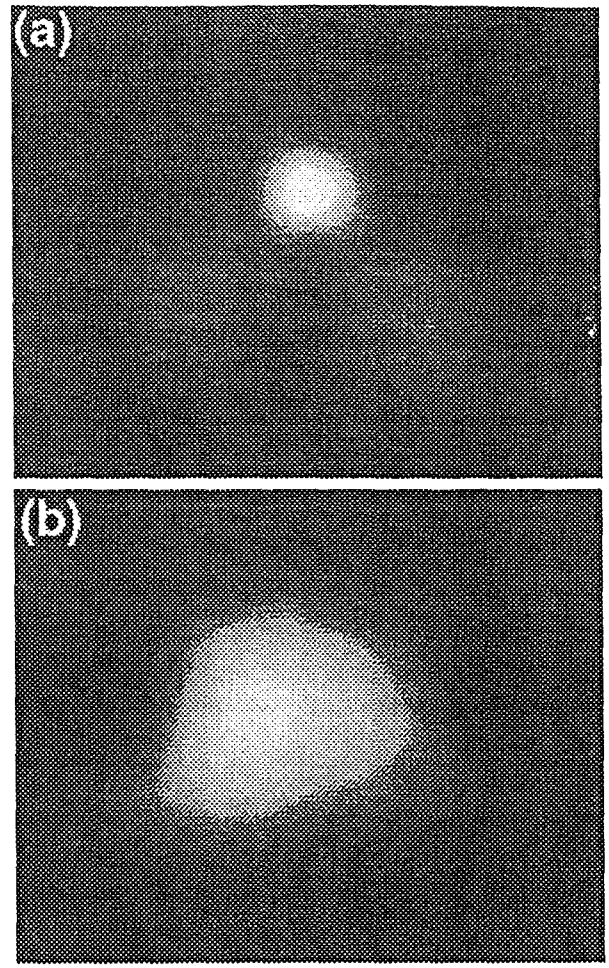


Fig. 18. Near-field images of the UID TRAFFiC waveguide input and output optical modes taken using an infrared video camera: (a) the small input optical mode with a rib width of 3.5 $\mu$m and (b) the large output optical mode with a 1-$\mu$m rib and 10-$\mu$m mesa waveguide. The images show effects of video saturation but are representative of the observed mode size and quality.

## VI. Summary

In summary, we have designed and demonstrated a monolithic tapered rib waveguide for spot-size transformation. The TRAFFiC device achieves 2-D expansion of the output optical mode of single-transverse-mode semiconductor waveguide modulators and lasers using a 1-D taper between noncritical initial and final taper widths which are compatible with optical lithographic techniques. Design details for (Al,Ga)As TRAFFiC waveguides have been given and effects of taper width, step size, etch depth, and etch profile simulated. Using the TRAFFiC device, total mode expansion losses of ~1.5–2.0 dB and semiconductor to fiber waveguide coupling losses of ~0.5–1.0 dB have been measured for doped pin optical-modulator-type waveguides at 1.32-$\mu$m wavelength. A TRAFFiC mode-expansion section has been integrated with a 980 nm rib-waveguide diode laser and stable fundamental mode operation with a narrow, 5.6° × 7.4° FWHM far-field observed well above lasing threshold. The observed mode size and far-field divergence are consistent with numerical simulation of

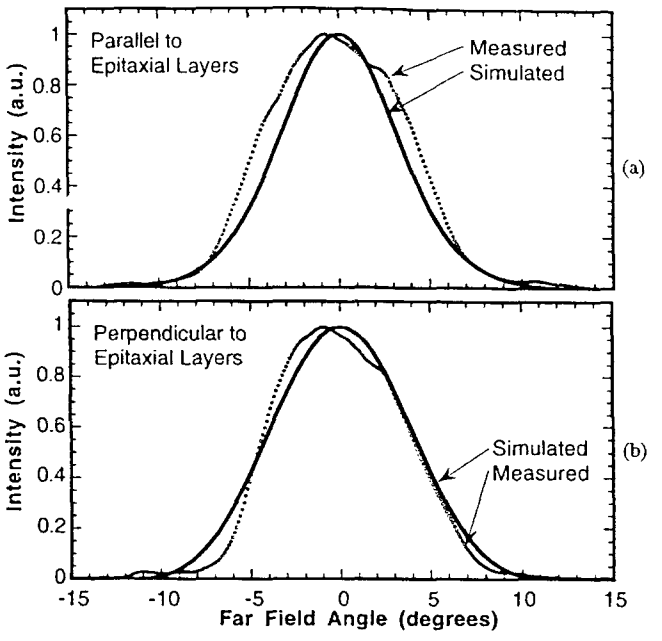


Fig. 19. Far-field emission patterns of UID TRAFFiC waveguide output along axes (a) parallel and (b) perpendicular to the epitaxial layers.

the TRAFFiC laser structure and measured coupling loss from the TRAFFiC laser output to single-mode, long-wavelength telecommunications fiber is only 0.9 dB. Finally, a TRAFFiC device has been design and demonstrated for UID waveguide modulators. For the UID structure total mode expansion losses of 1.84 dB and excellent modal behavior have been measured at 1.32-$\mu$m wavelength. All of these mode-expansion waveguides are fabricated using a single epitaxial growth followed by two lithography-and-etch procedures and use dimensions compatible with conventional photolithographic techniques. The UID waveguide mode-expanded has been demonstrated using standard contact printing lithography.

The TRAFFiC structure is particularly well suited for integration with both active and passive etched rib waveguide devices. Fabrication is relatively simple, requiring only patterning and etch of the tapered waveguide and uniform-width outer mesa waveguide without any epitaxial regrowth.

## ACKNOWLEDGMENT

The authors would like to thank D. Tibbetts-Russell, M. Romero, C. T. Fuller, M. B. Snipes, and R. Hadley for technical assistance. Sandia is a multiprogram laboratory operated by Sandia Corporation, a Lockheed-Martin Company, for the United States Department of Energy.

## REFERENCES

[1] H. F. Lockwood, P. Haugsjaa, C. Armiento, and R. Boudreau, Eds., "Hybrid optoelectronics integration and packaging," in *Optoelectronics Integration: Physics, Technology and Applications*. Norwell, MA: Kluwer Academic, 1994.

[2] T. L. Koch, U. Koren, G. Eisenstein, M. G. Young, M. Oron, C. R. Giles, and B. I. Miller, "Tapered waveguide InGaAs/InGaAsP multiple-quantum-well lasers," *IEEE Photon. Technol. Lett.*, vol. 2, pp. 88–91, 1990.

[3] R. Zengerle, H. J. Bruckner, H. W. Koops, H. J. Olzhausen, G. Zesch, A. Kohl, and A. Menschig, "Fabrication of optical beam width transformers for guided waves on InP using wedge-shaped taper structures," *J. Vac. Sci. Technol. B*, vol. 9, pp. 3359–3463, 1991.

[4] M. Chien, U. Koren, T. L. Koch, B. I. Miller, M. Oron, M. G. Young, and J. L. Demiguel, "Short-cavity distributed Bragg reflector laser with an integrated tapered output waveguide," *IEEE Photon. Technol. Lett.*, vol. 3, pp. 418–420, 1991.

[5] Mueller, B. Stegmueller, H. Westermiere and G. Wenger, "Tapered InP/InGaAsP waveguide structure for efficient fiber-chip coupling," *Electron. Lett*, vol. 27, pp. 1836–1838, 1991.

[6] T. Brenner and H. Melchior, "Integrated optical mode shape adapters in InGaAsP/InP for efficient fiber-to-waveguide coupling," *IEEE Photon. Technol. Lett.*, vol. 5, pp. 1053–1056, 1993.

[7] R. Ben-Michael, U. Koren, B. I. Miller, M. G. Young, M. Chien, and G. Raybon, "InP-based multiple quantum well lasers with an integrated tapered beam expander wave guide," *IEEE Photon.Technol. Lett.*, vol. 6, pp. 1412–1414, 1994.

[8] R. Zengerle, H. J. Bruckner, B. Hubner, and W. Weiershausen, "Low-loss beamwidth transformers on InP with reduced requirements on lithographic resolution," *J. Vac. Sci. Technol. B*, vol. 11, pp. 2641–2644, 1993.

[9] H. J. Bruckner, B. Mersali, S. Saison, M. Feuillade, A. Ougazzaden, P. Krauz, and A. Cernco, "Tapered waveguide integration for polarization insensitive InP/InGaAsP based optical amplifiers," *Electron. Lett.*, vol. 30, pp. 1290–1291, 1994.

[10] Y. Shani, C. H. Henry, R. C. Kistler, K. J. Orlowsky, and D. A. Ackerman, "Efficient coupling of a semiconductor laser to an optical fiber by means of a tapered waveguide on silicon," *Appl. Phys. Lett.*, vol. 55, pp. 2389–2391, 1989.

[11] R. E. Smith, C. T. Sullivan, G. A. Vawter, G. R. Hadley, J. R. Wendt, M. B. Snipes, and J. F. Klem, "Reduced coupling loss using a tapered-rib adiabatic-following fiber coupler," *IEEE Photon. Technol. Lett.*, vol. 8, pp. 1052–1054, 1996.

[12] G. A. Vawter, R. E. Smith, H. Hou, and J. R. Wendt, "Semiconductor laser with tapered-rib adiabatic-following fiber coupler for expanded output-mode diameter," *IEEE Photon. Technol. Lett.*, vol. 9, pp. 425–427, 1997.

[13] H. Sato, M. Aoki, M. Takahashi, M. Komori, K. Uomi, and S. Tsuji, "1.3 $\mu$m Beam-expander integrated laser grown by single-step MOVPE," *Electron. Lett.*, vol. 31, pp. 1241–1242, 1995.

[14] G. A. Vawter, R. E. Smith, B. Fuchs, J. R. Wendt, M. Hafich, and G. R. Hadley, "A rib optical waveguide with cutoff mesa isolation," *J. Lightwave Technol.*, vol. 14, pp. 169–172, 1996.

[15] G. A. Vawter, J. F. Klem, and R. A. Leibenguth, "Improved epitaxial layer design for real-time monitoring of dry-etching in III–V compound heterostructures with depth accuracy of $\pm$ 8 nm," *J. Vac. Sci. Technol. A*, vol. 12, pp. 1973–1977, 1994.

[16] G. A. Vawter, G. R. Hadley, J. R. Wendt, and J. F. Klem, "An integrated optical $X-Y$ coupler for phase-sensitive optical power combining and suppression of radiated light," in *Conf. Lasers and Electro-Optics, OSA Tech. Dig. Ser.* Washington, DC: Opt. Soc. Amer., 1994, vol. 8, p. 76.

[17] H. C. Casey and M. B. Panish, *Heterostructure Lasers Part A: Fundamental Principles*. San Diego, CA: Academic, 1978.

[18] C. T. Sullivan, G. A. Vawter, *et al.*, "Packaging of (Al,Ga)As photonic integrated circuits," presented at the 1997 IEEE MTT-S Int. Microwave Millimeter Wave Optoelectronic Integrated Circuit Module: Manufacturing and Applications Workshop, Denver, CO, June 1997.

[19] R. Spickermann, S. R. Sakamoto, M. G. Peters, and N. Dagli, "GaAs/AlGaAs traveling-wave electrooptic modulator with an electrical bandwidth greater than 40 GHz," *Electron. Lett.*, vol. 32, pp. 1095–1096, 1996.

**G. Allen Vawter** (S'86–M'87) received the Ph.D. degree in electrical engineering from the University of California, Santa Barbara, in 1987. His doctoral thesis involved design and fabrication of photonic integrated circuits, combining etched-facet AlGaAs diode lasers with passive optical routing waveguides for intra-chip optical interconnects.

While at UCSB, he also demonstrated the first etched-facet laser by reactive-ion etching and self-aligned Si and Zn diffusion into AlGaAs. Currently, he is a Principal Member of Technical Staff working in the Center for Compound Semiconductor Science and Technology (CCSS&T) at Sandia National Laboratories, Albuquerque, NM. His primary interests include optoelectonic device technology and reactive ion-beam etching of high-performance optoelectronic and photonic structures. Recent activities include high-power edge-emitting diode lasers, photonic integrated circuits, traveling-wave photodiodes, all-optical generation of millimeter waves, and artificially structured materials.

Dr. Vawter is a member of AVS and Tau Beta Pi, holds nine patents and has published more than 90 papers in recognized technical journals.

**Charles T. Sullivan** (S'76–M'83–SM'97) was born in El Paso, TX, on January 5, 1956. He received the B.S.E.E. and M.S.E.E. degrees from Washington University, St. Louis, MO, in 1978 and 1980, respectively, and the Ph.D. degree in electrical engineering (applied physics) from the University of California at San Diego, in 1985. His graduate work dealt with coupled cavity phenomena between diode laser gain media and external waveguide resonators built in lithium niobate and low-loss dielectrics.

During 1984, he worked as a Senior Engineer for General Dynamics, Electronics Division, San Diego, CA, on optical signal distribution technologies supporting microwave spectrum analysis for electronic warfare applications. From 1984 to 1993, he was with Honeywell Systems and Research Center, Bloomington, MN, as a Senior Principal Research Scientist where he was responsible for research and program development in (Al,Ga)As photonic devices and integrated circuits, monolithic optoelectronic integration, polymeric optical back planes, optical interconnects and packaging, and insertion of these technologies into sensored microsystems, avionic back planes, and satellites. In 1993 he joined Sandia National Laboratories as a Senior Member of Technical Staff in the Center for Compound Semiconductor Science and Technology where he has focused on research and development of (Al,In,Ga)As photonic devices and circuits, optomicroelectromechanical systems, and various optical waveguide components. He is now a Principal Member of Technical Staff leading programs in RF photonics, integrated photonic micro systems, and laser intersatellite communications.

Dr. Sullivan is a member of the American Physical Society, the Optical Society of America, and SPIE.

**Joel R. Wendt** (S'81–M'87) received the B.S.E.E. degree (*magna cum laude*) from Washington University, St. Louis, MO, in 1982, and the Ph.D. degree in electrical engineering from Cornell University, Ithaca, NY, in 1988. His Ph.D. research concerned the design, fabrication, and testing of sub micron vertical field effect transistors for the study of ballistic transport.

He joined Sandia National Laboratories, Albuquerque, NM, in 1988, and is currently a Principal Member of Technical Staff in the Compound Semiconductor Materials and Processes Department. Current work involves the application of electron beam lithography to nanofabrication in the areas of microoptics, photonics, and quantum electronics.

**Robert E. Smith** photograph and biography not available at the time of publication.

**Hong Q. Hou** received the Ph.D. in electrical engineering from the University of California, San Diego, in 1993. His thesis research centered on 1.3-$\mu$m optical modulators based on InAsP–InP strained quantum structures grown by gas-source molecular beam epitaxy.

Currently, he is a Senior Member of Technical Staff at Sandia National Laboratories, Albuquerque, NM. His principal interests include the design and epitaxial growth of a variety of optoelectronic and electronic devices by metal organic vapor phase epitaxy, especially vertical-cavity surface-emitting lasers. His past professional experience include a Research Assistant at the Institute of Physics, Chinese Academy of Science in Beijing (1985–1988), a Visiting Scholar at the Institute of Physical and Chemical Research (RIKEN), in Japan (1988–1990), and a Post-Doctoral Member of Technical Staff at AT&T Bell Laboratories, Holmdel, NJ (1993–1995), working on molecular beam epitaxy growth, heterostructure and exciton physics under high magnetic field and hydrostatic pressure, and 1.55-$\mu$m ultralow-chirp optical modulators, respectively.

Dr. Hou has published more than 90 papers in recognized technical journals. He is a Member of the American Physical Society, the Optical Society of America, and the Electrochemical Society.

**John Klem** received the B.S. degree in electrical engineering from Iowa State University in 1982, and the M.S. and Ph.D. degrees from the University of Illinois, Urbana-Champaign, in 1984 and 1987, respectively.

He joined Sandia National Laboratories, Albuquerque, NM, in 1987, and since then has been engaged in the molecular beam epitaxial growth of III–V compound semiconductors for a large number of electronic and Optoelectronic device programs. His current research interests include Sb-based materials for mid-IR optoelectronic devices, and the application of *in situ* monitors and feedback control for improved device epitaxy.

# High Speed Traveling Wave Electrooptic Intensity Modulator with a Doped PIN Semiconductor Junction

G.A. Vawter, V.M. Hietala, J.R. Wendt, B.A. Fuchs, M. Hafich,

M. Housel, M. Armendariz and C.T. Sullivan

Sandia National Laboratories

P.O. Box 5800, MS 0603

Albuquerque, NM 87185-0603

ph. (505) 844-9004; fax 844-8985

## Abstract

A high-electrooptic-efficiency Mach-Zehnder intensity modulator is demonstrated with a bandwidth exceeding 40 GHz. The 1 mm-long modulator has a switching voltage comparable to undoped semiconductor designs of much greater length.

This work was supported by the US/DOE under contract no. DE-AC04-94AL85000.

# High Speed Traveling Wave Electrooptic Intensity Modulator with a Doped PIN Semiconductor Junction

G.A. Vawter, V.M. Hietala, J.R. Wendt, B.A. Fuchs, M. Hafich,
M. Housel, M. Armendariz and C.T. Sullivan

Sandia National Laboratories, P.O. Box 5800, MS 0603
Albuquerque, NM 87185-0603, ph. (505) 844-9004; fax 844-8985

Extremely fast modulation response of optical phase delay in a waveguide modulator is required for photonic integrated circuits (PICs) to operate with mm-wave signals. Single phase modulators, paired phase modulators in a Mach-Zehnder interferometer, or more complex arrangements can be used for mm-wave modulation of light in either phase, amplitude, or frequency. Standard lumped-element devices are bandwidth limited by the RC time-constant of the structure. Distributed, or traveling-wave designs have been developed to surpass the RC limit. With distributed structures the bandwidth limit is determined by loss of phase synchronism between the optical and RF wavefronts within the length of the device. The generally different propagation constants of the optical and RF waves leads to a limiting length-bandwidth product in the modulation response. In the limit of zero velocity mismatch the modulation bandwidth is then limited by RF loss in the transmission line. Velocity matching in undoped or low-doped semiconductor optoelectronic modulators typically involves use of a slow-wave transmission line electrode structure. Several successful techniques have been developed[1-2], but undoped structures offer low electrooptic efficiency, resulting in undesirably large devices. We disclose a device using doped semiconductor structures to increase efficiency in a traveling-wave modulator. This new design is demonstrated to have a bandwidth greater than 40 GHz in a Mach-Zehnder intensity modulator operating at 1.32 μm wavelength while maintaining $V_\pi$ = 10V with a phase modulator section only 1mm-long.

Electrooptic efficiency can be dramatically increased through the appropriate use of doping in a semiconductor optical waveguide. A *p-i-n* junction centered on the optical mode of the waveguide concentrates the applied electric field within the optical mode, yielding higher optical phase shift per unit applied voltage compared to undoped waveguides. The improved efficiency permits the use of shorter modulators for a given applied voltage. Use of doped waveguides does increase the optical loss but the overall loss of the device can be similar to an undoped design due the reduced length.[3]

Figure (1) shows the cross-section of the optical phase modulator used in the high-speed Mach-Zehnder. The waveguide comprises an (Al,Ga)As cutoff-mesa rib optical waveguide.[4] A *p-i-n* junction with a 0.6 μm undoped thickness is centered on the 0.2 μm thick GaAs waveguide core. The upper waveguide rib is 2 μm wide, the waveguide mesa is 10 μm wide. The microwave transmission line comprises a 14 μm-wide Au strip balanced on the waveguide and ground-plane metalization contacting a continuous $n^+$ GaAs layer placed below the etched mesa. Vertical and horizontal spacing between the ground metalization and the center strip, is used to control the microwave phase velocity. The intrinsic region thickness also has a strong influence on the microwave phase velocity. However, this thickness is kept at a practical minimum in order to maintain the desired high optical modulation efficiency.

A quasi-TEM transmission-line model was used to predict the transmission line characteristics and phase modulation response versus frequency. At 30 GHz, the microwave index, loss and characteristic impedance are calculated to be 3.31, 2 dB/mm and (22 - 0.56j) Ohms respectively. The microwave index is well matched with the optical modal index of 3.3134 at the 1.32 μm wavelength calculated using a two-dimensional finite difference technique. Using theoretical transmission-line losses, ideal impedance matching at the source and load and a fixed electrooptic efficiency, the model indicates that a 1 mm-long device would have a bandwidth

between 50 and 100 GHz (Figure 2). This model is expected to overestimate the bandwidth to some extent as the RF loss is known to increase with frequency.

Mach-Zehnder intensity modulators were fabricated using epitaxial layers grown by molecular-beam-epitaxy. All etching was by chlorine reactive ion beam etching. A PMGI-based air-bridge metal plating technique was used to create the central metal strip balanced on the waveguide rib. The transmission line was terminated at both ends with pads placed directly on the semi-insulating substrate for Cascade microprobes. Final cleaved devices were 3 mm in length including the 1 mm-long phase modulator, input and output waveguides and optical power combiners/splitters occupied the remaining length. The two arms of the Mach-Zehnder were driven asymmetrically with one arm held to ground potential and the other comprising the high-speed phase modulator.

Small signal electrical response was measured to 40 GHz using an amplitude modulated microwave signal[5] and a DC-bias of -10 V. As seen in Figure (3), the response is fairly flat out to 20 GHz with a peak at 30 GHz. The device does not show a -3dB roll-off within the 40 Ghz measured frequency range. The peak at 30 GHz is most likely a resonance caused by the use of 50 Ohm probes, cables and output termination on the 22 Ohm transmission-line structure. This impedance mismatch was not included in the model of Figure (2). Use of proper impedance-matching techniques should flatten the resonance, providing a more uniform frequency response. S-parameter measurements up to 20 GHz were performed using a network analyzer. From this data, the measured RF loss of a 1 mm-long device is seen to increase monotonically from 1.3 to 2.4 dB/mm between 10 and 20 GHz.

In conclusion, a Mach-Zehnder intensity modulator at 1.32 μm wavelength has been demonstrated with a modulation bandwidth greater than 40 Ghz. The device uses a doped *p-i-n* semiconductor junction for high electrooptic modulation efficiency and small overall size. The 1 mm-long modulator section has a $V_\pi$ = 10V, comparable to undoped semiconductor designs of much greater length.

This work was supported by the United States Department of Energy under Contract DE-AC04-94AL8500.

References:

[1] R.G. Walker, Proceedings of the IEEE Lasers and Electrooptics Society 1995 Annual Meeting, Vol. 1, pp. 120-121, San Fransisco, CA, Oct. 30-Nov. 2, 1995.

[2] R. Spickermann, S. Sakamoto, M. Peters and N. Dagli, Proceedings of the IEEE Lasers and Electrooptics Society 1995 Annual Meeting, Vol. 1, pp. 118-119, San Fransisco, CA, Oct. 30-Nov. 2, 1995.

[3] G.A. Vawter, V.M. Hietala, S.H. Kravitz, M.G. Armendariz, Proceedings of the International 1994 IEEE MTT-S Topical meeting on Optical Microwave Interactions, pp. 3-6, Ile de France, France, Nov. 21-23, 1994.

[4] G.A. Vawter, R.E. Smith, B. Fuchs, J.R. Wendt, M. Hafich, G.R. Hadley, Proceedings of the IEEE Lasers and Electrooptics Society 1995 Annual Meeting, Vol. 1, pp. 137-138, San Fransisco, CA, Oct. 30-Nov. 2, 1995.

[5] S. Uehara, Applied Optics, Vol. 17, No. 1, pp. 68-71, 1978

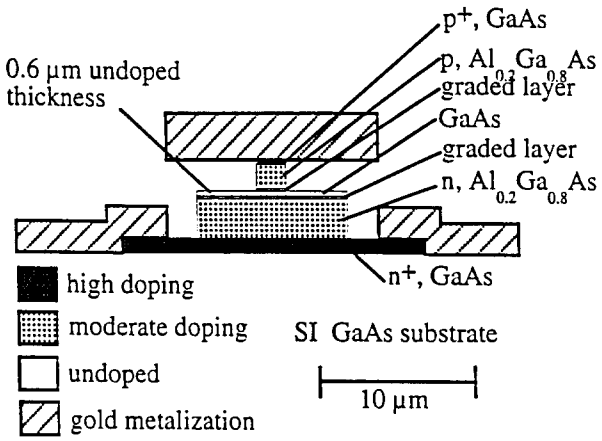


**Figure 1:** Cross-section view of the traveling-wave phased modulator with doped *p-i-n* waveguide design. Figure is drawn approximatly to scale. The outer Au ground-plane metalizations extend beyond the edges of the drawing.

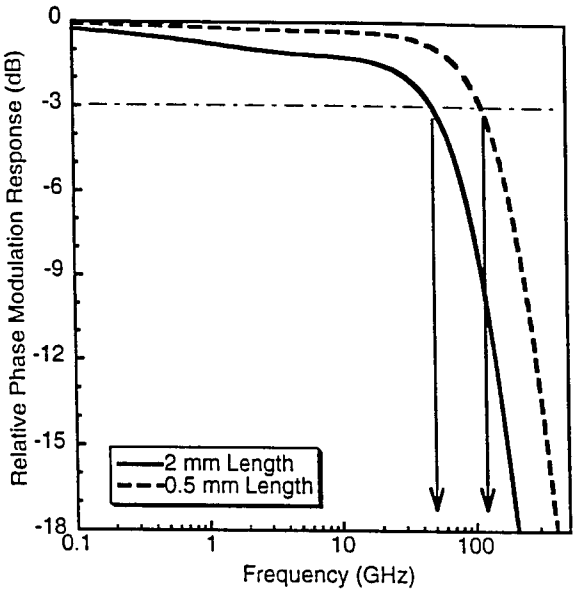


**Figure 2.** Theoretical traveling-wave phase modulator response as function of frequency. Dashed line is 0.5 mm long device. Solid line is 2 mm long device.

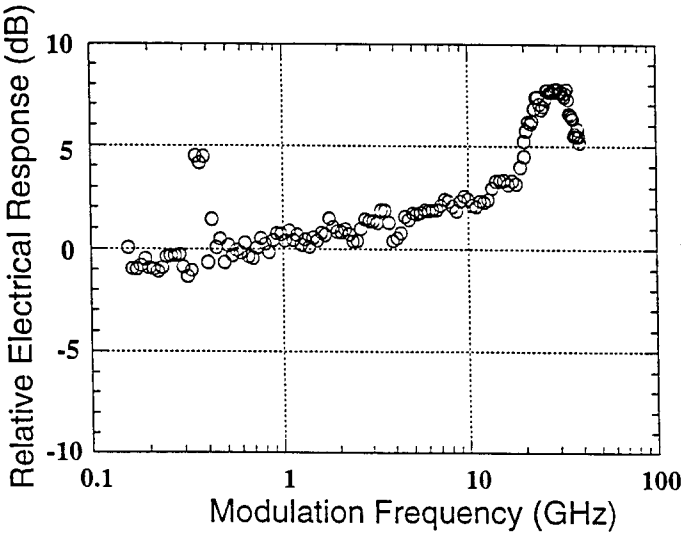


**Figure 3:** Relative small-signal electrical response of a Mach-Zehnder intensity modulator employing a 1 mm-long phase modulator of the design in Figure (1).

# Traveling-Wave Electrooptic Intensity Modulator Using a Doped PIN Semiconductor Junction for DC to >40 GHz Modulation Bandwidth

G.A. Vawter, V.M. Hietala, J.R. Wendt, B.A. Fuchs, M. Hafich

Sandia National Laboratories
Albuquerque, NM 87185-0603
USA

## Abstract

We present an AlGaAs Mach-Zehnder interferometric optical modulator for 1.3 μm wavelength combining both small size, low switching voltage and a modulation bandwidth exceeding DC to 40 GHz. Overall length of a Mach-Zehnder with a $v_\pi$ of 6.5 V is only 3.7 mm

## Introduction

To date, high-speed waveguide modulators have been largely undoped in order to reduce the device capacitance per unit length. Fast Mach-Zehnder interferometers (MZIs) have been built[Spickermann, 1995 #806; Walker, 1995 #805] using undoped waveguides. These devices have generally been greater than 10 mm in length. The long length is required to reduce the drive voltage below 10 V. Reducing the length of the MZI at a fixed drive voltage requires an increased phase modulation efficiency, greater than that available using thick, undoped semiconductor materials. Improved modulation can be achieved using doped pin semiconductor junctions where the applied electric field and the optical mode are confined within the depletion region of the diode. However, in so doing the capacitance of the resulting waveguide increases such that conventional velocity-matched RF waveguide structures are impractical.

We present an AlGaAs Mach-Zehnder interferometric optical modulator for 1.3 μm wavelength combining both small size, low switching voltage and a modulation bandwidth exceeding DC to 40 GHz. High speed, small size and low switching voltage are obtained through the use of a cutoff mesa rib-type optical waveguide and a novel cantilevered-beam microstrip RF transmission line.

## Design and Modeling

The integrated optical waveguides comprising the Mach-Zehnder use a cutoff-mesa rib optical waveguide.[Vawter, 1996 #804] The cutoff mesa rib waveguide permits process-tolerant fabrication of single-moded rib waveguides within wider, deeply etched isolation mesa structures. Conventional rib waveguides may become multi-moded when embedded within isolation mesas due to the refractive index discontinuity at the mesa edge. Fig. (1) shows both the (AlGa)As epitaxial structure and the resultant rib waveguide mode for single-mode propagation at 1.32 μm wavelength. The *pin* junction is centered on the optical mode for optimum interaction between light in the waveguide and the applied electric field.[Mendoza-Alverez, 1988 #371] Although a smaller depletion region would increase the modulation efficiency, a 0.6 μm-wide region is required to achieve an electrode velocity match while maintaining low electrical loss. An added benefit of the cutoff mesa design is that the top surface of the mesa is undoped material, this further reduces the device capacitance and RF loss compared to a p-type doped mesa surface.

A traveling-wave electrode is used to match the RF and optical phase velocities for maximum modulation bandwidth.[Walker, 1991 #523] Although the doped *pin* semiconductor waveguide simultaneously offers compactness and low drive voltage, the

relatively high capacitance, compared to undoped semiconductor and dielectric waveguide designs, has the effect of slowing the RF phase velocity to a value well below that of the optical phase velocity. Consequently, we have developed a cantilevered-beam microstrip RF transmission line to increase the group velocity to match that of light inside the waveguide. With this structure, Fig. (2), the p-contact metalization extends beyond the width of the rib waveguide so as to create an air gap between the electrode, the semicoductor mesa and metal ground planes. This design effectively lowers the inductance per unit length for the required velocity match while still concentrating the applied electric field within the region of the optical mode thereby improving the modulation efficiency at both low and high frequencies.

Characteristics of the RF line are established by the vertical and lateral air gaps and the width of the electrode. Dimension of the gap is readily adjusted during fabrication through the use of spin-coated polymers such as photoresist or PMGI. A quasi-TEM transmission-line model is used to calculate the characteristic impedance, loss and effective refractive index of the RF transmission line. Table I shows theoretical transmission line performance at 30 GHz for various center electrode widths and gaps. In all cases the calculated RF loss is 2.1 ±0.2 dB/mm. A 14-μm wide electrode and 0-μm lateral gap is expected to result in a transmission line velocity-matched with the optical waveguide design of Fig. (1) where the waveguide effective refractive index is 3.31.

Using the transmission line losses from the Quasi-TEM model, frequency-independent optical modulation efficiency and ideal impedance matching, the -3 dB response of a phase modulator in one arm of the MZI is calculated to be 50 and 100 GHz for 2 and 1 mm modulator lengths respectively.

## Fabrication and Test

Complete integrated MZI devices were fabricated using the design described above with 14-μm wide electrodes and both 0 and +2 μm lateral gaps. Multi-mode interference sections were used both for splitting light into the two MZI arms and recombining the two modulated beams at the output guide. Length of the completed MZIs was 3.7 and 4.7 mm for 1 and 2 mm-long phase modulator section respectively. Waveguides and mesas were etched using Cl2 reactive-ion-beam etching with in-situ reflectance endpoint monitoring.[Vawter, 1994 #698] The cantilevered center electrode was built using a PMGI air-bridge technique and thick Au electroplating. To facilitate device testing, contact pads for Cascade ACP40 high-speed probes were placed on semi-insulating GaAs at each end of the MZI. S-parameters of completed devices were measured from 150 MHz to 50 GHz. The actual characteristic impedance was 25 ohms. As seen in Fig. (3), the RF effective index was 3.7, and the RF losses increased with frequency monotonically from 0.5 to 3.5 dB/mm. The RF index is only 12% higher than the design value of 3.31.

Electrooptic response was measured using light from a CW diode-pumped ring-type Nd+ YAG laser at 1.32 μm butt-coupled into the rib waveguide. All testing was of devices with uncoated facets and using light polarized in the plane of the epitaxial layers to excite the fundamental TE optical mode. Straight test waveguides were measured to have 8.3 dB/cm propagation loss. Insertion loss of complete, 4.7 mm-long MZIs (2 mm modulator length) was measured as low as 4.7 dB exclusive of optical coupling loss at the cleaved ends. At 10 KHz modulation frequency modulation depths as high as 8.4 dB were observed. Switching voltage, $v_\pi$, of MZIs with 1-mm long phase modulators was typically 6.2 V. Although the 2-mm long modulators were expected to have $v_\pi$ values roughly one half those of the 1 mm devices, the typical value was ~8 V. This is likely due to non-uniform contact along the length of the longer devices. Improved processing is expected to reduce $v_\pi$ of the longer devices to ~3.1 V.

Amplitude modulation (AM) of the microwave drive signal was used to determine the small-signal response of the MZI.[Uehara, 1978 #791] The drive signal frequency was varied from 0.15 to 40 GHz with AM at 10.4 KHz. Output of the MZI was sent to a Ge photodiode and lock-in amplifier referenced to the AM signal. Care was taken to bias each device at the inflection point (maximum slope) of the low-frequency response. Fig. (4) shows the frequency response of 1- and 2-mm devices for both 0 and +2 μm lateral electrode gaps. Modulation response from 150 MHz to 40 GHz without significant rolloff. Two of the devices exhibit resonant dips above 35 GHz. Although the interpretation is difficult, the abrupt response dip at the high-frequency end of the data for the 1-mm-long, 0-μm gap is considered to be an electrical resonance.

## Analysis

The most striking features of the response curves for both 1 and 2 mm devices is their similarity and the broad peak at 30 GHz. Transmission line theory assuming ideal source/load impedances predicts a simple monotonic roll-off in the response determined almost entirely by RF losses within the device. In reality the device exhibits a 25 Ω impedance and is embedded within a 50 Ω system. As such a significant voltage standing wave may be established by reflections at each end of the device. Such a standing wave would have a length-dependent resonant frequency at AA and BB GHz for the two device lengths. However, since the resonance is frequency independent it is unlikely that simple reflections at the impedance discontinuity are responsible. Another possibility is that the metal pads for the coplanar probes form a localized reactive network between the 50 Ω external environment and the actual modulator. This concept was investigated by modeling the contact pads as a lumped capacitance, representing the square pad, and a short section of 50 Ω line, representing the transmission line on the SI substrate before bridging up onto the waveguide. The capacitance, 50 Ω line length and the impedance of the actual modulator were then used as adjustable parameters to fit this new circuit to the measured S-parameters. The resulting de-embedded values were 48 fF capacitance, 54 and 137 μm long 50 Ω line at the launch and load end respectively, and a 15 Ω real component of the characteristic modulator impedance. The fitted length of the 50 Ω sections were quite close to the actual lengths. The reasonable values resulting from the fitting process tend to support the concept of a resonant matching network created by the probe pads. Both the reduced characteristic impedance and increased index of the modulator indicate that the air gap is somewhat larger than the design value.

## Conclusions

In conclusion, an AlGaAs Mach-Zehnder interferometric optical modulator combining both small size (3.7 mm overall length), low switching voltage ($v_\pi$ = 6.5 V) and bandwidth exceeding 40 GHz has been designed and demonstrated. The design takes advantage of the combined effects of a doped *pin* semiconductor double heterostructure waveguide, a cutoff-mesa rib optical waveguide and a partial air-dielectric "fast-wave" distributed electrode. Future work is expected to result in slightly longer devices with 2-mm long modulator sections and $V_\pi < 3.5$ V. These devices have applications in both analog and digital optical communication systems. The flat response from DC to 40 GHz should give good noise margins in 20 to 30 Gbit/s data links. When used with a resistive matching network or embedded in a low impedance system multi-frequency RF optical data links are possible.

## Acknowledgments

The authors would like to thank C. T. Sullivan, M. G. Armendariz and M. Housel for technical assistance. This work was supported by United States Department of Energy under Contract DE-AC04-94AL85000.

| Electrode Width (μm) | Electrode Thickness (μm) | Lateral Gap (μm) | $n_{RF}$ | $Z_o$ (Ω) |
|---|---|---|---|---|
| 8 | 2 | 2 | 3.76 | 26-0.39j |
| 8 | 1 | 1 | 3.99 | 27.8-0.56j |
| 14 | 2 | -1 | 3.18 | 21-0.5j |
| 14 | 2 | 0 | 3.31 | 21.8-0.49j |
| 14 | 2 | 2 | 3.57 | 23.6-0.49j |
| 14 | 2 | 4 | 3.80 | 25.3-0.55j |

Table I: RF effective refractive index, $n_{RF}$, of the transmission line of Fig. (2) for various electrode dimensions at 30 GHz drive frequency.

Figure 1: (a) Cross-section schematic of rib optical waveguide used in the MZI. (b) Simulated constant-field contours of guided mode.

Figure 2: Cross-section schematic of microwave waveguide used in the MZI. Detail included in Fig. (1) is omitted for clarity.

Figure 3: Measured and simulated RF index and loss of the distributed phase modulator used in the MZI.

Figure 4: Frequency response of both 1 and 2 mm active length MZIs for both 0 and 2 μm lateral electrode gaps. In all cases the width of the center cantilevered electrode is 14 μm.

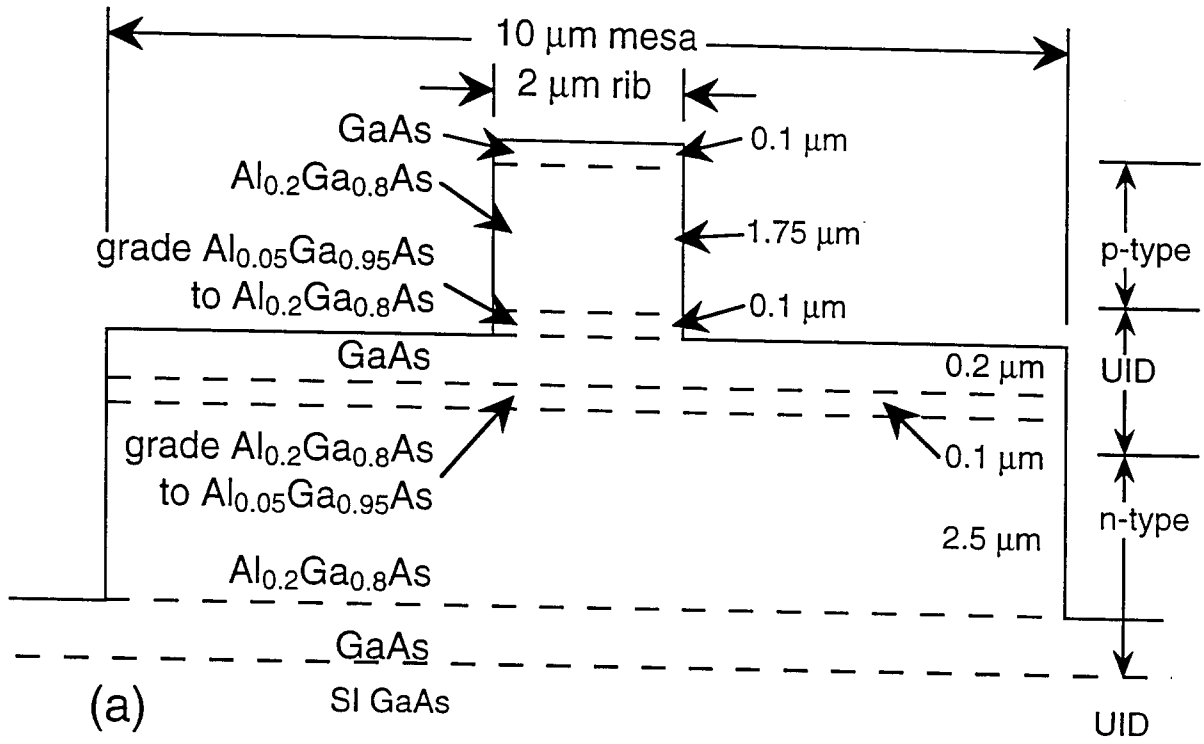
10 μm mesa
2 μm rib
GaAs
0.1 μm
$Al_{0.2}Ga_{0.8}As$
1.75 μm
grade $Al_{0.05}Ga_{0.95}As$
to $Al_{0.2}Ga_{0.8}As$
0.1 μm
p-type
GaAs
0.2 μm
UID
grade $Al_{0.2}Ga_{0.8}As$
to $Al_{0.05}Ga_{0.95}As$
0.1 μm
2.5 μm
n-type
$Al_{0.2}Ga_{0.8}As$
GaAs
SI GaAs
UID
(a)

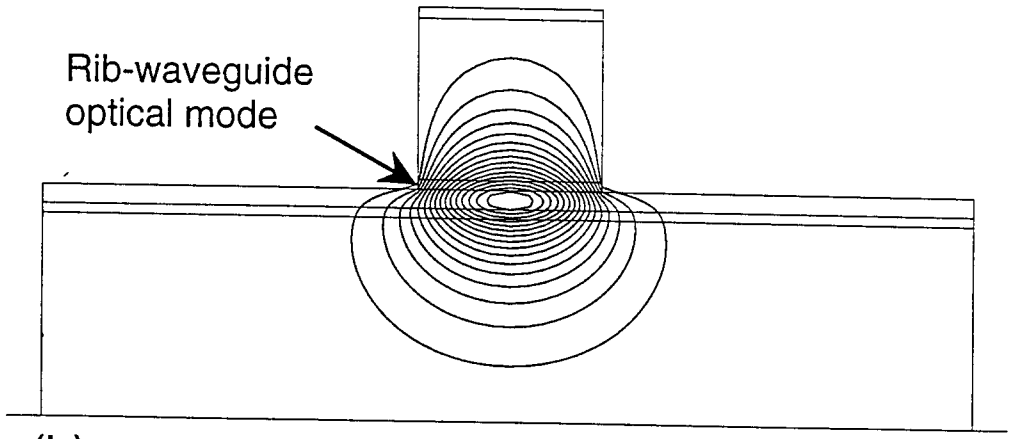
Rib-waveguide
optical mode
(b)

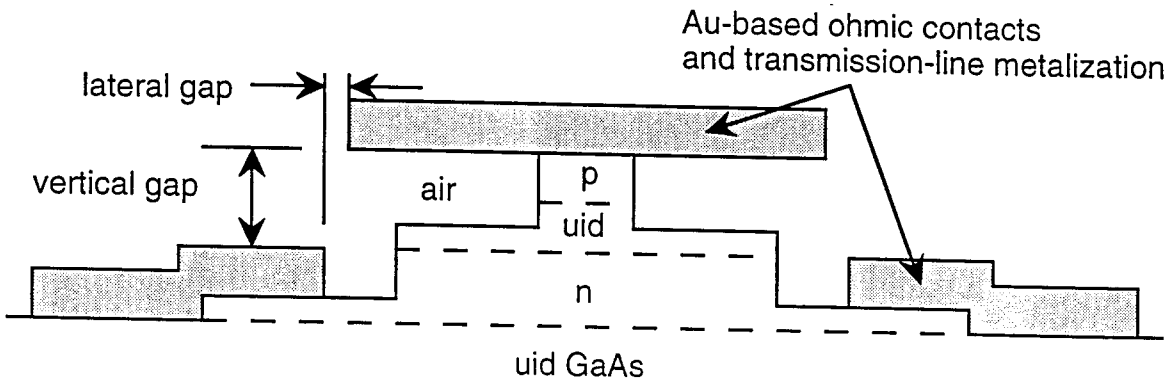
Au-based ohmic contacts
and transmission-line metalization
lateral gap
vertical gap
air
p
uid
n
uid GaAs

Figure 2

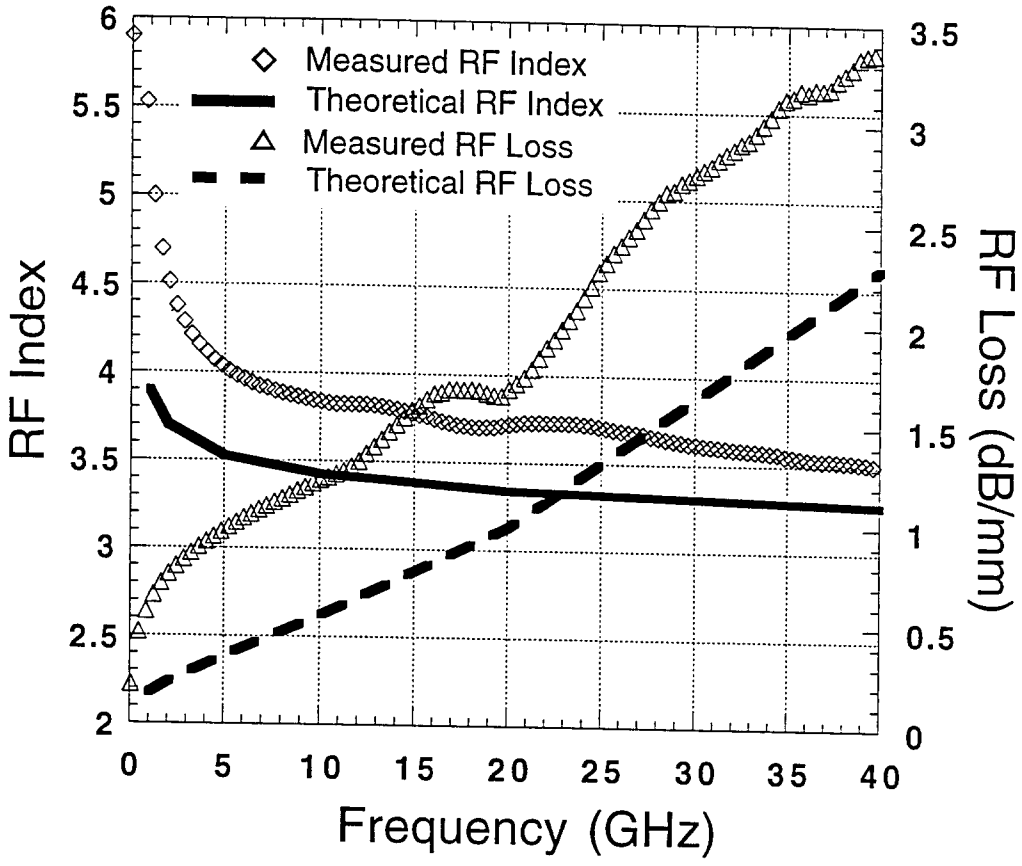
Measured RF Index
Theoretical RF Index
Measured RF Loss
Theoretical RF Loss
RF Index
RF Loss (dB/mm)
Frequency (GHz)
6
5.5
5
4.5
4
3.5
3
2.5
2
3.5
3
2.5
2
1.5
1
0.5
0
0
5
10
15
20
25
30
35
40

Figure 3

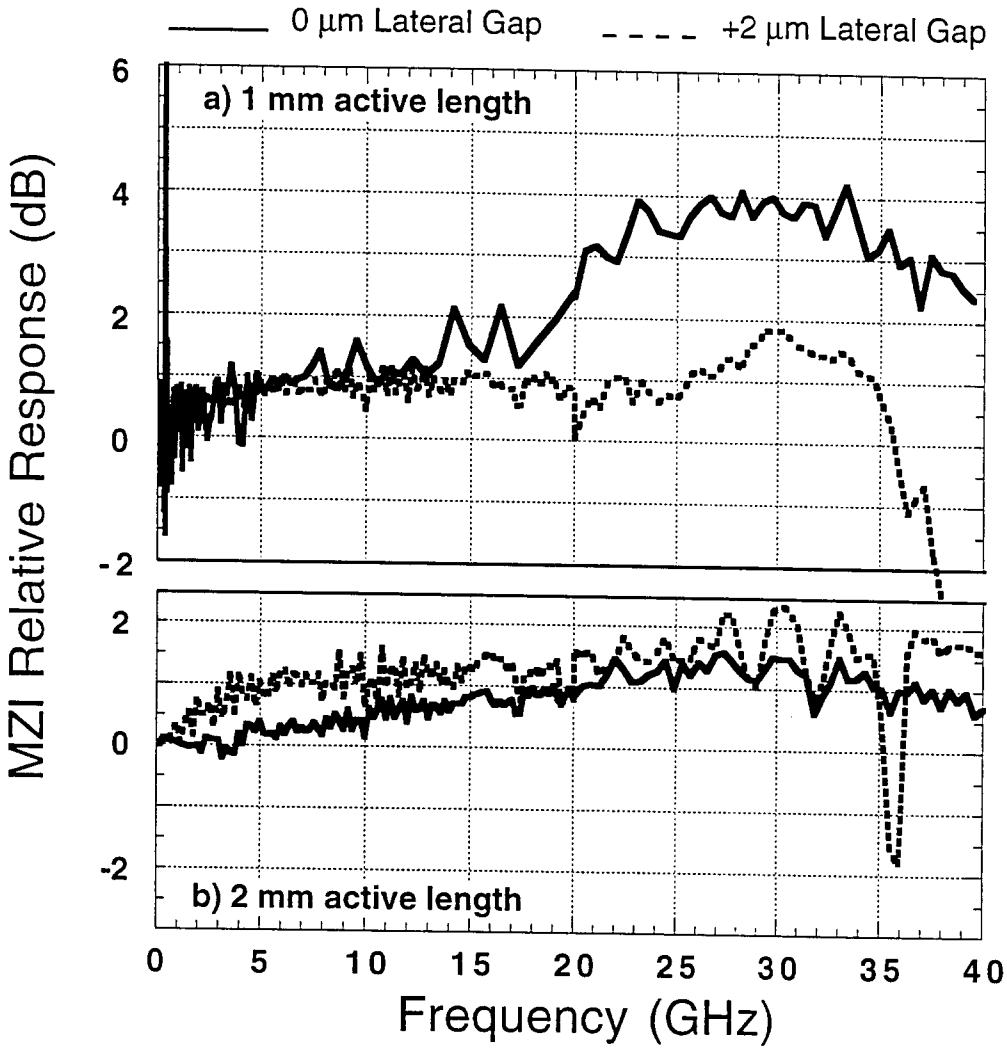
0 μm Lateral Gap
+2 μm Lateral Gap
a) 1 mm active length
b) 2 mm active length
MZI Relative Response (dB)
Frequency (GHz)
6
4
2
0
-2
2
0
-2
0
5
10
15
20
25
30
35
40

Figure 4

# Reduced Coupling Loss Using a Tapered-Rib Adiabatic-Following Fiber Coupler

R. E. Smith, C. T. Sullivan, *Member, IEEE*, G. A. Vawter, *Member, IEEE*, G. R. Hadley, *Senior Member, IEEE*, J. R. Wendt, *Member, IEEE*, M. B. Snipes, and J. F. Klem, *Member, IEEE*

***Abstract*—We present the design and experimental demonstration of a tapered-rib adiabatic-following fiber coupler (TRAFFiC). This device is an adaptation of a Shani–Henry mode converter fabricated in (Al)GaAs and designed to increase the coupling efficiency of conventional optical fibers to tightly-confined semiconductor rib waveguide devices. This approach offers the potential of significantly reducing fiber butt coupling losses from the typical values of 7 to 10 dB to values of <1 dB. This long-standing packaging problem is one of the major impediments to the widespread acceptance of semiconductor-based optoelectronics. Moreover, the design can be implemented with minimal increase in fabrication complexity since it uses only a straightforward modification to epitaxial growth, and one additional lithography and etching step.**

THE ABSENCE of an efficient and low-cost means of connecting optical fibers to semiconductor waveguide devices, e.g., diode lasers and photonic integrated circuits (PIC's), currently poses one of the largest barriers to wide scale commercialization of semiconductor optoelectronic devices. This problem arises because of the small size of semiconductor waveguides compared to optical fibers. The 1–2 $\mu$m elliptical modal spot of typical semiconductor waveguides is neither well-sized nor shaped to match to the standard 8–9 $\mu$m circular modal spot of conventional single-mode optical fibers. Directly coupling light from a fiber to the small waveguide typically results in 7 to 10 dB insertion loss. [1] Nonintegrated solutions that improve this coupling often increase coupling at the cost of tight alignment requirements (<1 $\mu$m) and are thus not well suited for passive alignment systems [2].

Recently several groups have presented monolithically integrated beam expanders for coupling semiconductor waveguides to single-mode fibers [3]–[10]. Among these solutions are adaptations of the Shani–Henry approach [11], which use a thin (~100 nm) buried waveguide at the output. Such buried waveguide solutions have been quite successful in reducing coupling losses to <3 dB, but these approaches require challenging taper sharpness. Furthermore, these designs are not applicable for use with PIC's and optoelectronic devices based on (Al)GaAs rib waveguides fabricated with a single epitaxial growth step. Here we present a design that uses lateral tapering in a tightly confined (Al)GaAs rib waveguide to convert the rib mode to the fundamental mode in an underlying mesa. The approach presented here is much more along the lines of that suggested in [12]. A schematic of our design is given in Fig. 1.

The epitaxy and upper rib dimension are chosen so that the rib supports only a single TE-polarized mode, and so that the GaAs epitaxy remaining outside the rib after etching supports no slab modes [13]. The lower mesa was designed to have a single TE mode and for that mode to be approximately matched to optical fiber, (~90%). Fig. 2 shows the field profiles of the fundamental TE mode of this structure for three separate values of the rib width, $w$. In Fig. 2(a), $w = 2.4$ $\mu$m and the fundamental mode is well confined to the rib waveguide. When the rib is initially narrowed, the mode remains well confined. As the waveguide rib is further narrowed to $w \sim 1.3$ $\mu$m, the fundamental mode is pushed down into the mesa, [Fig. 2(b)]. Fig. 2(c) shows that for $w \sim 1.0$ $\mu$m the fundamental mode has moved almost entirely into the mesa, where it is well suited for overlap with the approximately Gaussian shaped mode of an optical fiber. The fundamental mode remains in the mesa and is virtually unchanged as the rib width is narrowed further.

The small range of widths over which the majority of the power transfer occurs suggests a taper with a highly optimized nonlinear width variation in order to reduce the coupler length. Instead our tapers are chosen to be linear to improve fabrication tolerances. In particular this means that the power transition can occur centered at any width between 2.4 and 1.0 $\mu$m, so that the fabrication tolerances of the growth and processing parameters that might shift this transition are greatly increased. The results of three dimensional beam propagation calculations suggest that for this epitaxy linear tapers of 500–1000 $\mu$m in length and optimized-shape tapers of 350 $\mu$m have <1-dB theoretical excess insertion loss.

Although the required minimum taper widths of ~0.71–1.0 $\mu$m [Fig. 2(c)] can be achieved by using conventional contact lithography, a fabrication artifact strongly impacts these devices. When electron beam lithography is used for direct write or to fabricate masks for contact lithography, the pixelization of the electron beam grid size results in the tapers being approximated by a series of small stair steps. Theoretical models have shown that for TRAFFiC devices the excess taper loss due to pixelization measured in dB turns out to be essentially linearly proportional to the size of these stair steps (these theoretical investigations will be reported at length in a future publication). For this design, acceptable losses of <1 dB require stair steps of ~0.025 $\mu$m. Since masks with such

Manuscript received February 12, 1996; revised April 8, 1996. This work was supported by the United States Department of Energy under Contract DE-AC04-94AL85000.

The authors are with the Sandia National Laboratories, Albuquerque, NM 87185-0603 USA.

Publisher Item Identifier S 1041-1135(96)05840-5.

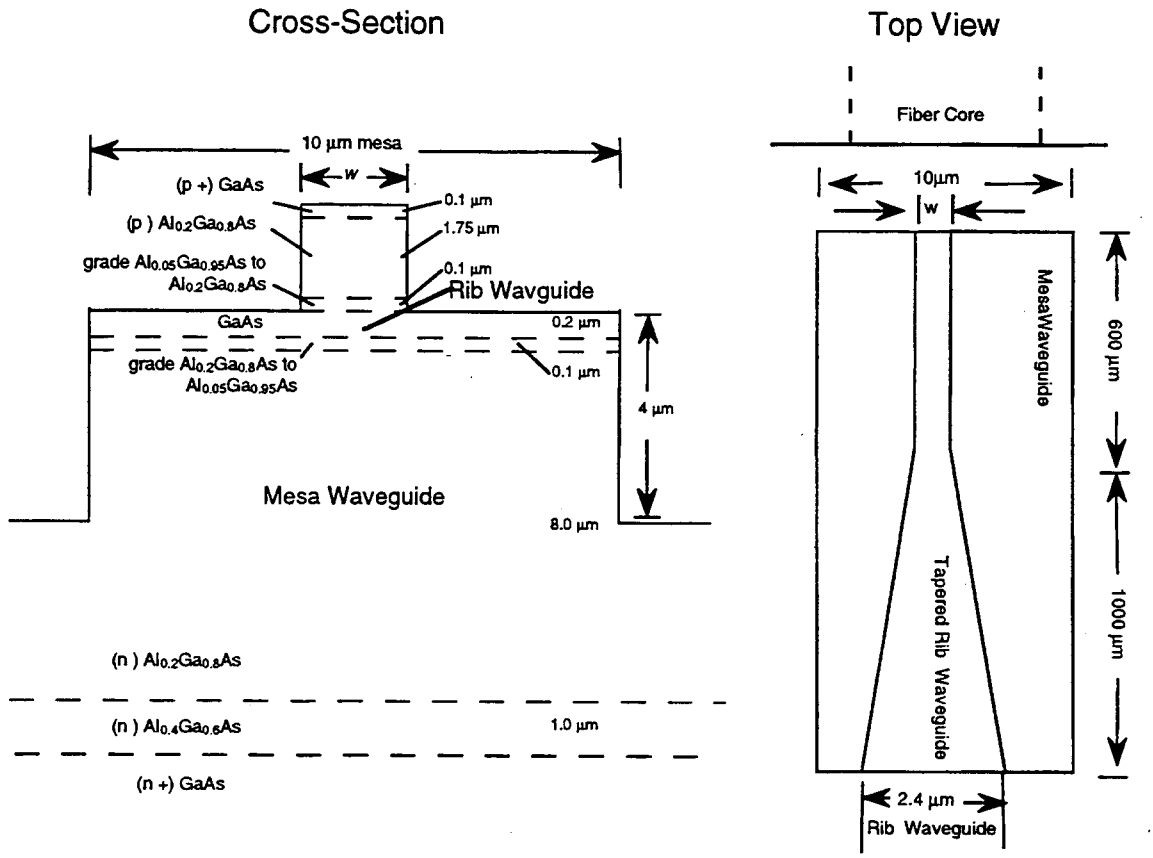


Fig. 1. A schematic drawing of a tapered-rib adiabatic-following fiber coupler (TRAFFiC) including (Al)GaAs composition profile and guide dimensions.

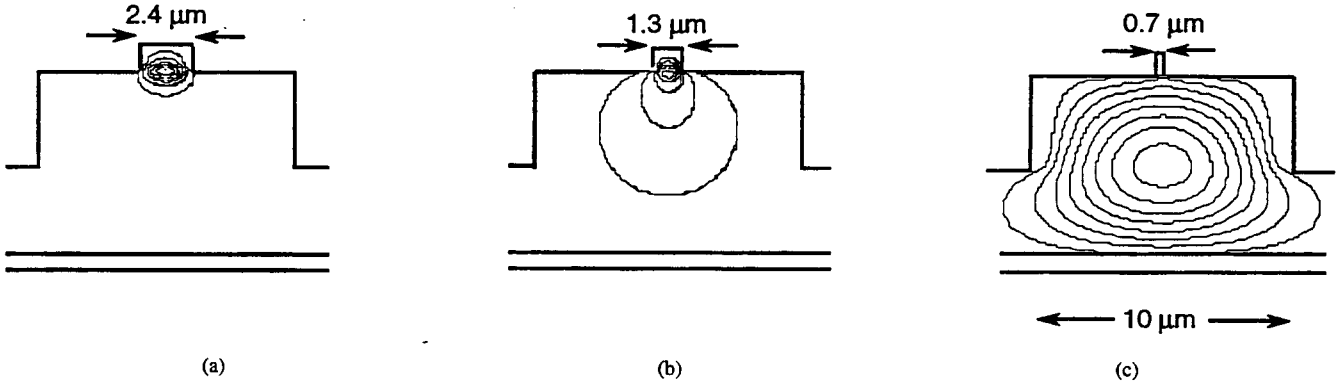


Fig. 2. The fundamental TE mode for three rib widths (electric field contours).

small grid sizes were unavailable commercially, these devices were prototyped by using direct write *e*-beam lithography. Notice that this same result could be accomplished by writing masks with a 0.025 $\mu$m grid spacing to achieve the necessary smoothness.

To demonstrate operation, fixed width rib waveguides [Fig. 2(a)], mesa waveguides [Fig. 2(c)], and tapered rib-width waveguide structures [Fig. 2(a)–(c)] were fabricated using (Al)GaAs waveguides identical to Fig. 1. Epitaxial layers were grown by molecular-beam epitaxy. The upper and lower cladding layers were doped p- and n-type, respectively, so that the 2.4 $\mu$m-wide rib waveguides are compatible with reverse-biased pn-junction phase modulators. Waveguide rib structures were patterned with negative-acting electron-beam resist and a 25-nm exposed pixel spacing. Etching of both the rib waveguide and mesa used chlorine reactive-ion-beam etching. [14]

For comparison, a mesa waveguide and a tapered rib mode converter were alternately excited using a single-mode fiber [15] emitting light at 1.31-$\mu$m wavelength. Near field images ($\sim$400$\times$) for the fiber, the mesa, and the tapered rib waveguide are shown in Fig. 3(a)–(c), respectively. Notice that the mesa guide and fiber are well matched and that the tapered rib output is very different. Unfortunately the limitations of the imaging optics result in the much smaller rib mode appearing relatively larger than its size compared to the mesa and fiber

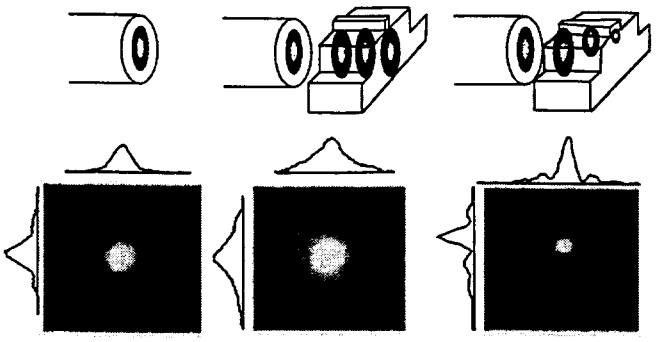


Fig. 3. Experimental results showing near-field images of: (a) light exiting the optical fiber (b) light coupled from a fiber and traveling though a mesa waveguide without a taper, and (c) light coupled from a fiber to a mesa waveguide then traveling through a tapered-rib adiabatic-following fiber coupler and exiting from a rib waveguide. (c) Demonstrates the desired spot size transformation. Each of the three images is accompanied with a schematic representation of the configuration used to obtain the image.

modes. Power measurements demonstrate total mesa to rib waveguide coupling losses of ~1.5–2.0 dB and fiber to mesa coupling losses of ~0.5 to 1.0 dB. The larger than expected total mesa to rib waveguide coupling losses are understood by the unusually large waveguide propagation losses of 0.8 to 1.0 dB/mm exhibited by both the rib and mesa waveguides on this sample.

The result of this simple test is encouraging, suggesting a conservative estimate of less than 3 dB total-fiber-to-rib-waveguide coupling loss. Based on these results and additional theoretical investigation we believe devices of this type are likely to provide a satisfactory solution to the fiber coupling problem. TRAFFiC devices using lower loss waveguides that have total theoretical losses—including excess taper, material, waveguide scattering, and mode-mismatch losses—of <1 dB are being fabricated.

## ACKNOWLEDGMENT

The authors wish to thank C. T. Fuller for assistance with the experimental measurements and T. R. Bauer and B. Fuchs for fabrication assistance.

## REFERENCES

[1] R. G. Hunsperger, A. Yariv, and A. Lee, "Parallel end-butt coupling for optical integrated circuits," *Appl. Opt.*, vol. 16, pp. 1026, 1977.

[2] H. F. Lockwood, P. Haugsjaa, C. Armiento, and R. Boudreau, "Hybrid Optoelectronics Integration and Packaging," in *Optoelectronics Integration: Physics, Technology and Applications*. Norwell, MA: Kluwer Academic, 1994.

[3] T. L. Koch, U. Koren, G. Eisenstein, M. G. Young, M. Oron, C. R. Giles, and B. I. Miller, "Tapered waveguide InGasAs/InGaAsP multiple-quantum-well lasers," *IEEE Photon. Technol. Lett.*, vol. 2, pp. 88–91, 1990.

[4] R. Zengerle, H.-J. Buckner, H. W. Koops, H.-J. Olzhausen, G. Zesch, and A. Kohl, and A. Menschig, "Fabrication of optical beam width transformers for guided waves on InP using wedge-shaped taper structures" *J. Vac., Technol. B*, vol. 9, pp. 3459–3463, 1991.

[5] M. Chien, U. Koren, T. L. Koch, B. I. Miller, M. Oron, M. G. Young, and J. L. Demiguel, "Short-cavity distributed bragg reflector laser with an integrated tapered output waveguide," *IEEE Photon. Technol. Lett.*, vol. 3, pp. 418–420, 1991.

[6] Mueller, B. Stegmueller, H. Westermeire, and G. Wenger, "Tapered InP/InGaAsP waveguide structure for efficient fiber-chip coupling," *Electron. Lett.*, vol. 27, pp. 1836–1838, 1991.

[7] T. Brenner and H. Melchior, "Integrated optical modeshape adapters in InGaAsP/InP for efficient fiber-to-waveguide coupling," *IEEE Photon. Technol. Lett.*, vol. 5, pp. 1053–1056, 1993.

[8] R. Ben-Michael, U. Koren, B. I. Miller, M. G. Young, M. Chien, and G. Raybon, "InP-based multiple quantum well lasers with an integrated tapered beam expander waveguide," *IEEE Photon. Technol. Lett.*, vol. 6, pp. 1412–1414, 1994.

[9] R. Zengerle, H. J. Buckner, B. Hubner, and W. Weiershausen, "Low-loss beamwidth transformers on InP with reduced requirements on lithographic resolution," *J. Vac. Technol. B*, vol. 11, pp. 2641–2644, 1993.

[10] H. J. Bruckner, B. Mersali, S. Saison, M. Feuillade, A. Ougazzaden, Ph. Krauz, and A. Cernco, "Taper-waveguide integration for polarization insensitive InP/InGaAsP based optical amplifiers," *Electron. Lett.*, vol. 30, pp. 1290–1291, 1994.

[11] Y. Shani, C. H. Henry, R. C. Kistler, K. J. Orlowsky, and Ackerman, "Efficient coupling of a semiconductor laser to an optical fiber by means of a tapered waveguide on silicon," *Appl. Phys. Lett.*, vol. 55, pp. 2389–2391, 1989.

[12] R. N. Thurston, E. Kapon, and A. Shahar, "Two-dimensional control of mode size in optical channel waveguide by lateral channel tapering," *Opt. Lett.*, vol. 16, pp. 306–308, 1991.

[13] G. A. Vawter, R. E. Smith, B. Fuchs, J. R. Wendt, M. J. Hafich, and G. R. Hadley, *J. Lightwave Technol.*, vol. 14, pp. 169–172, 1996.

[14] G. A. Vawter, J. F. Klem, and R. A. Leibenguth," Improved epitaxial layer design for real-time monitoring of dry-etching in III-V compound heterostructures with depth accuracy of ±8 nm," *J. Vac. Sci. Technol. A*, vol. 12, pp. 1973–1977, 1994.

[15] 3M, FS-HB-6621, design wavelength = 1.3 $\mu$m.

# A Rib Optical Waveguide with Cutoff Mesa Isolation

G. Allen Vawter, *Member, IEEE,* Robert E. Smith, Beth Fuchs, Joel R. Wendt, *Member, IEEE,* Mike Hafich, and G. Ronald Hadley

***Abstract*—A rib optical waveguide using the concept of optical cutoff to provide isolation between adjacent waveguides in a photonic integrated circuit is disclosed. Due to the evanescent nature of light propagation in cutoff waveguides, this cutoff mesa rib waveguide permits fabrication of single-moded rib waveguides with minimal self-interference and crosstalk by means of light guided in a remaining slab waveguide. Design rules are given and operation of a single-moded cut-off mesa rib waveguide and an MZI using this waveguide are demonstrated.**

## I. Introduction

PHOTONIC integrated circuits (PIC's) are attractive for their potential to perform complex coherent modulation and demodulation functions, generate complex switching meshes, and fill other optical communication and signal processing functions. Most PIC applications require single-moded waveguide structures in order to meet the needs of coherent communications systems. These waveguides have typically been either strip-loaded [1], [2] (using etched or deposited ribs), deeply etched [3] or buried heterostructure designs [4]. We have designed and demonstrated a single-mode semiconductor rib optical waveguide which differs from these conventional structures. Our design uses a highly asymmetric refractive index profile outside the rib to form a cutoff slab waveguide which does not support guided slab modes unless an upper rib of cladding material is introduced to reduce the asymmetry, permitting guiding of light under the rib (Fig. 1). Conventional strip-loaded rib waveguides support guided slab modes outside the actual rib resulting in high crosstalk between adjacent guides unless deep etched isolation trenches are used. When such trenches are used these same slab modes cause self-interference, i.e., "beating" between the fundamental rib mode and higher order modes bound to the etched slab waveguide. Fig. 2 illustrates the root cause of this self-interference. Whereas the fundamental "rib" mode is seen bound to the rib of a strip-loaded waveguide, the first higher order "mesa" mode is bound by an etched mesa such as might be used to isolate one rib from the next. Light scattered out of the fundamental mode is likely to be captured by these higher order mesa modes where it is guided alongside the rib or can scatter back into the rib mode. The cutoff mesa rib waveguide is a fundamental departure from the strip-loaded rib waveguide in that the two-dimensional slab of high refractive index material forms a slab waveguide in the strip-loaded

Manuscript received May 31, 1995; revised September 25, 1995. This work was supported by the United States Department of Energy under Contract DE-AC04-94AL85000.

The authors are with Sandia National Laboratories, Albuquerque, NM 87185 USA.

Publisher Item Identifier S 0733-8724(96)01423-5.

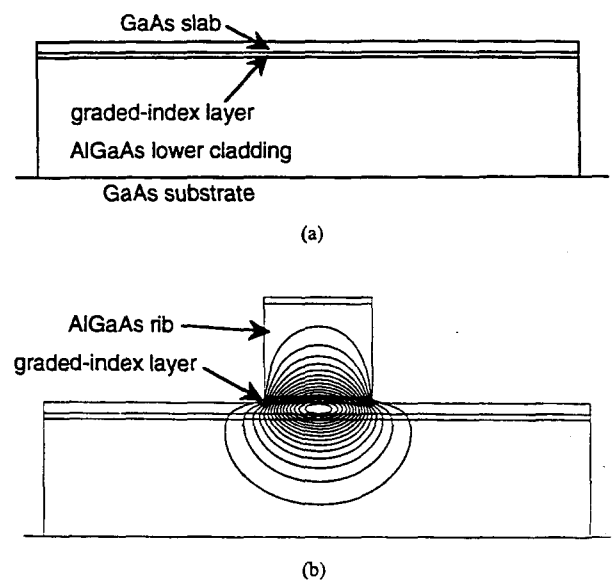


Fig. 1. (a) Cross section view of cutoff slab waveguide with etched mesa for isolation. The cutoff guide supports no guided modes. (b) Cutoff mesa with added rib of cladding material supports guided $TE_{00}$ and $TM_{00}$ modes only. Fifteen linearly spaced contours of constant electric field of the $TE_{00}$ mode are seen superimposed onto the 2 $\mu$m wide rib waveguide.

structure but is intentionally designed as a nonguiding cutoff waveguide in the cutoff mesa structure. The use of the cutoff slab eliminates self-interference and reduces crosstalk, since no slab modes are supported. With the cutoff slab in place, trenches are etched on either side of the rib to form a cutoff mesa, providing electrical isolation and simplified contacting of optical modulators. Although deeply etched heterostructure waveguides have been utilized to eliminate these same effects, etching through the pn-junction depletion region located in the waveguide core has been shown to cause material damage [5], [6] and can lead to compromised electrical and optical behavior of electrooptic modulators. Epitaxial regrowth of buried heterostructures eliminates such damage to the pn-junction, but is in general costly and impractical for AlGaAs structures.

## II. Design and Modeling of Waveguide

Design of a cutoff mesa rib waveguide begins with the design of a cutoff slab waveguide. The concept of optical cutoff is discussed in many textbooks [7]. In short, a slab waveguide with an asymmetric refractive index profile may be designed such that the transverse resonance condition can not be satisfied and no guided modes, including the $TE_0$, will propagate along the slab. The cutoff condition for the $TE_0$

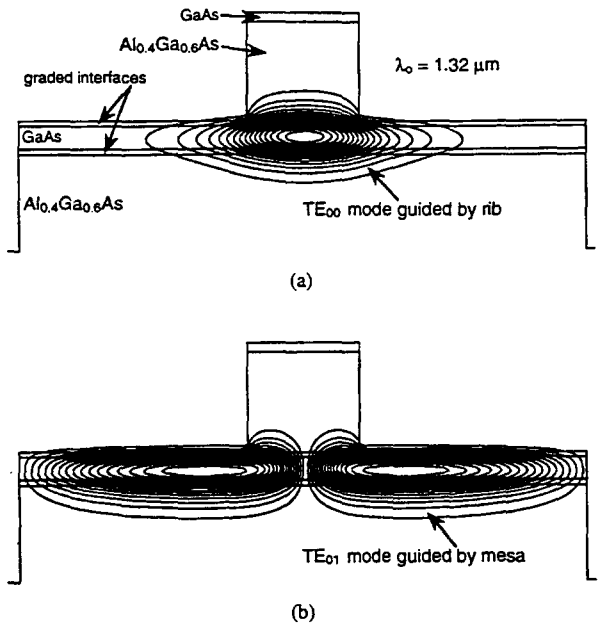


Fig. 2. Illustration of deep etched trench reflection effects in a conventional stripe-loaded rib waveguide. (a) Fundamental TE mode of single-moded rib. (b) The first of many higher-order modes induced by the mesa etch and guided coaxially with the central rib. Such high-order modes prevent effective coherent beam combining in PIC's with structures such as waveguide $y$-junctions since power meant to radiate out of the fundamental mode is captured by the mesa modes.

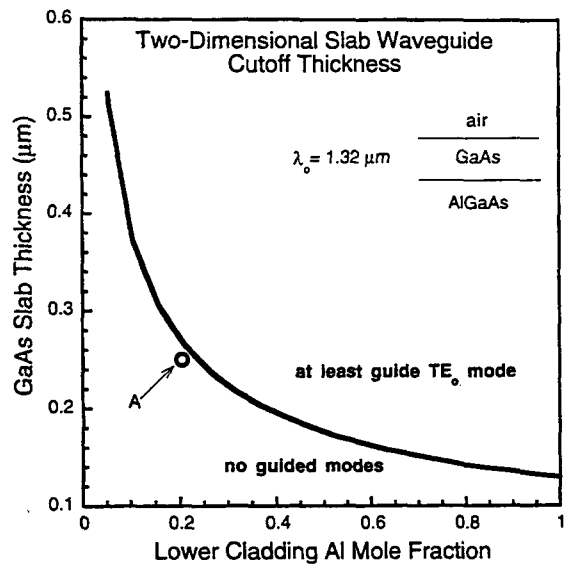


Fig. 3. Maximum thickness of a GaAs slab on AlGaAs for cutoff of optical waveguiding. Point A marks the design used in this demonstration of the cutoff mesa rib waveguide.

mode of a slab waveguide is given by

$$t_g = \frac{\tan^{-1}\sqrt{\frac{n_0^2-n_2^2}{n_1^2-n_0^2}}}{\frac{2\pi}{\lambda_o}\sqrt{n_1^2-n_0^2}} \qquad (1)$$

where $n_0, n_1$ and $n_2$ are the lower cladding, slab layer and upper cladding refractive indexes, respectively, $\lambda_o$ is the free space wavelength and $t_g$ the thickness of the slab. This relation is for the case of $n_1 > n_0 > n_2$. Using (1) a curve giving an upper limit on slab waveguide thickness as a function of $\Delta n = n_1 - n_0$ may be created. Fig. 3 shows the cutoff condition of an air/GaAs/AlGaAs slab waveguide at 1.32 $\mu$m wavelength for the $TE_0$ mode. Point A on Fig. 3 indicates the design value of an $Al_{0.2}Ga_{0.8}As$ lower cladding material under a 0.25 $\mu$m thick GaAs layer used in this first demonstration of a cutoff mesa rib waveguide.

Following the design of the cutoff slab waveguide, a rib of upper cladding material may now be designed which lies on top of the cutoff waveguide. This rib establishes both vertical and horizontal guiding of the desired optical mode. The presence of the rib allows for vertical guiding of light in the otherwise cutoff slab by reducing the asymmetry of the refractive index profile from an air/GaAs/AlGaAs structure to an AlGaAs/GaAs/AlGaAs structure so that, *under the rib*, the waveguide is no longer cutoff. Although lateral guiding does not differ significantly from standard waveguides, it is important to note that the conventional effective index method cannot be used to model the guiding properties of the cutoff mesa rib waveguide since the region outside the rib is in optical cutoff. An approximate effective index method may be used to calculate the modal index of the rib mode by setting the effective index of the slab region on either side of the rib to 1.0 [8]. However, use of this technique does not correctly predict the mode shape nor can it be used to verify (1), assuring that the remaining slab material outside the rib is cutoff and does not support higher-order guided modes. The final rib structure was designed with a personal computer using a two-dimensional iterative finite difference technique [9] to solve the 2-D vector Helmholtz equation. Since the rib waveguide design is intended for use with an electrooptic modulator, the simple air/GaAs/AlGaAs cutoff slab of 0.25 $\mu$m GaAs on $Al_{0.2}Ga_{0.8}As$ was modified by the introduction of a 0.1 $\mu$m graded interface heterojunction to reduce spikes in the conduction and valence bands and lower the device resistivity. The waveguiding behavior of a 0.25 $\mu$m GaAs layer with an abrupt interface should be essentially the same as a 0.20 $\mu$m GaAs layer with a 0.10 $\mu$m graded interface. In fact, although (1) is not valid for graded interfaces, the two-dimensional numerical model verified that the resulting slab with a graded interface was still cut off. Fig. 4 shows the cross-section of the cutoff mesa rib waveguide used for this demonstration. A contour plot of the resulting TE modal field profile is shown superimposed onto the waveguide cross section in Fig. 1(b). An essentially identical TM mode is also supported by the rib waveguide. No higher order modes of any sort are guided by the rib and cutoff mesa structure.

Elimination of the self-interference effect was investigated theoretically using three-dimensional BPM methods. A variety of centered and offset Gaussian TE excitation fields were launched in the structure described in Fig. 4 and the optical power distribution observed as the light propagated along the guide. In all cases a portion of the input optical power coupled into the $TE_{00}$ rib mode while the remainder radiated away from the rib. All radiated power left the modeled region through transparent boundary conditions resulting in a decay of the total power in the structure until all the power was in the $TE_{00}$ mode. No light remained guided by the mesa. The BPM model

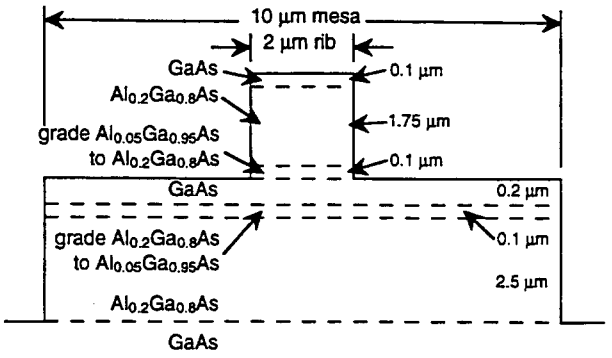


Fig. 4. Schematic cross-section diagram of the complete cutoff mesa rib waveguide.

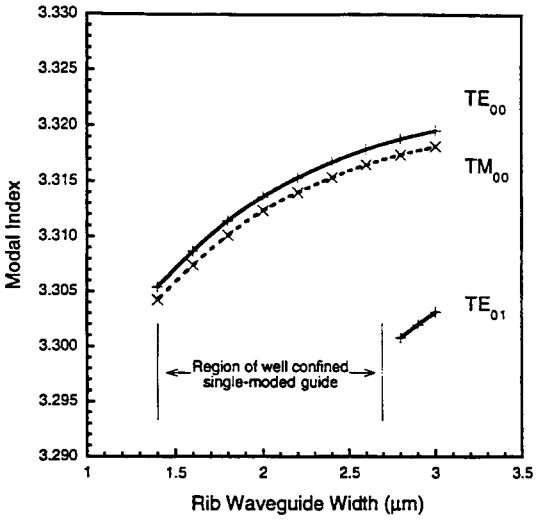


Fig. 5. Simulated modal index of the three lowest-order guided modes of the cutoff mesa rib waveguide as the rib width is varied from 1.4 to 3.0 $\mu$m.

suggests a typical decay length (propagation length needed to stabilize the guided power) of approximately 500 $\mu$m for gaussian input fields with 0.5 to 0.75 $\mu$m $1/e$ radius laterally offset by 0.1 $\mu$m.

Simulated modal indexes of the $TE_{00}$, $TM_{00}$ and $TE_{01}$ guided modes for the structure of Fig. 4 with various rib widths are shown in Fig. 5. Higher-order modes do not become guided until the rib width exceeds ~2.7 $\mu$m where the $TE_{01}$ mode becomes well confined. In these simulations a well confined mode is one which is fully confined within the waveguide structure using a 3.5 $\mu$m thick lower cladding layer. Modes whose field profiles extend beyond a 3.5 $\mu$m thick cladding are expected to radiate strongly into the GaAs substrate of the actual structure where a 2.5 $\mu$m thick lower cladding is used. The useful region of single-moded rib waveguide width extends from an upper limit of ~2.7 $\mu$m where the guide becomes multimoded, to a lower limit of 1.4 $\mu$m where the fundamental mode begins to penetrate quite far into the lower cladding layer and is no longer considered well-confined. In a similar fashion, the waveguide has been shown to exhibit single-mode behavior over a wide range of rib etch depths from well into the lower cladding to 0.14 $\mu$m above the designed etch endpoint at the upper interface of the GaAs waveguide layer. In the shallow etch limit the mesa becomes guiding and supports high-order modes. Preservation of single-moded behavior for deep rib etches below the actual waveguide layer is a consequence of our particular choice of rib width and material composition, not a feature of cutoff mesa rib waveguides in general. For example, increasing the rib width to 2.5 $\mu$m gives a waveguide which is single-moded for rib etches the same depth as Fig. 4 but multimoded for ribs extending into the lower cladding.

## III. Experimental Fabrication and Test

To demonstrate operation of the cutoff mesa rib waveguide, straight waveguides and Mach-Zehnder interferometers (MZI) using GaAs/AlGaAs rib waveguides identical to Fig. 4 were fabricated and tested with TE polarized, 1.32 $\mu$m wavelength light. Epitaxial layers were grown using molecular-beam epitaxy. The upper and lower cladding layers were doped $p$ and $n$-type respectively so that 2 mm long reverse-biased pn-junction phase modulators [10] could be used for MZI modulation and waveguide loss measurements, using the Fabry-Perot interference method [11]. MZI's used 4° included angle $Y$-type optical power splitters, $XY$-type power combiners [12] and 2 mm radius waveguide bends. Ribs for both straight waveguides and MZI's were fabricated using direct-write electron-beam lithography and chlorine reactive-ion-beam etching (RIBE) [13]. Mesas were patterned using optical contact printing and etched by chlorine RIBE.

Waveguides and MZI's were tested using uncoated cleaved facets and end-fire coupling of light from a diode pumped YAG ring laser at 1.32 $\mu$m wavelength. The waveguides are single-moded with no evidence of mesa modes. Attempts were made to launch mesa modes by misalignment of the $NA = 0.85$ lens used to couple light into the waveguide. Such misalignment led only to extinction of the observed $TE_{00}$ mode. Measured loss is $0.26 \pm 0.07$ dB/mm assuming a facet reflectivity of $0.32 \pm 0.02$. Loss is limited by scattering at process-induced defects and by free-carrier absorption [14] resulting from the doped pn-junction. Simulations including the effects of free-carriers due to impurity doping show that the lower limit of absorption due to free-carriers is 0.05 dB/mm. MZI's have on-off contrast ratios as high as 14 dB, as seen in Fig. 6. It is believed that the contrast ratio is limited by process-induced asymmetry in the $y$-splitter.

## IV. Conclusion

In conclusion, a new cutoff mesa rib waveguide has been designed and demonstrated. Using the principal of the cutoff slab waveguide, this waveguide provides single-mode performance regardless of any deep etches that might be used for electrical isolation between integrated electrooptic devices. Single-mode operation is achievable with a wide range of rib widths and does not require demanding etch depth tolerances. Stable single-moded cutoff mesa waveguides with low propagation loss and MZI's with 14 dB contrast have been demonstrated in GaAs/AlGaAs. This new waveguide design eliminates reflection effects, or self-interference, commonly seen when rib waveguides are combined with deep isolation etches and

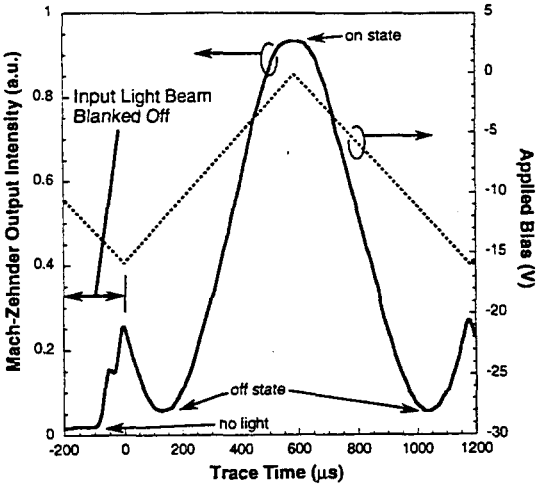


Fig. 6. Modulation characteristics of MZI fabricated with cutoff mesa rib waveguide. The modulator is being driven beyond the "off" state to −16 V applied bias in order to clearly measure the modulation depth.

is expected to dramatically reduce crosstalk compared to conventional rib waveguides.

## REFERENCES


[1] H. Takeuchi and K. Oe, "Low-loss single-mode GaAs/AlGaAs miniature optical waveguides with straight and bending structures," *J. Lightwave Technol.*, vol. 7, pp. 1044–1054, July 1989.

[2] G. Wenger, L. Stoll, B. Weiss, M. Schienle, R. Muller-Nawrath, S. Eichinger, J. Muller, B. Acklin, and G. Muller, "Design and fabrication of monolithic optical spot size transformers (MOST's) for highly efficient fiber-chip coupling," *J. Lightwave Technol.*, vol. 12, pp. 1782–1790, Oct. 1994.

[3] C. T. Sullivan, S. D. Mukherjee, M. K. Hibbs-Brenner, A. Gopinath, E. Kalweit, T. Marta, W. Goldberg, and R. Walterson, "Switched time delay elements based on AlGaAs/GaAs optical waveguide technology at 1.32 $\mu$m for optically controlled phased array antennas," in *Optic. Technol. Microwave Appl. VI and Optoelectron. Signal Processing for Phased-Array Antennas III Proc. SPIE*, 1992, vol. 1703, pp. 264–271.

[4] Y. Shani, U. Koren, B. Miller, M. Young, M. Oron, and R. Alferness, "Buried rib passive waveguide Y junctions with sharp vertex on InP," *IEEE Photon. Technol. Lett.*, vol. 3, pp. 210–212, Mar. 1991.

[5] A. C. Papadopoulo, C. Dubon-Chevallier, J. F. Bresse, A. M. Duchenois, and F. Heliot, "Etching procedures of GaAs: Cathodoluminescence study of the induced damages and of the recovering techniques," *J. Vac. Sci. Technol. B*, vol. B8, pp. 407–412, May/June 1990.

[6] A. Scherer, H. G. Craighead, M. L. Roukes, and J. P. Harbison, "Electrical damage induced by ion beam etching of GaAs," *J. Vac. Sci. Technol. B*, vol. 6, pp. 277–279, Jan./Feb. 1988.

[7] H. Kogelnik, "Theory of optical waveguides," in *Guided-Wave Optoelectronics*, T. Tamir Ed. New York: Springer-Verlag, 1988, p. 15.

[8] M. W. Austin, "GaAs/GaAlAs and $n/n+$ GaAs rib waveguides; variational analysis and experimental study," *J. Lightwave Technol.*, vol. LT-2, pp. 688–694, Aug. 1985.

[9] G. R. Hadley and R. E. Smith, "Full-vector waveguide modeling using iterative method with transparent boundary conditions," *J. Lightwave Technol.*, vol. 13, pp. 465–469, Mar. 1995.

[10] J. G. Mendoza-Alverez, L. A. Coldren, A. Alping, R. H. Yan, T. Hausken, K. Lee, and K. Pedrotti, "Analysis of depletion edge translation lightwave modulators," *J. Lightwave Technol.*, vol. 6, pp. 793–808, June 1988.

[11] R. G. Walker, "Simple and accurate loss measurement technique for semiconductor optical waveguides," *Electron. Lett.*, vol. 21, pp. 581–582, 1985.

[12] G. A. Vawter, G. R. Hadley, J. R. Wendt, and J. F. Klem, "An integrated optical $X$-$Y$ coupler for phase-sensitive optical power combining and suppression of radiated light," *IEEE Photon. Technol. Lett.*, vol. 7, pp. 394–396, Apr. 1995.

[13] G. A. Vawter, J. F. Klem, and R. A. Leibenguth, "Improved epitaxial layer design for real-time monitoring of dry-etching in III–V compound heterostructures with depth accuracy of ±8 nm," *J. Vac. Sci. Technol. A*, vol. 12, pp. 1973–1977, July/Aug. 1994.

[14] R. G. Hunsperger, *Integrated Optics: Theory and Technology*, Springer Series in Optical Sciences, T. Tamir, Ed. New York: Springer-Verlag, 1982, vol. 33, p. 78.


**G. Allen Vawter** (S'86–M'87) received the B.S., M.S., and Ph.D. degrees in electrical engineering from the University of California, Santa Barbara in 1982, 1983, and 1987, respectively.

During his graduate work at the University of California, he studied reactive-ion-etching of GaAs/AlGaAs laser diode facets and integration of laser diodes into waveguide circuits. He then joined Sandia National Laboratories, Albuquerque, NM, and is currently a Senior Member of Technical Staff. His research interests include design and fabrication of diode lasers and optoelectronic integrated circuits in III-V compound semiconductors as well as application of reactive-ion-beam etching in the fabrication of novel optoelectronic devices.

Dr. Vawter is a member of Tau Beta Pi, Eta Kappa, Nu, and the American Vacuum Society.

**Robert E. Smith**, photograph and biography not available at the time of publication.

**Beth Fuchs** received the Bachelor of Engineering degree with a specialization in microelectronics processing from the University of New Mexico in 1987.

She is currently a microelectronic research engineer with Ktech Corporation on contract to Sandia National Laboratories.

Ms. Fuchs is a member of the Americal Vacuum Society and is currently listed in Who's Who of American Women and Who's Who in Science and Engineering.

**Joel R. Wendt** (S'81–M'87) received the B.S.E.E. degree (*magna cum laude*) from Washington University, St. Louis, MO, in 1982, and the Ph.D. degree in electrical engineering from Cornell University, Ithaca, NY, in 1988. His Ph.D. research was concerned with the design, fabrication, and testing of submicron vertical field effect transistors for the study of ballistic transport.

He joined Sandia National Laboratories, Albuquerque, NM, in 1988, and is currently a Senior Member of Technical Staff in the Compound Semiconductor Technology Department. Current work involves the application of electron beam lithography to the fabrication of micro-optics and photon devices.

**Mike Hafich**, photograph and biography not available at the time of publication.

**G. Ronald Hadley**, photograph and biography not available at the time of publication.

# An Integrated Optical XY Coupler for Phase-Sensitive Optical Power Combining and Suppression of Radiated Light

G. Allen Vawter, *Member, IEEE*, G. Ronald Hadley, *Senior Member, IEEE*, Beth Fuchs, Joel R. Wendt, *Member, IEEE*, and John F. Klem, *Member, IEEE*

*Abstract*—**We have designed and fabricated a new type of XY coupler for phase-sensitive combining of coherent light in waveguide PIC's. The XY coupler uses two input waveguides and couples in-phase light into the middle of its three output waveguides. Out-of-phase light is coupled into the two outer waveguides. 15.5-dB extinction ratio is demonstrated in a Mach–Zehnder interferometer using this new XY coupler. Switching from the inner to the outer waveguides at the output is also demonstrated.**

## I. Introduction

MACH–ZEHNDER interferometers (MZI's) are extremely valuable for use in photonic integrated circuits (PIC's) for intensity modulation of light. However, in a conventional MZI with a Y-type waveguide power combiner at the output end, on-state light travels out of the MZI output waveguide but off-state light is forced to couple into radiation modes, contributing to crosstalk. Directional couplers [1] and multimode interference sections [2] have been used to switch the off-state light into a separate waveguide. However, these structures are fairly large and intolerant of process-induced dimensional variations. We have developed a new type of XY coupler [3] capable of capturing *out of phase* light into guided modes such that this light may be removed from the PIC in a desirable manner or actually used by other portions of the PIC. The XY coupler does not use relative phase-velocity differences between orthogonal modes of one or more waveguides, and so can be made relatively compact and does not have challenging dimensional tolerance requirements.

Single-mode Y-junction poewer combiners radiate light that is mutually $\pi$ radians out of phase in the two input waveguides. When etched-rib waveguides are used, this radiated light is forced to couple into either substrate modes, air modes, or one-dimensionally guided slab-waveguide modes supported by high-refractive-index material remaining at the upper surface of the semiconductor after the etched rib is formed. The bulk of the light radiated out of the rib waveguide couples into the slab waveguide, if present, allowing for crosstalk between adjacent waveguides.

Manuscript received September 14, 1994; revised December 16, 1994. This work was supported in part by the United States Department of Energy under Contract DE-AC04-94AL85000.

The authors are with Sandia National Laboratories, Albuquerque, NM 87185-0603 USA.

IEEE Log Number 9409253.

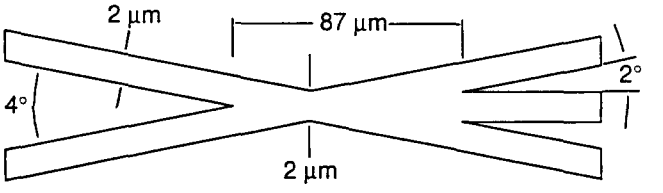


Fig. 1. Top-view schematic of a rib-waveguide XY-coupler. Light is input from the two waveguides on the left and leaves the coupler from the three waveguides on the right.

In order to eliminate the slab waveguide crosstalk problems of the Y-junction combiner without suffering the tight dimensional requirements of either directional couplers or multimode interference couplers, we have developed the XY coupler. As shown in Fig. 1, the XY coupler resembles a pair of crossed waveguides with an added waveguide exiting the crossing point along the symmetry axis. The on-axis output guide accepts in-phase light from the two input guides while the two off-axis output guides accept the out-of-phase light. The rib waveguide was designed using an iterative two-dimensional finite difference method [4]. Rib composition, width, and etch depth were chosen to provide single-mode operation of the waveguide. The rib waveguide comprised a 420–nm GaAs layer placed between 100-nm $Al_{0.05}Ga_{0.95}As$-to-$Al_{0.4}Ga_{0.6}As$ graded layers and $Al_{0.4}Ga_{0.6}As$ cladding. 2–$\mu$m-wide ribs were etched down to the bottom of the upper cladding layer. The XY coupler was designed using two-dimensional effective index beam propagation method (BPM) modeling with strict power conservation and transparent boundary conditions. Modal index of the rib waveguide obtained using the effective index BPM model differed from the two-dimensional finite-difference technique by only $1.2 \times 10^{-3}$, thus confirming the validity of the model. Fig. 2 shows results of the BPM modeling of the XY coupler. In the figure, adding a $\pi$ phase difference between the input guides is seen to switch the output from the middle to the outer waveguides. The XY coupler has a theoretical contrast ratio in the side output waveguides of $-8.07$ dB and an insertion loss to the middle and side output waveguides of $-1.09$ and $-0.28$ dB, respectively. Calculated contrast ratio of the middle output waveguide is infinite due to the perfectly antisymmetric input conditions used in the "off" state.

At the center of the crossing section of the XY-coupler, the rib structure supports only a single guided mode. As a result,

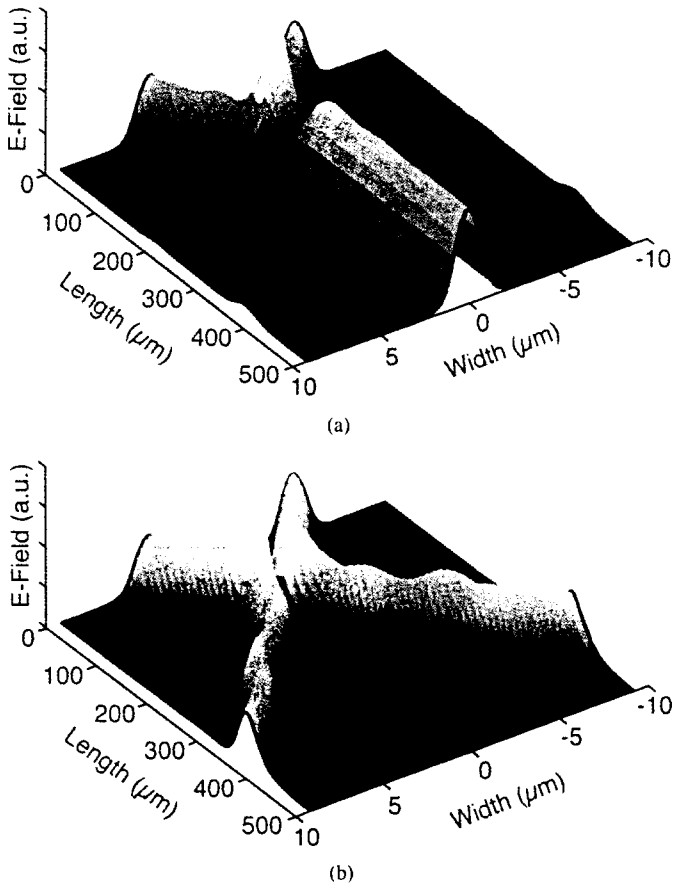


Fig. 2. Results of two-dimensional effective-index beam propagation analysis for a waveguide XY-coupler fabricated using the design of Fig. 1. (a) With the two input waveguides carrying in-phase light, nearly all of the input couples into the output waveguide. (b) When the two input signals are out of phase, nearly all of the light couples into the outer pair of waveguides.

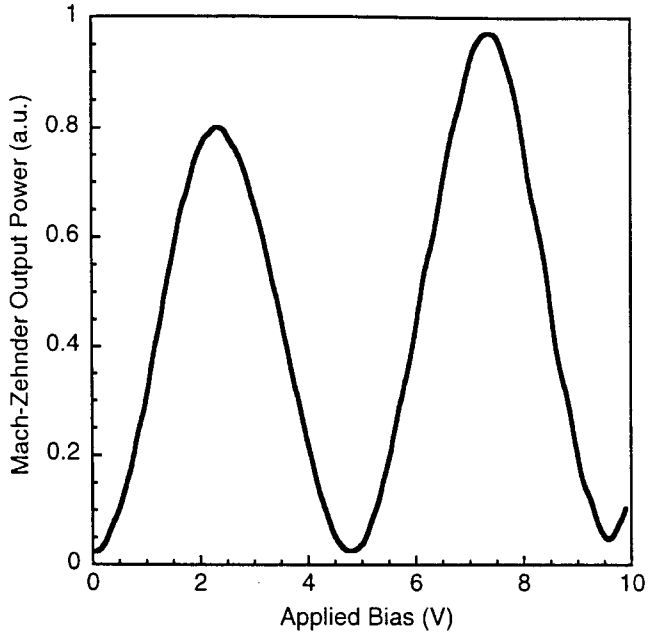


Fig. 3. Measured modulation performance of an integrated rib waveguide MZI with an XY-coupler as the optical power combining element at the output of the two Mach–Zehnder arms. Modulation depth is 15.5 dB with an applied bias swing of only 2.6 V. The increased output signal at high applied bias is due to the improved transparency of the depletion-edge translation phase modulator used in the Mach–Zehnder.

anti-symmetric modes excited by out-of-phase light from the input guides are forced to radiate into the outer waveguides at the waist of the coupler. It is the single-mode behavior at the coupler waist that both forces out-of-phase light into the outer waveguides and makes the XY-coupler comparatively easy to fabricate, as compared to directional couplers and lateral-mode interference devices, since only the maximum waveguide width is constrained. However, in practice the minimum guide width will be determined by factors external to coupler operation, such as desired mode shape and quality.

To demonstrate operation of the XY-coupler, MZI's were fabricated using GaAs–AlGaAs rib waveguides and tested with TE-polarized, 1.32-$\mu$m wavelength light. Optical power splitting at the input end of the Mach–Zehnder was achieved using a simple four-degree included-angle waveguide Y-junction. Phase modulation within the two arms of the MZI was obtained using two-millimeter-long integrated depletion-edge-translation waveguide phase modulators [5]. All waveguide structures were fabricated in a single etch step using direct-write electron-beam lithography and chlorine reactive-ion-beam etching [6]. MZI's were built both with and without the outer waveguides extending to the cleaved output edge of the device. Extending the outer waveguides to the output cleave allowed for measurement of optical switching from the inner to the outer guides while terminating the outer waveguides at an etched 45° mirror prior to the cleave simplified fiber coupling of the MZI for operation as a conventional two-port modulator. However, sufficient length of outer waveguide was left in place to ensure that the inner and outer waveguides were fully decoupled at the point of termination. As control devices, standard MZI's with conventional Y-junction power combiners were fabricated on the same chip using the identical waveguide design as the XY-coupler MZI's and a four-degree included angle at the output Y-combiner. Total length of the integrated MZI's was only 4.3 mm.

Completed MZI's with the XY-coupler showed a 15.5-dB modulation depth with a 2.6-V bias swing on one arm of the MZI (Fig. 3). Data in Fig. 3 are from an MZI with terminated outer waveguides. The limitation on the modulation depth appears to be a small amount of optical power coupled into a $TE_{01}$ mode in the central output waveguide. Measurements of straight waveguides adjacent to the MZI's indicated that the waveguides, as fabricated, support both the $TE_{00}$ and $TE_{01}$ modes. This is most likely due to a slight overetch of the rib waveguide. The presence of a double-moded rib waveguide implies that the waist of the XY coupler is also double-moded, allowing for enhanced coupling of out-of-phase light into the central output waveguide. Measured insertion loss of the XY-coupler was $-2.8$ dB while insertion loss of the Y-junction splitter was measured at $-2.3$ dB. The actual insertion loss of the XY-coupler is 1.71 dB greater than the calculated value. This additional XY-coupler insertion loss is likely due to scattering at imperfections within the coupler. Straight waveguide propagation loss was measured to 1.9 $cm^{-1}$ using the Fabry–Perot interference technique and an assumed facet reflectivity of 0.32.

Testing of the control MZI's with a conventional Y-junction output coupler showed very little actual output power modu-

lation. These devices functioned as mode converters with the output light switching from $TE_{00}$ to $TE_{01}$ with a 2.6-V applied bias swing. This mode-switching behavior is expected with double-moded rib waveguides, due to the efficient coupling of out-of-phase input light into odd symmetry output light. It is of greater interest that the XY coupler demonstrates better than 15 dB modulation with the same double-moded waveguides. Clearly, the XY configuration is an effective mode filter, switching $TE_{01}$ light to the outer waveguide pair while placing $TE_{00}$ light in the central guide.

Switching behavior of the XY-coupler was examined using devices with all three waveguides continued out to the cleaved output edge. Ideally, power in the two outer guides switches nearly inversely with power in the middle guide. Fig. 4 (top) shows BPM simulations of the relative power in each waveguide versus applied bias to the MZI. The two outer arms are predicted to carry maximum power at close to the same voltage, peaking at roughly 40% of the maximum power carried in the middle waveguide. The slightly asymmetric switching behavior of the two outer output arms is caused by multimode propagation within portions of the XY coupler. Since the crossed waveguide structure is only single-moded near the coupler waist, a relative phase difference slightly less (or greater) than 90° between the two input arms can preferentially excite a combination of modes within the XY-coupler that will couple relatively more light into the one of the outer exit guides as compared to the other. The slight difference in height of the curves for the outer arms is due to accumulated numerical error. Measured switching behavior is shown in Fig. 4 (bottom). Although Fig 4 (bottom) does show strong switching behavior, the outer guides do not switch as closely together as we expect from the simulation and all three waveguides carry close to the same peak power. We believe that this is a consequence of the unintended double-moded waveguide system. In the double-moded XY-coupler, the MZI excites linear combinations of $TE_{00}$ and $TE_{01}$ modes that remain guided throughout the length of the device, such that the phase velocity difference between these two modes will influence the output coupling. The reduced modulation depth of this device compared to the MZI of Fig. 3 is due to process-induced asymmetry at the Y-splitter.

This first fabrication of an XY coupler demonstrates its utility as a waveguide power combiner and phase-sensitive switch, as evidenced by its good modulation behavior. It further shows excellent tolerance to process-induced dimensional variations, as demonstrated by the preservation of 15.5-dB modulation even though a slight overetch of the rib resulted in double-moded waveguides. For future work, we are designing a new rib waveguide for use with the XY-coupler. This new design is intended to place the $TE_{01}$ mode much further into cut-off, allowing for single-mode waveguides to be fabricated with more relaxed processing constraints.

## II. Conclusion

We have designed and fabricated a new type of XY coupler for phase-sensitive combining of coherent light in waveguide PIC's. The XY-coupler uses two input waveguides and couples in-phase light into the middle of its three output waveguides. Out-of-phase light is coupled into the two outer waveguides. We have demonstrated 15.5-dB extinction ratio in an MZI using this new XY coupler as the optical power combining element. Switching from the inner to the outer waveguides at the output is demonstrated but shows limited extinction and asymmetry caused by double-moded waveguides. Although an MZI circuit has been used to demonstrate operation of the XY coupler, it is suitable for integration into a wide variety of PIC's where phase-sensitive coherent power combining of light is needed but where generation of radiated light resulting from destructive interference is not desired.

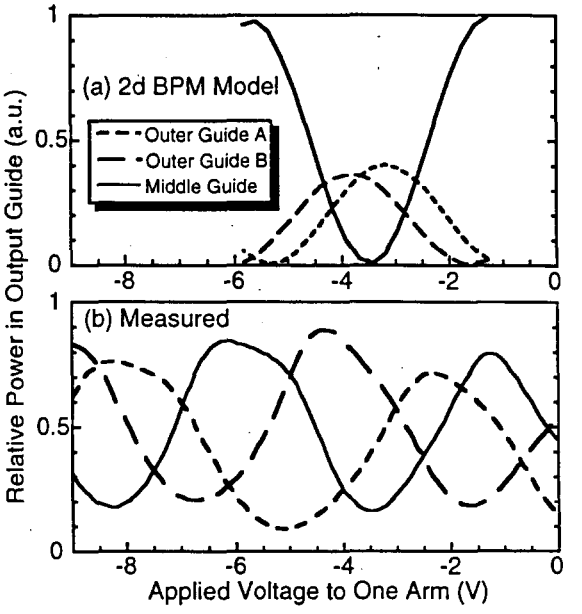


Fig. 4. Optical power in each arm of the XY-coupler as a function of bias applied to one arm of the Mach–Zehnder: (top) Two-dimensional BPM model results. (bottom) Measured data. Switching between the three waveguides is clearly seen.

## References


[1] R. G. Walker, "High-speed III–V semiconductor intensity modulators," *IEEE J. Quantum Electron.*, vol. 27, pp. 654–667, 1991

[2] E. Pennings, R. Deri, A. Scherer, R. Bhat, T. Hayes, and N. Andreadakis, "Ultracompact, low-loss directional couplers on InP based on self-imaging by multimode interference," *Appl. Phys. Lett.*, vol. 59, pp. 1926–1928, 1991.

[3] G. A. Vawter, G. R. Hadley, J. R. Wendt, and J. F. Klem, "An integrated optical X-Y coupler for phase-sensitive optical power combining and suppression of radiated light," in *Conf. Lasers Electro-Optics*, vol. 8, *1994 OSA Technical Digest Series*. Washington, DC: Optical Society of America, 1994, p. 76.

[4] G. R. Hadley and R. E. Smith, "Full-vector waveguide modeling using iterative method with transparent boundary conditions," *IEEE J. Lightwave Technol.*, in press.

[5] J. G. Mendoza-Alverez, L. A. Coldren, A. Alping, R. H. Yan, T. Hausken, K. Lee, and K. Pedrotti, "Analysis of depletion edge translation lightwave modulators," *IEEE J. Lightwave Technol.*, vol. 6, pp. 793–808, 1988.

[6] G. A. Vawter, J. F. Klem, and R. A. Leibenguth, "Improved epitaxial layer design for real-time monitoring of dry-etching in III–V compound heterostructures with depth accuracy of ±8 nm," *J. Vac. Sci. Technol. A*, vol. 12, pp. 1973–1977, 1994.

# ATTENUATION LOSSES IN ELECTRON CYCLOTRON RESONANCE PLASMA ETCHED AlGaAs WAVEGUIDES

R. J. SHUL[1], C. T. SULLIVAN[1], M. B. SNIPES[1], G. B. McCLELLAN[1], M. HAFICH[1], C. T. FULLER[1], C. CONSTANTINE[2], J. W. LEE[3] and S. J. PEARTON[3]

[1]Sandia National Laboratories, Division 1322, Albuquerque, NM 87185, [2]Plasma-Therm IP, St. Petersburg, FL 33716 and [3]Department of Materials Science and Engineering, University of Florida, Gainesville, FL 32611, U.S.A.

*(Received 27 December 1994; in revised form 19 February 1995)*

**Abstract**—AlGaAs/GaAs ridge waveguides with fundamental mode attenuation $\leqslant 1\ dBcm^{-1}$ at a wavelength of 1.32 $\mu$m and channel widths of 4–4.5 $\mu$m are realized by ECR (Electron Cyclotron Resonance) plasma etching in $BCl_3/Cl_2/Ar/N_2$ chemistries. The choice of both plasma chemistry and initial mask scheme (single layer photoresist or trilevel resist) has a significant effect on the attenuation losses.

## INTRODUCTION

Index-guided III–V semiconductor lasers are used for applications ranging from laser printers and compact disk players to fiber-optic communications [1]. To reduce the current threshold for lasing, smaller active widths are necessary. Accordingly, there is much interest in developing anisotropic dry etching processes which have the capability for much higher fidelity pattern transfer than the more common wet etching techniques[2–10]. There is also a requirement for low ion energies in the plasmas used for dry etching in order to avoid creation of non-radiative damage centers in the active layer and to minimize sputter-erosion of the masking material. The former situation reduces the output power of the laser and degrades its lifetime, whereas the latter leads to uncontrolled sidewall angles on the etched features[11].

In this paper we report on fundamental mode attenuation in AlGaAs/GaAs/AlGaAs waveguide structures etched under Electron Cyclotron Resonance (ECR) conditions in a novel $BCl_3/Cl_2/N_2/Ar$ chemistry, using either a single layer thick photoresist mask, or a trilevel scheme. Measured mode attenuations of $\leqslant 1\ dBcm^{-1}$ at 1.32 $\mu$m wavelength are found for channel widths of ~4–4.5 $\mu$m using either masking scheme, provided the plasma chemistry is optimized.

## EXPERIMENTAL

A typical waveguide structure consisted of 4.0 $\mu$m of $Al_{0.04}Ga_{0.96}As$ bottom clad layer, ·2.0 $\mu$m GaAs guide and 0.5 $\mu$m $Al_{0.04}Ga_{0.96}As$ top clad layer, grown on semi-insulating GaAs substrates by Molecular Beam Epitaxy (MBE). All layers were undoped in this experiment. The targeted etch depth for this structure was 3.0 $\mu$m. A schematic of the waveguide is shown in Fig. 1. The individual etch rates for GaAs and AlGaAs were determined on separate single-layers, also grown on GaAs. The waveguides were patterned either with a single layer of AZ P4620 photoresist ~7 $\mu$m thick, or with a trilevel scheme consisting of a 1.1 $\mu$m thick bottom layer (OCG 875-20CS photoresist) hard baked at 200°C/3 h, a 500 Å e-beam evaporated Ti transfer layer, and a 1.5 $\mu$m thick imaging resist (AZ5214). The trilevel mask was opened by a sequence of $Cl_2$ and $O_2$ reactive ion-beam plasma etching steps. The channel width was varied from ~3 to 10 $\mu$m and was directly measured by SEM. The range of channel widths for singlemode propagation at 1.3 $\mu$m was 3–4.4 $\mu$m with this waveguide design. The 10 $\mu$m-wide channels had measured attenuations of $0.8 \pm 0.2$ dB/cm which we attribute primarily to scattering in the as-grown planar epilayer materials. The increased losses for the narrower single channel widths are primarily attributable to sidewall scattering caused by the channel masking and etching processes. The advantage of the single-layer resist scheme is its simplicity, however the required resist thickness limits the resolution of the lithography process and therefore the minimum channel width obtainable. The trilevel scheme is more complex but is capable of much higher resolution ($\leqslant 1$ $\mu$m) if very narrow laser stripes are required[12]. Dry etching was performed in a Plasma-Therm SLR 770 system utilizing a 2.45 GHz ECR electromagnet source and separate r.f. (13.56 MHz) biasing on the sample.

## RESULTS AND DISCUSSION

The etch rates of GaAs and $Al_xGa_{1-x}As$ ($x$ up to 0.3) were found to be identical in $BCl_3$-containing

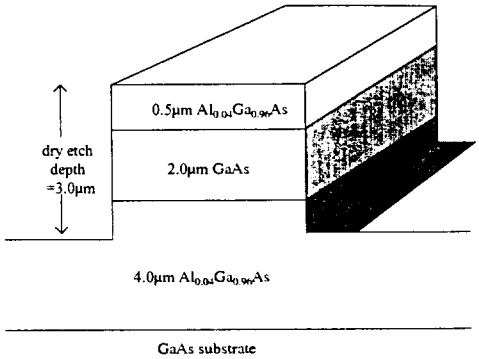


Fig. 1. Schematic of the AlGaAs/GaAs waveguide.

plasmas, whereas the etch rates were slower for AlGaAs in $Cl_2$-based mixtures. This is due to the ability of $BCl_3$ to etch aluminium oxides and to getter water vapor in the chamber, which minimizes reoxidation of the exposed AlGaAs during etching[13–15]. Figure 2 shows the GaAs/AlGaAs etch rate in 10 $BCl_3$/40Ar (total flow rate 50 sccm) discharges at 1 mtorr, 10°C (controlled by clamping and backside cooling) and 850 W microwave power, as a function of applied r.f. power. The etch rate is linearly dependent on r.f. power, suggesting that ion-induced sputter deposition of the etch products is the limiting step. The selectivity over photoresist is such that $\sim 1\,\mu$m of resist is lost during etching of the waveguide.

We noticed that the etching was highly anisotropic at microwave powers $\leqslant 850$ W in $BCl_3$/Ar, but that lateral etching was present for higher powers. To avoid this undercut one can either substantially reduce the sample temperature, or provide a sidewall protection mechanism. Addition of $N_2$ can be used to intentionally degrade resist in $Cl_2$-plasma chemistries for sidewall polymer protection. We found with $BCl_3$ this was much more controllable, probably due to the reduced free chlorine radical density available to degrade the resist. The $N_2$ addition is very helpful in producing a wider window for anisotropic etching, and in our case addition of 2 sccm led to very straight sidewalls even at microwave powers up to 1250 W (Fig. 3). It also means that $Cl_2$ can be added to the plasma chemistry to increase the GaAs/AlGaAs etch rate (typically by at least 50%) without causing undercut of the waveguide sidewalls.

Waveguides were etched using either $BCl_3/Ar/N_2$ (flow rates 10/40/2 sccm) or $BCl_3/Cl_2/Ar/N_2$ (flow rates 5/5/40/2 sccm) ECR plasmas at 1 mtorr, 10°C, 75 W r.f. power ($\sim 50$ V d.c.) and 850 W microwave power. The fundamental mode attenuation was obtained by Fabry–Perot interferometry at 1.32 $\mu$m wavelength assuming a calculated modal reflectivity of 0.296[16]. Figure 4 shows that the waveguides patterned with the trilevel mask have lower mode attenuation when etched with the $BCl_3/Ar/N_2$ chemistry, while the reverse is true when $BCl_3/Cl_2/N_2/Ar$ is employed (Fig. 5). We expect the differences in the loss of guided wave intensity are due to variations in waveguide sidewall roughness. For example, a linearly polarized wave encountering a bend or angle

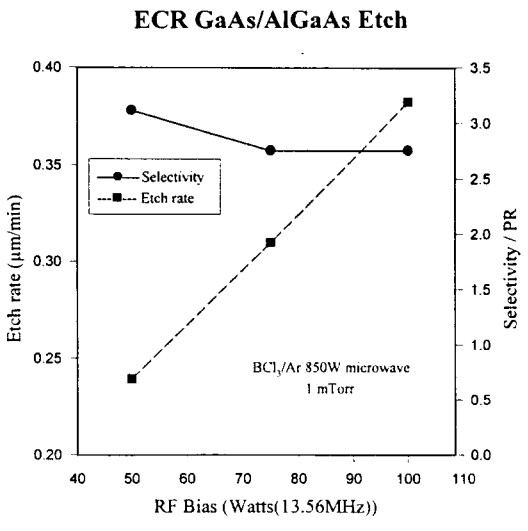


Fig. 2. Etch rates for $Al_xGa_{1-x}As$ ($x = 0$–0.8) and selectivity over photoresist in $BCl_3$/Ar plasmas/850 W microwave power, 1 mtorr, as a function of r.f. power.

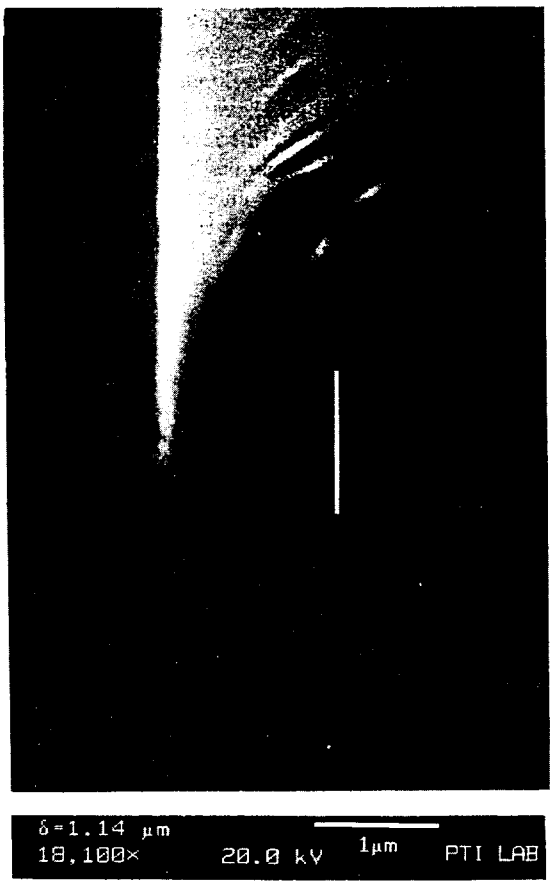


Fig. 3. SEM micrograph of multi-layer AlGaAs/GaAs structure etched in $BCl_3/N_2/Ar$ with a resist mask which is still in place.

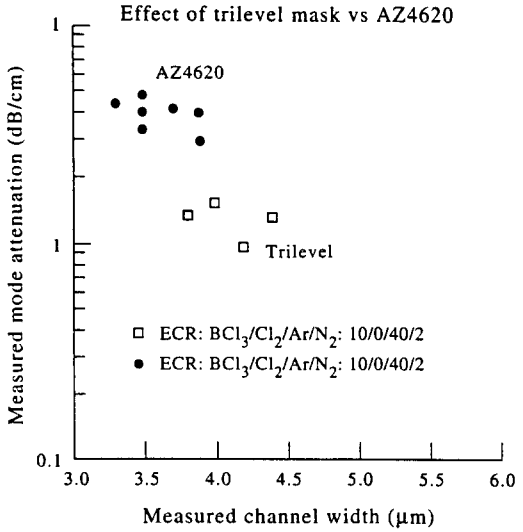


Fig. 4. Fundamental mode attenuation as a function of channel width for $Al_xGa_{1-x}As$ waveguides etched in $BCl_3/N_2/Ar$ using either single layer resist or trilevel resist masks.

when propagating down a waveguide will suffer a 3 dB attenuation for an angle of[17]:

$$\phi_{3dB} = 1.42\lambda/n_f b,$$

where $\lambda$ is the waveguide of the propagating wave, $n_f$ is the refractive index of the guiding medium and $b$ is channel width. Under our conditions, such a 3 dB attenuation would occur if an angle of $\sim 2.5°$ were present. Equivalent attenuation could be produced by sidewall corrugations and other forms of microroughness resulting from the particular etch chemistry employed, and the initial smoothness of mask edges. In our case it is found that the choice of both etch chemistry and mask material can make significant differences in waveguide quality. The sidewall protection mechanism with $BCl_3/N_2/Ar$ is most effective with the trilevel mask, whereas when $Cl_2$ is added to increase etch rates, the AZ4620 resist mask produces better results.

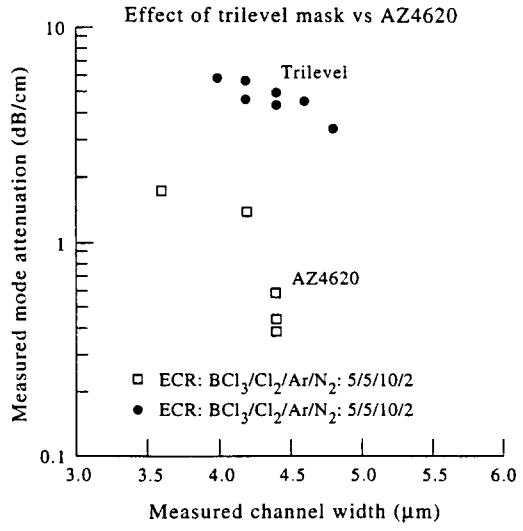


Fig. 5. Fundamental mode attenuation as a function of channel width for $Al_xGa_{1-x}As$ waveguides etched in $BCl_3/Cl_2/N_2/Ar$ using either single layer resist or trilevel resist masks.

## SUMMARY AND CONCLUSIONS

In conclusion we find that high quality AlGaAs ridge waveguides can be produced by ECR dry etching using $BCl_3/N_2/Ar$ plasmas. Addition of $Cl_2$ enhances the etch rate, but may induce larger attenuation losses depending on the masking materials employed during the etch step. Mode attenuations of $\leqslant 1$ dBcm$^{-1}$ at 1.32 $\mu$m were obtained for waveguide stripe widths of 4–4.5 $\mu$m.

*Acknowledgements*—The work at Sandia National Laboratories was supported under US Dept of Energy contract No. DE-AC04-94AL850000. The authors at the University of Florida acknowledge the staff of the Microfabritech facility and its director, Professor P. H. Holloway, and also the support of the National High Magnetic Field Laboratory in Tallahassee. The authors at Sandia would like to thank P. L. Glarborg for her technical support.

## REFERENCES

1. J. Hecht, *The Laser Guidebook*, 2nd edn. McGraw-Hill, New York (1992).
2. R. J. Shul, R. P. Schneider and C. Constantine, *Electron. Lett.* **30,** 817 (1994).
3. D. L. Melville, J. G. Simmons and D. A. Thompson, *J. Vac. Sci. Technol. B* **11,** 2038 (1993).
4. K. D. Choquette, R. S. Freund, M. Hong, H. S. Luftman, S. N. G. Chu, J. P. Mannaerts and R. C. Wetzel, *J. Vac. Sci. Technol. B* **11,** 2025 (1993).
5. S. J. Pearton, U. K. Chakrabarti, A. Katz, F. Ren and T. R. Fullowan, *Appl. Phys. Lett.* **60,** 838 (1992).
6. C. D. W. Wilkinson, *Superlatt. Microstruct.* **7,** 381 (1990).
7. C. Constantine, D. Johnson, S. J. Pearton, U. K. Chakrabarti, A. B. Emerson, W. S. Hobson and A. Kinsella, *J. Vac. Sci. Technol. B* **8,** 596 (1990).
8. K. K. Ko and S. W. Pang, *J. Vac. Sci. Technol. B* **11,** 2275 (1993).
9. R. J. Shul, M. L. Lovejoy, D. L. Hetherington, D. J. Rieger, G. A. Vawter, J. F. Klem and M. R. Melloch, *J. Vac. Sci. Technol. A* **12,** 1351 (1994).
10. S. J. Pearton, *J. Vac. Sci. Technol. A* **12,** 1966 (1994).
11. S. J. Pearton, W. S. Hobson, F. Ren, C. R. Abernathy and C. Constantine, *J. Mater. Sci.-Mater. Electron.* **5,** 185 (1994).
12. W. M. Moreau, *Semiconductor Lithography—Principles, Practices and Materials*. Plenum Press, New York (1991).
13. S. Salimian and C. B. Cooper III, *J. Electrochem. Soc.* **136,** 2420 (1989).
14. S. J. Pearton, W. S. Hobson, C. R. Abernathy, F. Ren, T. Fullowan, A. Katz and A. Perley, *Plasma Chem. Plasma Proc.* **13,** 311 (1993).
15. R. H. Bruce and G. P. Malafsky, *J. Electrochem. Soc.* **130,** 1369 (1983).
16. R. J. Deri and E. Kapon, *IEEE J. Quantum Electron.* **27,** 626 (1991).
17. K. J. Eberling, *Integrated Opto-electronics*. Springer, Berlin (1992).

# Etching of GaAs/AlGaAs rib waveguide structures using $BCl_3/Cl_2/N_2/Ar$ electron cyclotron resonance

C. Constantine
*Plasma Therm IP, St. Petersburg, Florida 33716*

R. J. Shul, C. T. Sullivan, M. B. Snipes, G. B. McClellan, M. Hafich, and C. T. Fuller
*Sandia National Laboratories, Albuquerque, New Mexico 87185*

J. R. Mileham and S. J. Pearton
*University of Florida, Gainesville, Florida 32611*

(Received 23 February 1995; accepted 3 June 1995)

An anisotropic nonselective etch for GaAs/AlGaAs rib waveguides has been developed for use under electron cyclotron resonance conditions. The plasma chemistry features $BCl_3$ to minimize AlGaAs oxidation effects and small additions of $N_2$ to induce sidewall protection when using photoresist masks. The fundamental mode attenuation in GaAs/AlGaAs waveguides is sensitive to the choice of both plasma chemistry and masking material, but can be reduced to $<1$ dB $cm^{-1}$ for channel widths of 4–5 $\mu$m. © *1995 American Vacuum Society.*

## I. INTRODUCTION

GaAs/AlGaAs laser diodes operating over the wavelength range of 750–850 nm are used for a variety of applications, including compact disk playback (generally using low power diodes at 780 nm), optical data storage, laser printers, short-distance fiber-optical communications and as Nd laser pump sources.[1–8] Two of the research thrusts for these devices are

(i) the reduction of laser thresholds and improvement in efficiency, and
(ii) the development of arrays which might increase the speed of laser printers and optical data storage systems.

Photonic integrated circuits (PICs) constructed from GaAs/AlGaAs optical waveguides have also been the subject of research over the past decade for optical communications and control applications at 0.830, 1.3, and 1.55 $\mu$m wavelengths,[9–12] although these circuits have not yet seen as significant a commercial impact as GaAs/AlGaAs lasers. The layer compositions and thicknesses for these PICs are roughly similar to that used in laser diodes. Three of the research thrusts for these devices and circuits are

(i) the reduction of mode attenuation, primarily by reduction of sidewall scattering losses,
(ii) the reduction of fiber-to-waveguide coupling loss by modifying the waveguide design to achieve good mode matching with optical fibers or by the incorporation of waveguide tapers for controlled mode evolution, and
(iii) the development of abrupt waveguide turning mirror structures that permit much smaller chip path lengths and areas.

A key requirement for such advances is the development of high-resolution pattern transfer processes involving low pressure ($\sim$1 mTorr) plasmas with a relatively large ionization efficiency (1%–10%) and ion energies of $\leq$100 eV. Under these conditions the etching of the semiconductor layers is generally quite anisotropic and there is minimal disruption of the lattice due to energetic ion displacements or creation of nonstoichiometric surfaces.[13–21] Dry etching allows for fabrication of narrower stripe geometries, and therefore lower threshold current lasers. Recently most attention has been paid to the development of high etch-rate plasma chemistries for the long wavelength InGaAsP/InP lasers used in telecommunications, where it is necessary to use elevated substrate temperatures during $Cl_2$-based plasma etching in order to achieve practical etch rates. A sidewall polymer creating gas such as $CH_4$ or $SiCl_4$ (the latter in conjunction with a photoresist mask) is added to prevent undercutting, and other gases such as $H_2$ may be added to optimize the surface morphology and stoichiometry.[13,22–31] Similar work needs to be performed for the GaAs/AlGaAs system. While $Cl_2$-containing plasma chemistries are generally employed for GaAs, there has been little investigation into optimizing the etching under high microwave power conditions in the type of electron cyclotron resonance (ECR) single-wafer reactors now finding increasing application in III–V device technology.

In this article we show that a $BCl_3/Cl_2/N_2/Ar$ plasma chemistry can produce highly anisotropic ECR etching of GaAs/AlGaAs multilayer structures in conjunction with photoresist-based masks, even for very high microwave powers (1250 W). Some simple waveguide structures were fabricated using variants of this plasma chemistry and either single layer or trilevel resist masks.

## II. EXPERIMENT

Single layers of GaAs or $Al_xGa_{1-x}As$ ($x \leq 0.8$) grown on GaAs by metalorganic chemical vapor deposition and patterned with AZ5214 photoresist were used for etch-rate measurements. Etch depths were obtained by stylus profilometry after removal of the resist. The etch anisotropy was examined by scanning electron microscopy (SEM). Waveguide structures consisting of a 4 $\mu$m $Al_{0.04}Ga_{0.96}As$ bottom clad, a 2.0 $\mu$m GaAs guide, and a 0.5 $\mu$m $Al_{0.04}Ga_{0.96}As$ top clad

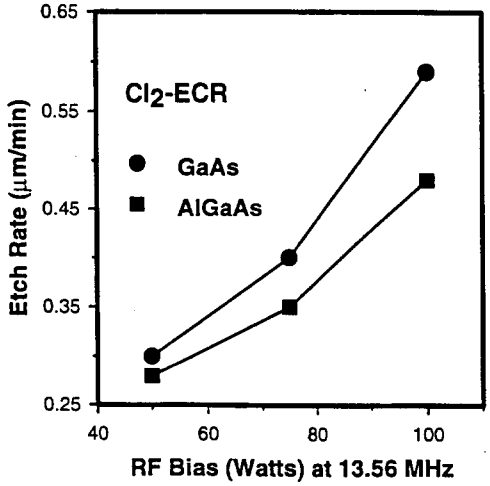


FIG. 1. Etch rates of GaAs and $Al_{0.3}Ga_{0.7}As$ in $Cl_2$/Ar ECR discharges (1 mTorr, 850 W microwave) as a function of applied rf bias.

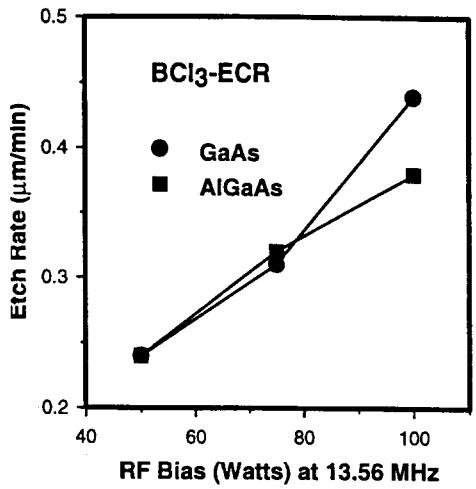


FIG. 2. Etch rates of GaAs and $Al_{0.3}Ga_{0.7}As$ in $BCl_3$/Ar ECR discharges (1 mTorr, 850 W microwave) as a function of applied rf bias.

were also grown by molecular beam epitaxy on semi-insulating GaAs substrates. The etch depth was nominally 3.0 $\mu$m. Fabry–Perot interferometry at 1.32 $\mu$m wavelength was used to measure the fundamental mode attenuation in these waveguides.[32] Two types of initial masking schemes were employed for dry etching of the waveguides. The first was a single layer of AZP4620 photoresist $\approx$7 $\mu$m thick. The second was a trilevel scheme, consisting of 2.1 $\mu$m of OCG875-90CS photoresist hard baked at 200 °C for 3 h, 500 Å of e-beam evaporated Ti, and 1.5 $\mu$m of AZ5214 imaging photoresist. After lithographically patterning the imaging resist, the Ti and hard baked resist layers were opened in a reactive ion beam etcher (RIBE) equipped with *in situ* end-point monitoring using $Cl_2$ and $O_2$, respectively.

All dry etching was performed in a Plasma-Therm SLR 770 system using an Astex low profile ECR source operating at 2.45 GHz. In this source the input power was varied from 850 to 1250 W. The sample position was separately biased with rf bias (13.56 MHz) at powers from 50 to 100 W, corresponding to dc biases from approximately $-30$ to $-70$ V. The process pressure was held constant at 1 mTorr and the sample temperature maintained at 10 °C using wafer clamping and He backside cooling (He pressure $\sim$5 Torr). Various ratios of $BCl_3$, $Cl_2$, $N_2$, and Ar were introduced through electronic mass flow controllers at a total gas flow rate of $\sim$50 standard cubic centimeters per minute (sccm).

## III. RESULTS AND DISCUSSION

We noticed in etching GaAs/AlGaAs rib waveguide structures in $Cl_2$Ar that there was a noticeable difference in etch rate between the GaAs and AlGaAs. This effect was most obvious with structures in which there was a graded composition confinement layer approaching a quantum well active region, typically varying from an [AlAs] mole fraction of 0.3$\rightarrow$0.8. An example is shown in Fig. 1, in which the etch rate of GaAs and $Al_{0.3}Ga_{0.7}As$ in a 1:10 $Cl_2$:Ar, 850 W microwave discharge is plotted as a function of applied rf bias. There is an etch rate difference of $\leq$20% between GaAs and 30% AlGaAs under these conditions.

A more uniform and more nonselective etch is obtained using a 1:10 $BCl_3$:Ar plasma under the same conditions. Figure 2 shows the etch rates for GaAs and $Al_{0.3}Ga_{0.7}As$ are the same within experimental error for this plasma chemistry. This has been reported previously under higher pressure reactive ion etching conditions,[33] and at much lower microwave powers (250 W) in an ECR system using permanent magnets.[34] The $BCl_3$ is known to attack aluminum oxides, and to getter water vapor in the reactor chamber,[35] thereby preventing reoxidation of the AlGaAs.

Figure 3 shows the microwave power dependence of $Al_xGa_{1-x}As$ ($x$=0–0.8) etch rate in $BCl_3$/Ar at 75 W rf bias. There is a smooth rise with microwave power, typical of a species-limited process. The etch rate was linearly dependent on rf bias between 50 and 100 W at fixed microwave power (850 W), signifying an ion/sputter desorption mechanism. $BCl_3$ does not form a high density of free chlorine radicals except at very high microwave powers, and therefore it can display diffusion-limited processes and substantial undercut at microwave powers$\geq$1000 W, or purely anisotropic etching

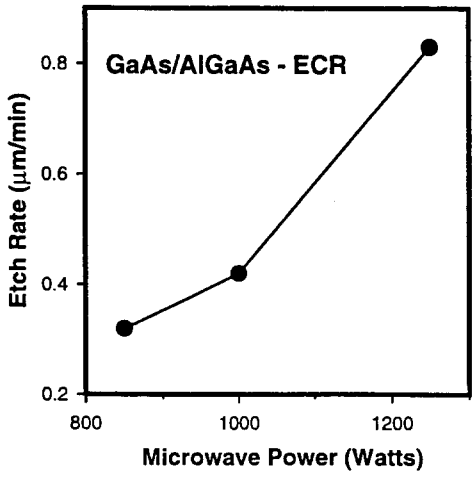


FIG. 3. Etch rate of $Al_xGa_{1-x}As$ ($x$=0–0.8) in $BCl_3$/Ar ECR discharges (1 mTorr, 75 W rf) as a function of applied microwave power. The etch rate is the same for all $x$ values under these conditions.

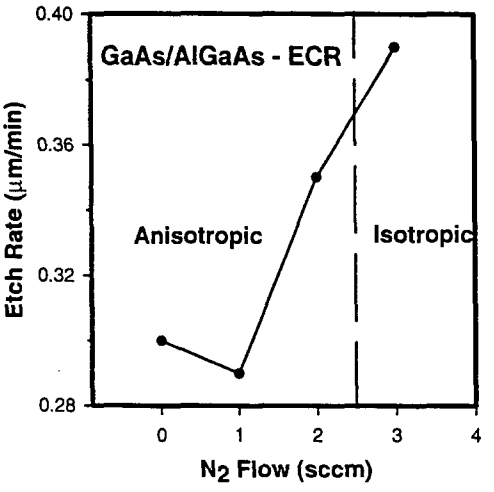


FIG. 4. Etch rate of $Al_xGa_{1-x}As$ ($x=0-0.8$) in $BCl_3$/Ar ECR discharges (1 mTorr, 850 W microwave, 750 W rf) as a function of $N_2$ flow rate.

at moderate powers (~850 W). The selectivity for etching AlGaAs over photoresist was typically 3 in the $BCl_3$/Ar mixtures, and is adequate for the waveguide structures under investigation.

The addition of $N_2$ to $Cl_2$ plasma chemistries has long been used to intentionally degrade resist for sidewall polymer protection.[35] We found that with $BCl_3$, rather than pure $Cl_2$, the polymer thickness is more controllable, due most likely to the reduced free chlorine radical density available to degrade resist. This produces a useful method for maintaining anisotropy of etched features in production situations, leading to a much larger window of etch conditions for anisotropy. Figure 4 shows the AlGaAs etch rate as a function of $N_2$ flow rate in a 75 W (rf), 850 W (microwave), 1 mTorr $BCl_3/N_2$/Ar discharge (5 sccm $BCl_3$, 50 sccm Ar). Above ~2.5 sccm $N_2$, the etch was found to begin to become isotropic. The mechanism may be the excess nitrogen radicals reacting with B to form BN, liberating free chlorine. This would allow the etch to become radical (diffusion) dominated. As the $N_2$ flow was increased from 1 to 3 sccm, the optical emission signal for Cl* at 725 nm also increased.

Figure 5 (top) shows an AlGaAs feature etched in a 5 $Cl_2$/50 Ar/2 $N_2$ discharge (1 mTorr, 75 W rf, 850 W microwave), with the resist mask still in place. There are clearly polymer sheets decorating the sidewalls. These were not removed when the resist was soaked off in acetone. Figure 5 (center and bottom) shows two views of features etched in a 5 $BCl_3$/50 Ar/2 $N_2$ discharge under the same conditions. The resist is still intact on these samples, but there is no indication of sidewall polymer sheets. This shows the more controllable nature of the latter chemistry for this application.

A scanning electron microscope (SEM) micrograph of a AlGaAs feature etched in 5 $BCl_3$/50 Ar/2 $N_2$ after removal of the resist mask is shown in Fig. 6. The etching is smooth and straight, with the corrugated features on the sidewall having been transferred into the semiconductor from the initial roughness in the edges of the resist mask, as reported previously.[36]

Figure 7 (top) shows a feature etched with 2.5 sccm $N_2$ flow in which the onset of polymer sheet formation is obvious. When the rf bias was reduced to 50 from 75 W, and the microwave power lowered from 850 to 500 W we still observed anisotropic etching [Fig. 7 (center)], but with a reduced rate near the feature relative to the field. When the $N_2$ flow rate was increased to 3 sccm (at 75 W rf and 850 W microwave), we observed the sidewall beginning to undercut, as shown at the bottom of Fig. 7.

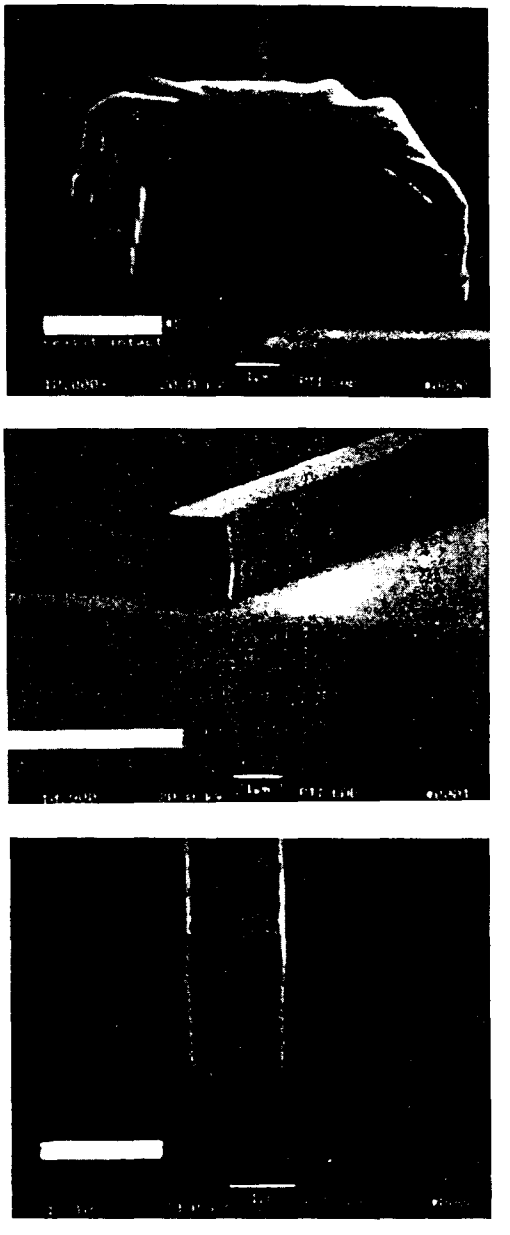

FIG. 5. SEM micrographs of features etched into AlGaAs/GaAs waveguide structures with ECR discharges (1 mTorr, 850 W microwave, 75 W rf) of (top) $Cl_2$/Ar/$N_2$ and (center and bottom) $BCl_3$/Ar/$N_2$. The resist mask is still in place in all cases.

As mentioned earlier, the two mask schemes used for actual waveguide fabrication involved either a single layer of thick resist, or a trilevel resist. The advantage of the former is its simplicity and application to a wide range of ECR etching recipes, including via hole processes for both InP and GaAs substrates. The major disadvantages of thick resist are poor dimensional control below 2–4 $\mu$m and obtaining straight wall profiles. The trilevel scheme, on the other hand,

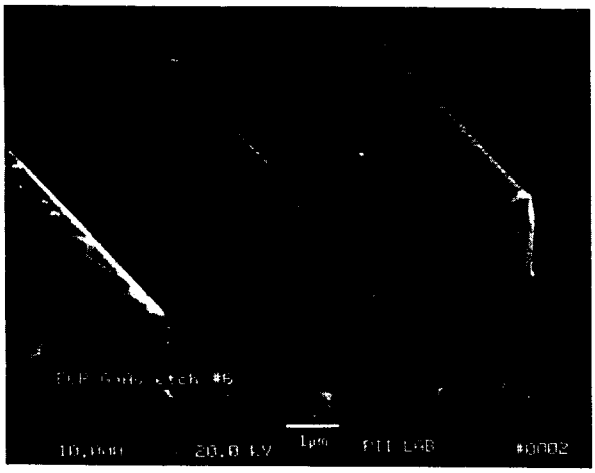

FIG. 6. SEM micrograph of feature etched into an AlGaAs/GaAs structure using a $BCl_3/Ar/N_2$ ECR discharge (1 mTorr, 75 W rf, 850 W microwave). The resist mask has been removed.

is more time consuming to fabricate since it involves many more steps, but it can be used for feature sizes down to submicron with near-vertical smooth mask profiles. Waveguides were fabricated with channel widths between ~3 and 10 $\mu$m using both masking schemes and several etch chemistries, including $BCl_3/Cl_2N_2/Ar$, $BCl_3/N_2/Ar$, and $Cl_2/N_2/Ar$. Some waveguide loss results are shown in Fig. 8 for the trilevel mask. The attenuation at 1.32 $\mu$m is comparable for waveguides etched with either the ECR $BCl_3/N_2/Ar$ chemistry as with reactive ion beam etching with a 0.25 mTorr, 300 V chlorine beam (an etch rate of ~700 Å $min^{-1}$). The latter is a completely polymer-free situation, and the equivalence with the ECR $BCl_3/N_2/Ar$ etching shows that the sidewalls under these ECR conditions are not affected by any remnant deposition. By contrast, ECR etching with $BCl_3/Cl_2/N_2/Ar$ produces much greater mode attenuation at similar channel widths and must therefore result from increased light scattering at nonuniformities on the feature sidewalls.[2] The coupling efficiency of the light propagating in a waveguide of width $b$ with a deflection angle of $\phi$ is given by[2]

$$|\eta_0|^2 = \left( \frac{\sin\frac{(\beta\phi b)}{2}}{\frac{\beta\phi b}{2}} \right)^2,$$

where $\eta_0$ is the ratio of power coupled into the fundamental mode to the total incident power and $\beta$ is the propagation constant. This relation shows that strong mode attenuation can be created by small irregularities in the waveguide sidewall, which scatter light out of the propagating beam.

When using the single photoresist mask, lower attenuation losses in the waveguides were obtained with $Cl_2$ addition to the plasma chemistry, as shown in Fig. 9. This suggests an optimum amount of chlorine must be available for the best sidewall protection, since the $BCl_3/Cl_2/N_2/Ar$ etching produced better results than either $BCl_3/N_2/Ar$ or $Cl_2/N_2/Ar$. A global representation of data obtained from all the waveguides is shown in Fig. 10, and emphasizes how the

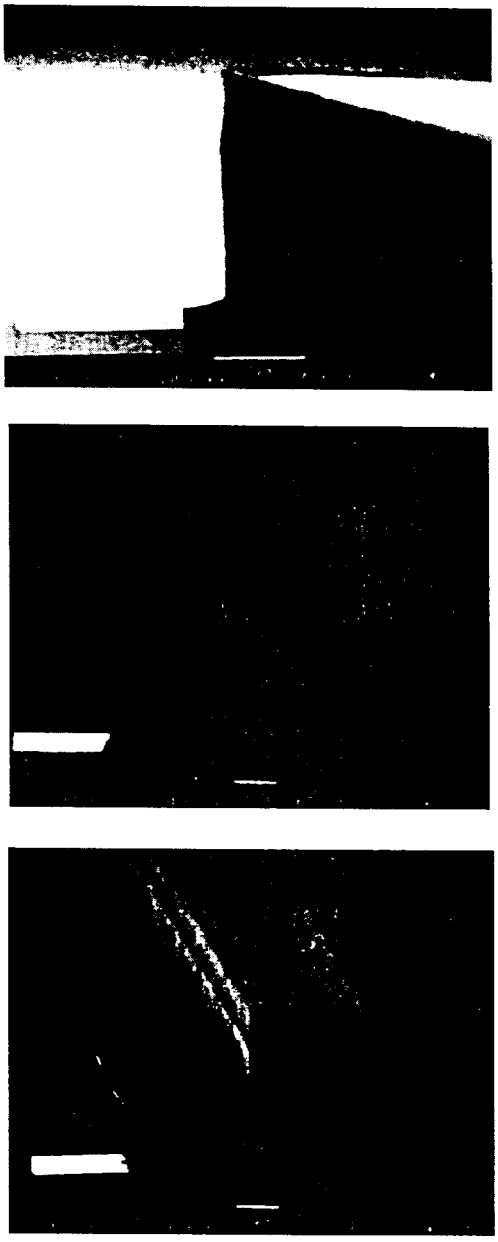

FIG. 7. SEM micrographs of features etched into AlGaAs/GaAs structures using $BCl_3/Ar/N_2$ with (top) 2.5 sccm $N_2$, rf power of 75 W and microwave power of 850 W, (center) a reduced rf power of 50 W and microwave power of 500 W, 2 sccm $N_2$ and (bottom) 3 sccm of $N_2$ and standard rf power (75 W) and microwave power (850 W).

choice of both plasma chemistry and mask material can strongly influence the quality of the resulting waveguide. Note that in all cases the mode attenuation increases as the channel width is decreased, resulting from increased influence of the sidewalls. Finally, we note all etching was performed on 2 in. $\phi$ wafers, and etch uniformities of $\leq$3% were obtained over the wafer diameter when employing $N_2$ in the plasma chemistry.

## IV. SUMMARY AND CONCLUSIONS

A $BCl_3/Cl_2/N_2/Ar$-containing plasma chemistry used under ECR conditions nonselectively etches AlGaAs/GaAs waveguide structures. Addition of $N_2$ at low relative concentrations (~5% of total flow rate) produces a wider window of

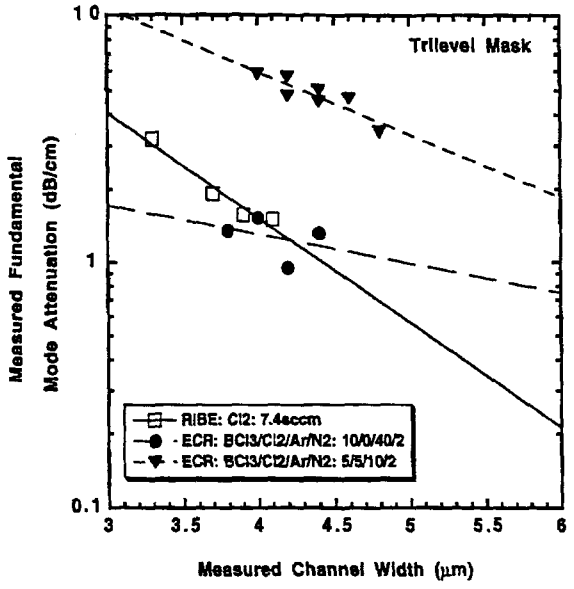


FIG. 8. Mode attenuation in AlGaAs/GaAs waveguides as a function of channel width in features patterned with $Cl_2$(RIBE), $BCl_3/Ar/N_2$ (ECR), or $BCl_3/Cl_2/Ar/N_2$ (ECR) discharges using a trilevel mask.

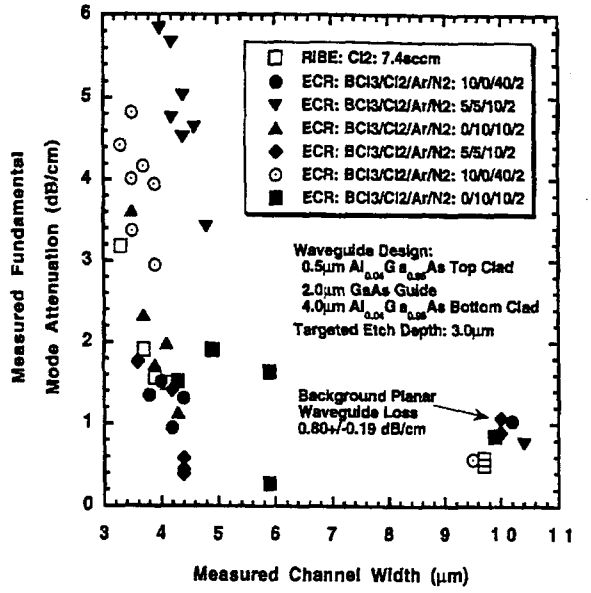


FIG. 10. Mode attenuation in AlGaAs/GaAs waveguides as a function of channel width in structures patterned with various plasma conditions and mask materials. The data with closed circles, inverted triangles, and regular triangles were obtained using trilevel masks, while all others were obtained with single layer resist masks.

conditions under which anisotropic etching is obtained, and careful choice of both plasma chemistry and mask materials is necessary to achieve the lowest attenuation losses in narrow ($\leq 5$ $\mu$m) stripe waveguides. Both trilevel and simple photoresist masks were investigated, and each can give low waveguide losses, depending on the $N_2$ concentration in the plasma. Attenuation losses as low as 1 dB $cm^{-1}$ were obtained in the waveguides.

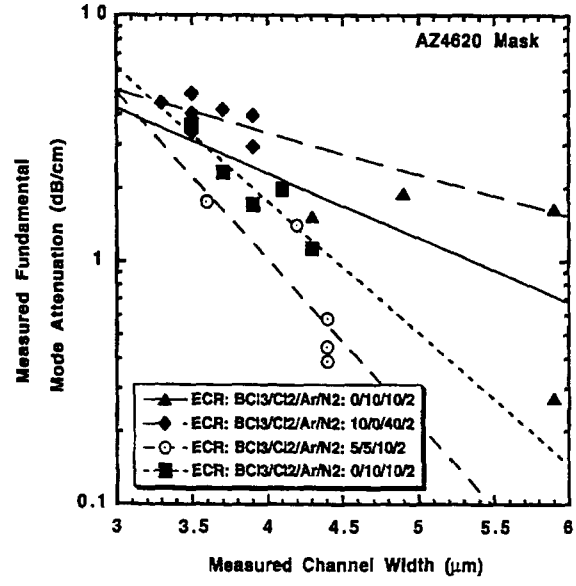


FIG. 9. Mode attenuation in AlGaAs/GaAs waveguides as a function of channel width in features patterned with $BCl_3/Ar/N_2$, or $BCl_3/Cl_2/Ar/N_2$ECR discharges using a single-layer photoresist mask. The data marked with triangles is for 850 W microwave power, while that with squares is with 500 W microwave power.

## ACKNOWLEDGMENTS

The work performed at Sandia National Laboratories was supported under U. S. Department of Energy Contract No. DE-AC04-94AL850000. The authors at the University of Florida would like to thank the staff of the Microfabritech facility and its director, Professor P. H. Holloway, and also the support of the National High Magnetic Field Laboratory in Tallahassee, FL. The authors at Sandia National Laboratories would like to thank P. L. Glarborg for her technical support.

[1]E. Kapon, in *Handbook of Solid State Lasers*, edited by P. K. Cheo (Dekker, New York, 1989), pp. 1–112.
[2]K. J. Ebeling, *Integrated Optoelectronics* (Springer, New York, 1992).
[3]J. Hecht, *The Laser Guidebook* (McGraw-Hill, New York, 1992).
[4]M. Ohtsu, *Highly Coherent Semiconductor Lasers* (Artech House, Norwood, MA, 1992).
[5]M. Fukuda, *Reliability and Degradation of Semiconductor Lasers and LED's* (Artech House, Norwood, MA, 1991).
[6]*Quantum Well Lasers*, edited by P. S. Zory (Academic, San Diego, 1993).
[7]*Photonics in Switching*, edited by J. E. Midwinter (Academic, San Diego, 1993), Vol. 1.
[8]G. P. Agrawal and N. K. Dutta, *Long Wavelength Semiconductor Lasers* (Van Nostrand Reinhold, New York, 1986).
[9]M. K. Hibbs-Brenner and C. T. Sullivan, Appl. Phys. Lett. **56**, 1529 (1990).
[10]C. T. Sullivan, S. D. Mukherjee, M. K. Hibbs-Brenner, A. Gopinath, E. Kalweit, T. Marta, W. Goldberg, and R. Walterson, Proc. SPIE **1703**, 163 (1992).
[11]C. T. Sullivan, S. D. Mukherjee, E. Kalweit, T. Marta, W. Goldberg, M. K. Hibbs-Brenner, R. Walterson, and M. N. Khan, Proc. SPIE **1703**, 207 (1992).
[12]R. J. Devi and E. Karpon, IEEE J. Quantum Electron. **27**, 626 (1991).
[13]C. Constantine, C. Barratt, S. J. Pearton, F. Ren, and J. R. Lothian, Appl. Phys. Lett. **61**, 2899 (1992).
[14]S. J. Pearton, Int. J. Mod. Phys. **8**, 1781 (1994).
[15]K. K. Ko and S. W. Pang, J. Vac. Sci. Technol. B **11**, 2275 (1993).
[16]C. Thirstrup, S. W. Pang, O. Albreksten, and J. Hanberg, J. Vac. Sci. Technol. B **11**, 1214 (1993).

[17]G. F. McLane, W. R. Buchwald, L. Casas, and M. W. Cole, J. Vac. Sci. Technol. A **12**, 1356 (1994).
[18]R. J. Shul, M. L. Lovejoy, D. L. Hetherington, D. J. Rieger, G. A. Vawter, J. F. Klein, and M. R. Melloch, J. Vac. Sci. Technol. A **12**, 1351 (1994).
[19]S. J. Pearton, J. Vac. Sci. Technol. A **12**, 1966 (1994).
[20]R. J. Shul, R. P. Schneider, and C. Constantine, Electron. Lett. **30**, 817 (1994).
[21]M. A. Foad, S. Thomas, and C. D. W. Wilkinson, J. Vac. Sci. Technol. B **11**, 20 (1993).
[22]G. J. van Gurp and J. M. Jacobs, Philips J. Res. **44**, 211 (1989).
[23]R. van Roijen, C. W. T. Bulle-Lieuwma, and E. A. Montie, J. Vac. Sci. Technol. B **10**, 2188 (1992).
[24]R. van Roijen, M. B. Kemp, C. W. T. Bulle-Lieuwma, L. J. van Izendoorn, and T. Thijssen, J. Appl. Phys. **70**, 3983 (1991).
[25]P. J. A. Thijs, L. Tiemeijer, P. Kuindersma, J. J. Binsma, and T. van Dongen, IEEE J. Quantum Electron **27**, 1426 (1991).
[26]S. J. Pearton, W. S. Hobson, F. Ren, C. R. Abernathy, and C. Constantine, J. Mater. Sci.: Mater. Electron. **5**, 185 (1994).
[27]G. J. van Gurp, J. M. Jacobs, J. J. M. Binsma, and L. F. Tiemeijer, Jpn. J. Appl. Phys. **28**, L1236 (1989).
[28]F. Ren, S. J. Pearton, B. Tseng, J. Lothian, B. Segner, and C. Constantine, J. Electrochem. Soc. **140**, 3294 (1993).
[29]J. Schneider, M. Moser, and K. Affolfer, Proceedings of the 6th International Conference on InP and Related Materials, 1994 (unpublished), pp. 216–219.
[30]S. J. Pearton, Mater. Sci. Eng. B **27**, 61 (1994).
[31]C. Constantine, C. Barratt, S. J. Pearton, F. Ren, and J. Lothain, Electron. Lett. **28**, 1749 (1992).
[32]E. Kapon and R. Bhat, Appl. Phys. Lett. **50**, 1628 (1987).
[33]S. Salimian and C. B. Cooper III, J. Electrochem. Soc. **136**, 2420 (1989).
[34]S. J. Pearton, W. S. Hobson, C. R. Abernathy, F. Ren, T. R. Fullowan, A. Katz, and A. Perley, Plasma Chem. Plasma Process. **13**, 311 (1993).
[35]R. H. Bruce and G. P. Malafsky, J. Electrochem. Soc. **130**, 1369 (1983).
[36]U. K. Chakrabarti, S. J. Pearton, and F. Ren, Semicond. Sci. Technol. **6**, 408 (1991).

(Invited Paper)

# Unlimited-Bandwidth Distributed Optical Phase Modulators and Detectors: Design and Fabrication Issues

G. A. Vawter, V. M. Hietala, S. H Kravitz, M. G. Armendariz

Sandia National Laboratories
P.O. Box 5800
Albuquerque, NM 87185-0603 USA
tel: (505)844-9004 fax: (505)844-8985

**Abstract**

Practical and theoretical limits on the bandwidth of distributed optical phase modulators and traveling-wave photodetectors are given. For the case of perfect velocity matching, RF transmission losses are the main performance-limiting factor. However, some high-performance modulators require highly-capacitive transmission lines making proper slow-wave operation difficult to achieve. Trade-offs between high and low figure-of-merit phase modulators are given. The newly developed travelling-wave photodetector is discussed as a means to achieve detection of mm-wave modulated light beams at high power levels.

## Introduction

Extremely fast modulation response of optical phase delay in a waveguide modulator is required for photonic integrated circuits (PICs) to operate with mm-wave signals. Single phase modulators, paired phase modulators in a Mach-Zehnder interferometer, or more complex arrangements can be used for mm-wave modulation of light in either phase, amplitude, or frequency. The primary limitations on the operating frequency are the modulation bandwidth of the phase modulator and the photodetector used to receive the modulated light. Standard lumped-element devices are bandwidth limited by the RC time-constant of the structure. Distributed, or traveling-wave, modulators and, more recently, detectors have been developed to surpass the RC limit. With distributed structures the bandwidth limit is determined by loss of phase synchronism between the optical and RF wavefronts within the length of the device[1]. The generally different propagation constants of the optical and RF waves leads to a limiting length-bandwidth product in the modulation response. In the limit of zero velocity mismatch the modulation bandwidth is then limited by RF loss in the transmission line. We discuss the application of slow-wave transmission lines to both phase modulators[2] and photodiodes[3], [4] as a means to increase the length-bandwidth product by matching the propagation constants of the optical and RF waves.

$$length \bullet bandwidth \propto \frac{1}{velocity\ mismatch} \quad (1)$$

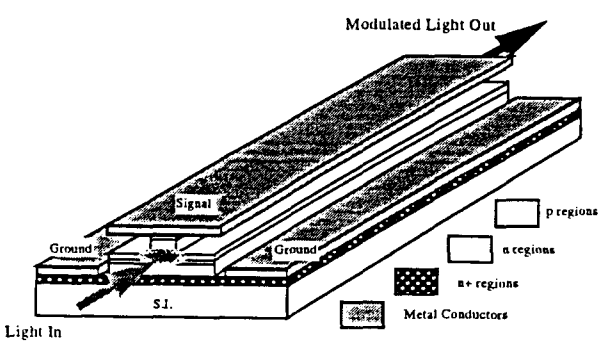


Figure 1. Diagram of traveling-wave phase modulator.

## Distributed Phase Modulators

The (Al)GaAs material system is attractive for use with high-speed optical phase modulators due to the extremely high modulation figure-of-merit (FOM) obtainable at 1.3 μm wavelengths without excessive absorption modulation. Properly designed PIN double heterostructure waveguides[5] can have an FOM between 35 and 90 °/V/mm (degrees phase shift per unit voltage and length). These very high efficiencies allow for reduced modulation bias swing and device size, thus easing the RF drive power required and allowing relatively greater velocity mismatch for a given bandwidth as compared to conventional low-doped or dielectric structures. Velocity match in the phase modulator is obtained using a slow-wave transmission line. Slow-wave propagation is achieved through the insertion of a heavily-doped, n+, GaAs layer beneath the diode structure, connecting the two ground planes and serving as the electrical connection between the ground planes and the diode. However, the high capacitance of the PIN structure requires minimizing the transmission line's inductance with very small spacing between ground and signal metalizations.

Initial attempts to fabricate distributed phase modulators with a high FOM used a asymmetric ground-signal configuration[2] with a 4 μm gap between the ground and signal metalizations. This small gap was used to reduce the inductance per unit length of the device so as to match the phase velocity of the optical and RF signals. Measurements of the performance of the ground-signal design showed a bandwidth of ~10 GHz. We believe that this low bandwidth is due primarily to the asymmetric metalization design, allowing the electric-field vector within the depletion-zone of the diode to rotate away from perpendicular to the epitaxial layers, reducing the effective modulation efficiency at high frequencies.

In order to force the electric field vector to remain perpendicular to the epitaxial layers we are investigating symmetric ground-signal-ground electrode configurations. Fig. 1 shows a schematic diagram of one such design. The optical waveguide is an etched rib type with outer mesa

etches used to provide contact of the ground metal with the $n^+$ GaAs layer. A quasi-TEM transmission-line model is used to calculate the frequency response of the modulator. As seen in Fig. 2(a), this model predicts a 280 GHz -3 dB bandwidth (limited by loss within the metalization) for perfect velocity matching. This calculation assumes that a high FOM ( about 40°/V/mm) design is used. Such modulators do give relatively high RF transmission losses, 2 dB/mm at 30 GHz, in the resultant slow-wave transmission line but this high loss is compensated by the short modulator length, 1 mm, such that a significant speed increase compared to low FOM devices is seen. Fig. 2(b) shows a similar calculation for a low FOM (about 4°/V/mm) device where the bandwidth drops to 12 GHz in spite of the assumed 1 dB/mm, at 30 GHz, RF loss due to the 10 mm length needed to compensate for the low modulation efficiency.

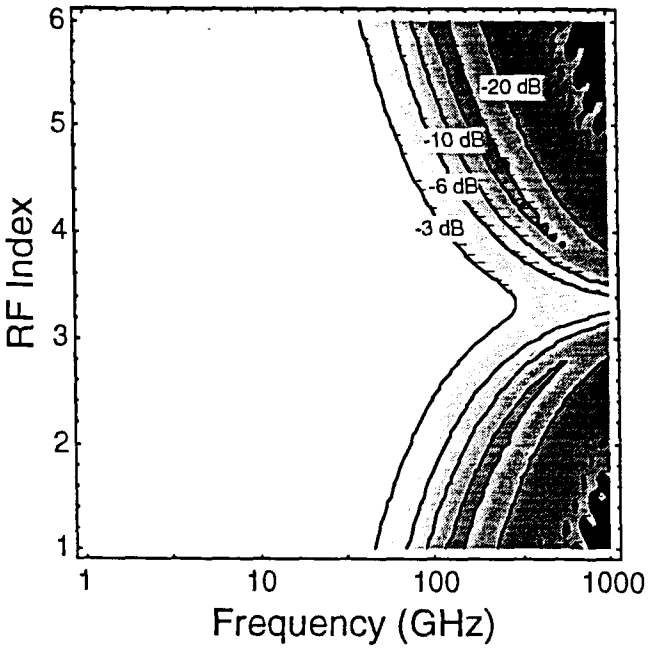


(a)

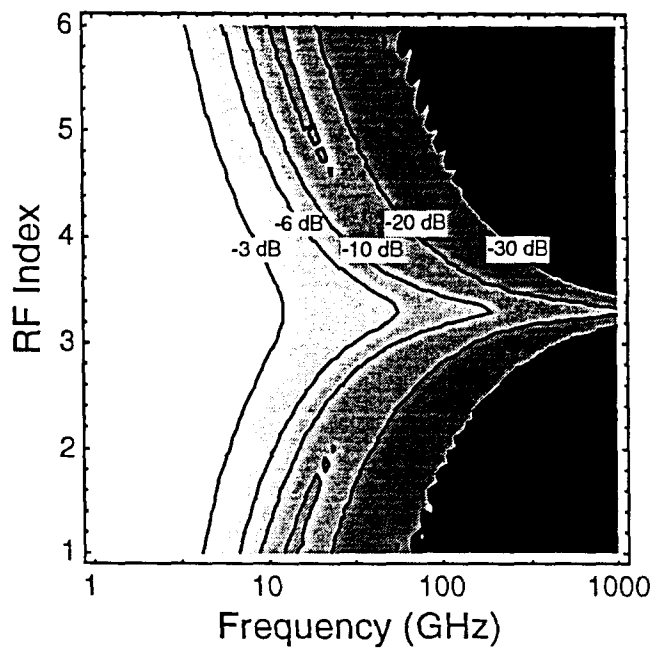


(b)

**Figure 2.** Theoretical traveling-wave phase modulator response as a function of frequency and RF index. (a) Response of high FOM device with 2 dB/mm RF loss but requiring only 1 mm length. The -3 dB bandwidth is 280 GHz. (b) Response of low FOM device with only 1 dB/mm RF loss but requiring only 10 mm length. The -3 dB bandwidth is 12 GHz.

### Distributed Photodetector

The traveling-wave photodetector (TWD) (Fig.3) is also a slow-wave structure. This device takes advantage of a low-confinement-factor single quantum well centered in a larger optical waveguide, similar to a GRINSCH laser diode, to spread absorption of the guided light over a very long distance, 0.5 to 2 cm, so that detection of high-power signals can be achieved at mm-wave frequencies. As the light is absorbed along the length of the device, the resulting photocurrent couples into an RF wave propagating along the electrodes. If velocity synchronism is obtained these photocurrents will add in phase with the RF wave, increasing its amplitude as it travels down the device. Depending on the impedance at the termination of the RF waveguide, this device can generate very high RF power levels in the mm-wave regime.

The authors have developed a detailed model for detection along the length of a TWD[3], this model is similar to a time-domain model described recently by Giboney et al.[4]

Assuming no back reflection at the far end of the device (100% optical absorption), and excitation by light with a 100% modulation depth at the RF operating frequency, the

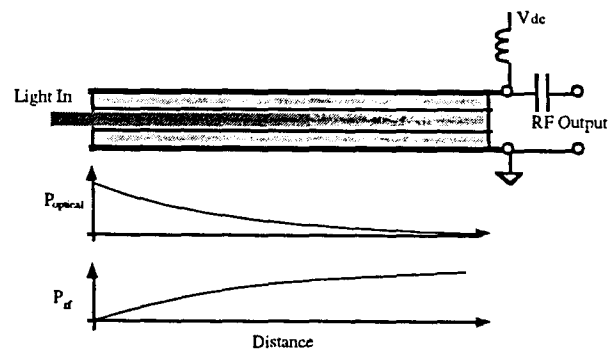


a)

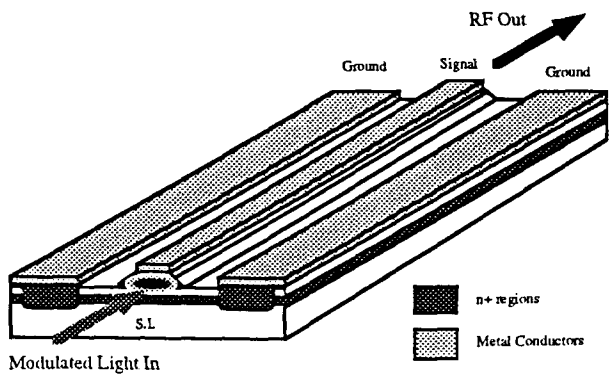


b)

**Figure 3.** Diagram of traveling-wave photodetector. a) Optical and RF power levels are shown along the detector's length. b)Physical diagram.

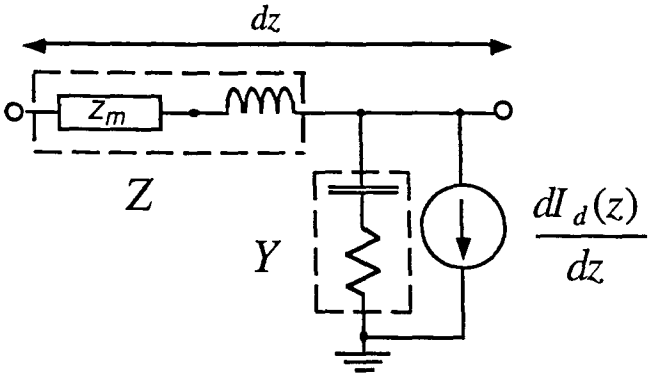


**Figure 4.** Equivalent transmission-line circuit for TWD.

optical intensity ($P_l$) within the photodetector can be described by:

$$P_l(z,t) = 2P_o\left(1+\sin\left(\omega_{rf}t-\beta_o z\right)\right)e^{-\alpha_o z} \quad (2a)$$

in which $\omega_{rf}$ is the angular rf beat frequency, $z$ is the position along the length of the detector, $\alpha_O$ attenuation constant of the optical mode and $\beta_O$ is the propagation constant of the rf modulated light ($\beta_O \approx 2\ \pi\ n_O/\lambda_{rf}$). Dropping the DC term, equation (2) can be rewritten in phaser-wave notation at the RF-operating frequency $\omega_{rf}$:

$$p_l(z) = 2P_o e^{-\gamma z} \quad (2b)$$

in which $\gamma = \alpha_O + \beta_O$. The exponential decay of the light as it propagates is due to photons being absorbed and hence electrons and holes generated (e.g. a current). The local current generated at any point along the detector is related to the amount of light absorbed at the point multiplied by the responsivity:

$$\frac{dI_d(z)}{dz} = \Re\frac{d|p_l(z)|}{dz}e^{-j\beta z} \quad (3a)$$

in which ($\Re$) is the responsivity given by:

$$\Re = \frac{\xi e \lambda_o}{hc} \quad (3b)$$

where $\xi$ is the quantum efficiency, $e$ is the charge of an electron, $h$ is Planck's constant, and $c$ is the speed of light. Carrier transit times within the detector are neglected allowing for Equation (3) to be valid at all operating frequencies. Combining Equations (2) and (3) gives:

$$\frac{dI_d(z)}{dz} = k_o e^{-\gamma_o z} \quad (4a)$$

in which

$$k_o = \frac{\alpha_o \xi e P_o \lambda_o}{2hc} \quad (4b)$$

and

$$\gamma_o = \alpha_o + j\beta_o\ . \quad (4c)$$

This distributed current source can be coupled to the electrical propagation along the detector by incorporating it into the time-harmonic telegraphist's equations:

$$\frac{dV}{dz} = -ZI \quad (5a)$$

and

$$\frac{dI}{dz} = -YV - \frac{dI_d(z)}{dz} \quad (5b)$$

in which the second term is the differential current source described by Equation 4. The transmission line equivalent circuit is shown in Fig. 4. This model is only approximately correct as physically the current source should be in parallel with the capacitance. The incorporation of the current source as shown in Fig. 4 is appropriate provided that the transverse electrical loss is small compared to the electrical energy storage along the detector. This is true for this type of transmission line. Using this approximate model allows for an analytical solution. Equation 5 can be combined to form a second order differential equation describing the voltage ($V$) along the line:

$$\frac{d^2V}{d^2z} - \gamma^2 V = Zk_o e^{-\gamma_o z} \quad (6)$$

in which $\gamma = \sqrt{Z\,Y}$ is the traditional electrical propagation constant along the detector.

Equation (6) has a simple analytical solution which can be found by elementary methods (i.e. variation of parameters):

$$V(z) = V_1 e^{\gamma z} + V_2 e^{-\gamma z} + \frac{Z\,k_o}{\left(\gamma_o^2 - \gamma^2\right)}e^{-\gamma_o z}\ . \quad (6)$$

The first and second terms in the right hand side of Equation (6) are the traditional backward and forward propagating waves along a transmission line. The third term the detected light's signal impressed along the line. Applying boundary conditions allows for the determination of $V_1$ and $V_2$ .

With the input open and output ends terminated, the appropriate boundary conditions are:

$$I(0) = 0 \quad \text{and} \quad \frac{V(l)}{I(l)} = Z_l\ . \quad (7)$$

Applying these boundary conditions to Equation (6) gives a relationship which is plotted as Fig. 5. showing the theoretical TWD response as a function of frequency and

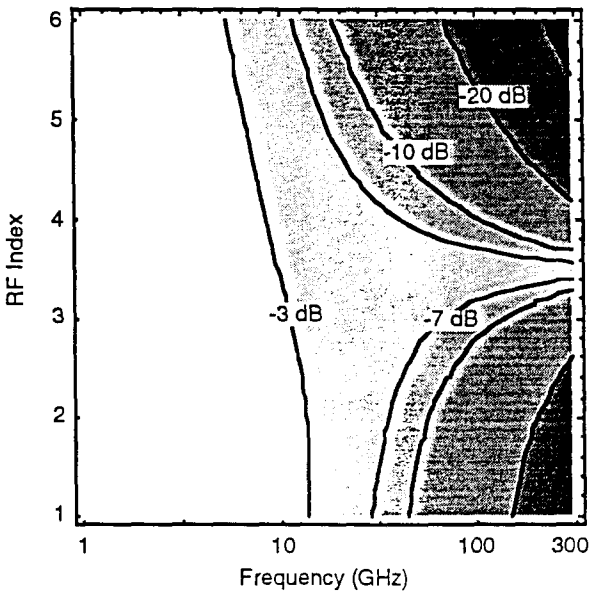


**Figure 5.** Theoretical traveling-wave photodetector response as function of RF index and frequency.

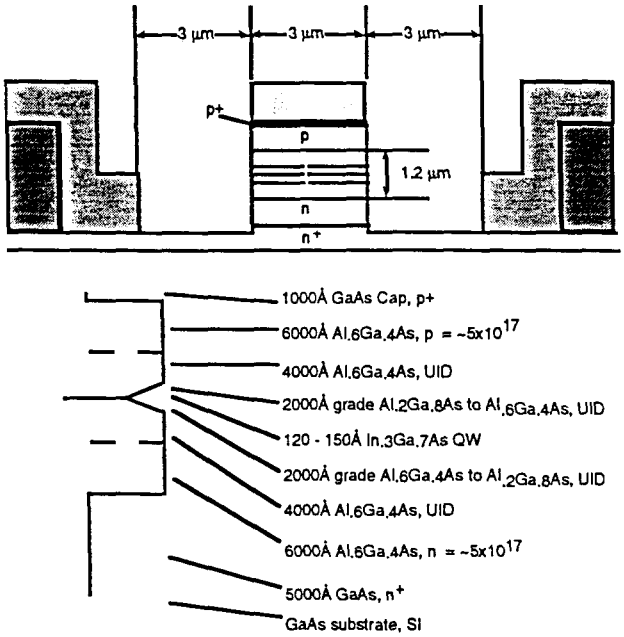


**Figure 6**. Cross-section schematic of the TWD for 1.06 µm operation (top) and diagram of material composition and thicknesses through the center axis of the waveguide (bottom).

RF index. This particular design has a 6 dB bandwidth in excess of 200 GHz.

Based on these design calculations a GaAs/AlGaAs/InGaAs TWD was fabricated as shown in Fig. 6. This structure is intended to have both a high bandwidth and a maximum usable input power of up to 200 mW at 1.06 µm wavelength. SEM micrographs or of the finished device are shown in Figs. 7 and 8. Testing of these 1250 µm long TWDs yielded an 8 GHz 6 dB bandwidth ( 4.8 GHz 3 dB bandwidth). Modulation response of the actual detectors does not yet achieve the theoretical limit due primarily to transit-time effects of photogenerated carriers. Upper power limits have not yet been measured. More recently, an extremely short TWD optimized for response bandwidth has been demonstrated [6] to have a 172 GHz 3 dB bandwidth. This device was only 7 µm long and was tested in an electrooptic sampling system to eliminate performance limitations due to large size or electrical loading effects.

## Conclusions

Distributed modulators offer an excellent bandwidth advantage compared to lumped-element designs. With the proper optical and RF modeling tools modulation responses well into the hundreds of GHz are achievable. High FOM phase modulators can be exploited to aid in achieving these extremely high bandwidths as the excess RF loss associated with the high FOM is more than offset by the resulting reduced device length. Travelling-wave detectors are a new type of photodiode offering simultaneous high speed and high power operation, unlike conventional lumped photodiodes offering high-speed operation only at very low signal levels. A TWD model has been derived and used to show that these new devices have potential bandwidths in excess of 200 GHz. To date, efforts to fabricate and test TWDs have yielded a 1250 µm long detector optimized for high-power operation with a 4.8 GHz bandwidth (this work) and 7 µm long device optimized for high speed [6] with a

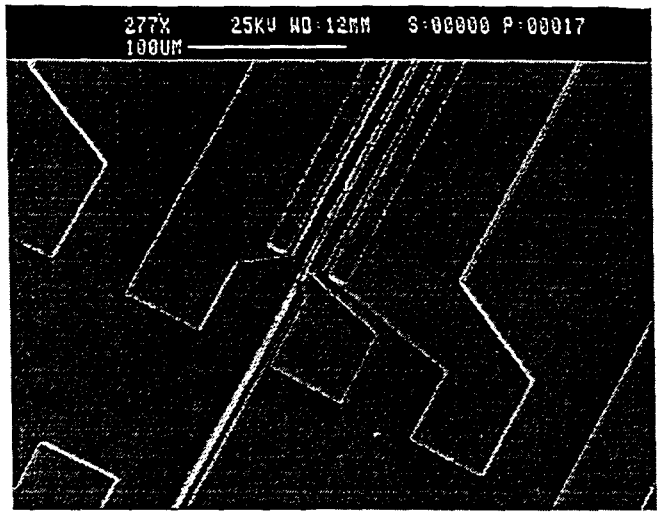


**Figure 7.** SEM micrograph of top view of traveling-wave photodetector. Optical guide extends diagonally for lower-left to upper-right at center. Center electrical contact connected to optical guide's contact is the signal. Ground lines exist to either side.


**Figure 8** SEM micrograph of TWD showing connection to center electrode on top of the optical guide to the offset metal used by Cascade probes.

172 GHz bandwidth.


## Acknowledgements

This work was supported by the United States Department of Energy under Contract DE-AC04-94AL85000.

## References

[1] Walker, "High-speed III-V semiconductor intensity modulators," IEEE J. Quantum Electron., vol. 27, pp. 654, 1991.

[2] V. M. Hietala, S. H. Kravitz, M. G. Armendariz, G. A. Vawter and R. E. Leibenguth, "High-Performance GaAs/AlGaAs Optical Phase Modulators for Microwave/Photonic Integrated Circuits", in Proceedings of the SPIE, Optoelectronic Signal Processing for Phased-Array Antennas IV, SPIE, Los Angeles, CA, 1994, 2155, pp. 29-36.

[3] V. M. Hietala and G. A. Vawter, "Traveling Wave Photodetector", U.S. Patent No. 5,270,532 issued Dec. 14, 1993.

[4] K. Giboney, M. Rodwell and J. Bowers, "Travelling-wave photodetectors," IEEE Phot. Technol. Lett., vol. 4, pp. 1363-1366, 1993.

[5] Mendoza-Alverez, Coldren, Alping, Yan, Hausken, Lee and Pedrotti, "Analysis of Depletion Edge Translation Lightwave Modulators," IEEE J. Lightwave Technol., vol. 6, pp. 793, 1988.

[6] K. Giboney, R. Nagarajan, T. Reynolds, S. Allen, R. Mirin, M. Rodwell and J. Bowers, "172 GHz, 42% Quantum Efficiency p-i-n Travelling-Wave Photodetector", in 52nd Annual Device Research Conf. (late paper), Boulder, CO, June, 1994, pp. VIA-9.

**Distribution:**

| | | |
|---|---|---|
| 3 | MS 0603 | Charles Sullivan, 01313 |
| 1 | MS 0161 | Patent and Licensing Office, 11500 |
| 1 | MS 9018 | Central Technical Files, 08940-2 |
| 2 | MS 0899 | Technical Library, 04916 |
| 2 | MS 0619 | Review and Approval Desk, 12690<br>For DOE/OSTI |